EFFECTS OF ADDITIVES ON RHEOLOGY AND FILM BLOWING OF POLYPROPYLENE/CLAY NANOCOMPOSITES

By

Weijie Ren

A DISSERTATION

Submitted to
Michigan State University
in partial fulfillment of the requirements
for the degree of

Chemical Engineering - Doctor of Philosophy

2016

ABSTRACT

EFFECTS OF ADDITIVES ON RHEOLOGY AND FILM BLOWING OF POLYPROPYLENE/CLAY NANOCOMPOSITES

By

Weijie Ren

Polymer nanocomposites with organically modified nanoclay have two different types of interface sites: edges with hydroxyl groups and gallery faces with oxygen atoms. In this study, the polymer-particle interface was strengthened by a coupling agent, aminoalkyldimethoxysilane, which allowed the formation of covalent bonds between silane treated organoclay and maleic anhydride groups of the long chain compatibilizer. The objective of this research is to investigate effects of reactive coupling at these interfacial sites on rheology of polypropylene (PP)/clay nanocomposites in dynamic shear and uniaxial extensional flow for blown film applications.

For preparation of PP nanocomposites, two different organoclays, with different aspect ratios and surfactants, before and after silane treatment via a wet process were used as the additives. In the case of organoclay with the greater interlayer packing of surfactants (Nanocor I.44P), the silanols reacted only at the nanolayer edges while in the other case with primary onium ion surfactants (Nanocor I.30P), the silanols entered the interlayer galleries. The effect of reactive coupling in both cases was noticeably improved dispersion with thinner stacks of clay nanolayers. The uniaxial extensional viscosity of these melts displayed greater strain hardening and more so in the case of reactive coupling at both faces and edges despite the aspect ratio of this organoclay being significantly lower. Upon reprocessing, the nanostructure and strain hardening behavior were stable for nanocomposites with silylated I.44P while severe aggregation of nanoclays and drastic reduction of extensional viscosity were observed for nanocomposites

with silylated I.30P. This was attributed to detachment of loosely held silanes from the gallery sites.

A dry, solvent-free process was also introduced for silane treatment. This approach was shown to lead to better penetration of the interlayer galleries of the I.44P organoclay by silanes than through the solvent based or wet process. As an additional advantage of this treatment, good thermal stability was maintained for silylated I.44P. This ensured its applicability for high temperature processing. The silylated I.44P nanoclay was then compounded with the compatibilizer to prepare masterbatch additives for letting down with a high molecular weight polypropylene. Blown films with a thickness of 25 μm were prepared with these compounds and exhibited elevated bubble stability and thickness uniformity. These films were also evaluated for mechanical properties and the transverse direction mechanical properties were much closer to those along the machine direction and hence much greater than the values for the base polypropylene film. In particular, the strain to failure in the transverse direction was significantly greater than for the base polypropylene film.

A linear viscoelastic model proposed by Sarvestani was applied to the dynamic shear rheology of PP nanocomposites prepared with non-silylated and silylated organoclays. The model described the dynamics of free chains and particle-attached chains that formed two different types of entanglements to account for the effects of attractive polymer-particle interactions on chain relaxation. The volume fraction of attached chains in different compounds was estimated from the dynamic shear moduli, along with the effect of particle attachment on slowing of the chain relaxation. The parameters revealed that silylation reduced the volume fraction of polymer chains attached to nanolayers, which was responsible for the lower dynamic storage modulus of nanocomposite with silylated I.44P compared to that with non-silyated I.44P.

DEDICATED
TO
MY PARENTS

ACKNOWLEDGEMENTS

Along the journey of my graduate studies at Michigan State University, I have been encouraged, supported and inspired by many people. First and foremost, I would like to express my sincere gratitude to my academic advisor, Dr. K. Jayaraman, for his valuable guidance and consistent encouragement during the past five years. His deep insights helped me establish the overall direction of the research and move forward with investigation in depth. I consider it as a great fortune to do my doctoral program under his guidance and to learn from his research expertise. Thank you, Dr. Jay, for all your help and support. I would also like to thank my committee members, Dr. R. Narayan, Dr. A. Lee and Dr. T. Pence for their devoted suggestions and comments during the course of my research.

My thanks also go out to the support I received from my fellow colleagues, Rahul, for his help in getting me started with my research during the early stages of my graduate studies, and Xinting and Christopher, for their scholarly interactions and suggestions at various points of my research program. I would like to thank Mike Rich, Brain Rook and Per Askeland at CMSC for generously offering their time in training me on various instruments. I am also very grateful to all those at the CHEMS office, who were always so helpful and provided me with their assistance throughout my graduate studies. I would also like to thank my friends, especially my roommate Hao, for their support and all the fun we have at MSU.

A special thanks to my family. Words cannot express the feelings I have for my Mom, Dad and brother for their constant unconditional love. I would like to acknowledge the tremendous sacrifices that my parents made to ensure that I had an excellent education. For this and much more, I am forever in their debt. It is to them that I dedicate this dissertation. This last

word of acknowledgment I have saved for my dear fiancée, Ran Qi, for her understanding and love during the past few years. She has been my best friend and great companion, encouraged, and helped me get through my Ph.D. studies in the most positive way.

TABLE OF CONTENTS

LIST OF TABLES

LIST OF FIGURES

CHAPTER 1

INTRODUCTION

1.1 Research Background and Motivation

Over the past decade, polymers have replaced many conventional materials (metals, ceramics, paper) due to their functionality, lightweight, ease of processing, and low cost. Among the various applications, extruded plastic film is one of the most significant polymeric products and comprise around 25 percent of all plastic used worldwide.

Two major industrial methods have been used to convert resin into an extruded film: cast film extrusion and blown film extrusion. In the cast film extrusion process, the molten polymer travels through a flat die system to adopt its final flat film shape. Immediately after exiting the die, the molten curtain enters the cooling unit where its temperature is lowered with a water cooled chill roll to "freeze" the film. The film is then passed downstream where surface treatment is applied and the film is wound into rolls. Between the die and the quench roll, thick edges called edge beads form due to surface tension, die swell, and an edge stress effect, which have to be trimmed from the film, and are often scrapped. As many cast film line dies are fixed slot width, the amount of edge trim that must be taken could be a large percentage of the overall film.

Blown film extrusion, as schematically shown in Figure 1.1, involves extrusion of a plastic through a circular die, followed by a "bubble-like" expansion process. Plastic melt is first extruded through an annular slit die, usually vertically, to form a thin walled tube. Air is introduced via a hole in the center of the die to blow up the tube like a balloon. The tube of film is then continuously stretched upwards under air cooling, until it passes through nip rolls where

the tube is flattened to create what is known as a “lay-flat” tube of film. Regulation of film width and thickness is by control of the volume of air in the bubble, the output of the extruder and the speed of the haul-off. Compared to the cast film process, the principal advantages of manufacturing film by film blowing process include the ability to eliminate end effects such as edge bead trim and produce films with more balanced physical properties along machine direction and transition as a result of biaxial orientation. Also, depending on processing conditions, the blown film bubble has a shape freedom that allows almost any number of profiles within a designed range of diameter and thickness. This high level of flexibility in the process leads to less scrap material and higher productivity.

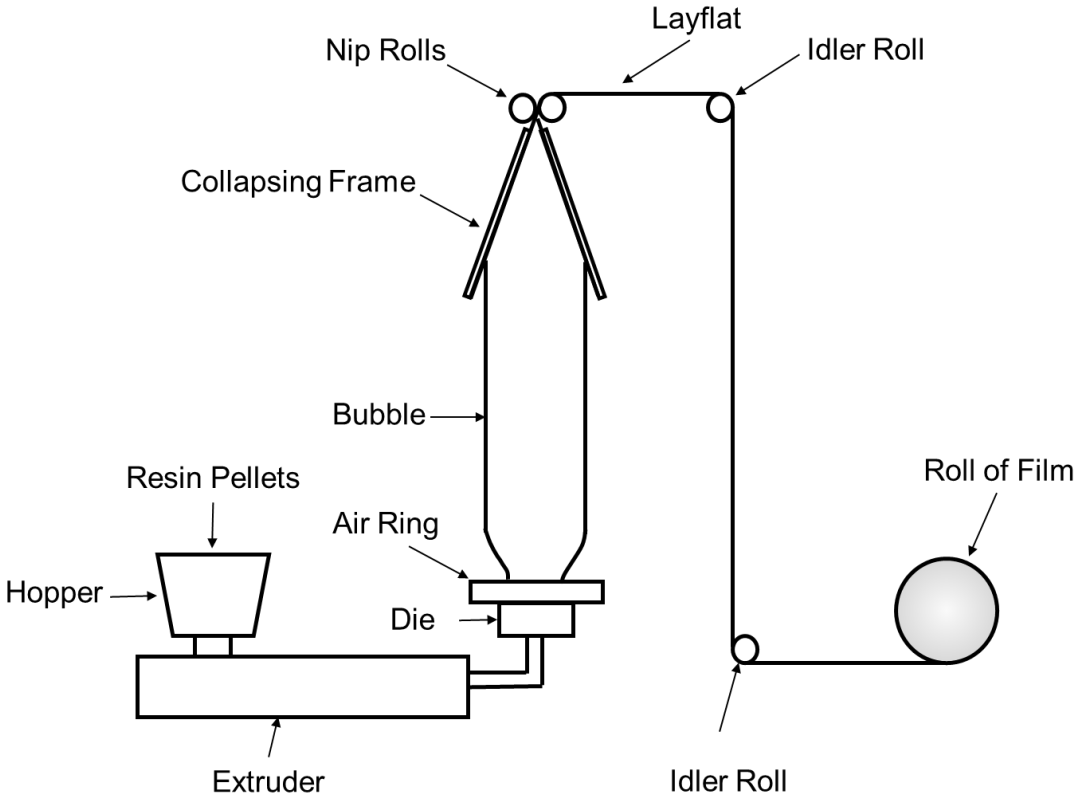

Figure 1.1 Schematic view of blown film extrusion process.

There are numerous applications for blown films such as grocery sacks, garbage bags, and flexible packaging and so on[1]. Many types of polymers, including polyethylene (PE)[2-5], polypropylene (PP)[6-11], polyamide (PA)[12, 13], ethylene-vinyl acetate (EVA)[14, 15], ethylene vinyl alcohol (EVOH)[16-18], polyethylene terephthalate (PET)[19], polylactic acid (PLA)[20-22], high impact polystyrene (HIPS)[23], etc., have been extruded into blown films. Among all blown film products, various grades of polyethylene comprise the vast majority of the market. It is lightweight, water-resistant and has a good balance of strength and flexibility. More importantly, as a polymer that has been development for over 50 years and very well understood scientifically, it allows for the design and control of molecular structure to yield specific property values over a very wide range.

Polypropylene has excellent chemical resistance, moisture barrier, clarity, dimensional stability and other benefits. Compared to polyethylene, it has a higher melting point and is generally stiffer, which allows it to be used in applications requiring a higher usage temperature and more strength. However, polypropylene for films is today almost exclusively used for cast films but not blown films. This is because the selection of polymeric materials for blow film application depends on not only their physical properties, but also processing properties. However, linear polypropylene homopolymer has been proved to be difficult to process on blown film extrusion equipment[24]. Various types of bubble instability as shown in Figure 1.2, which include (1) a periodic oscillation of the bubble diameter, (2) variations in the vertical position of the frost line height, and (3) a helicoidal motion of bubble around its axial direction, are the major issues in blown film process of polypropylene[24, 25]. Consequently, the range of processing conditions is quite narrow and difficult to control. This drawback makes it difficult to

downgauge polypropylene blown films, which is one of the important trends identified for flexible packaging in order to reduce costs and minimize waste after use.

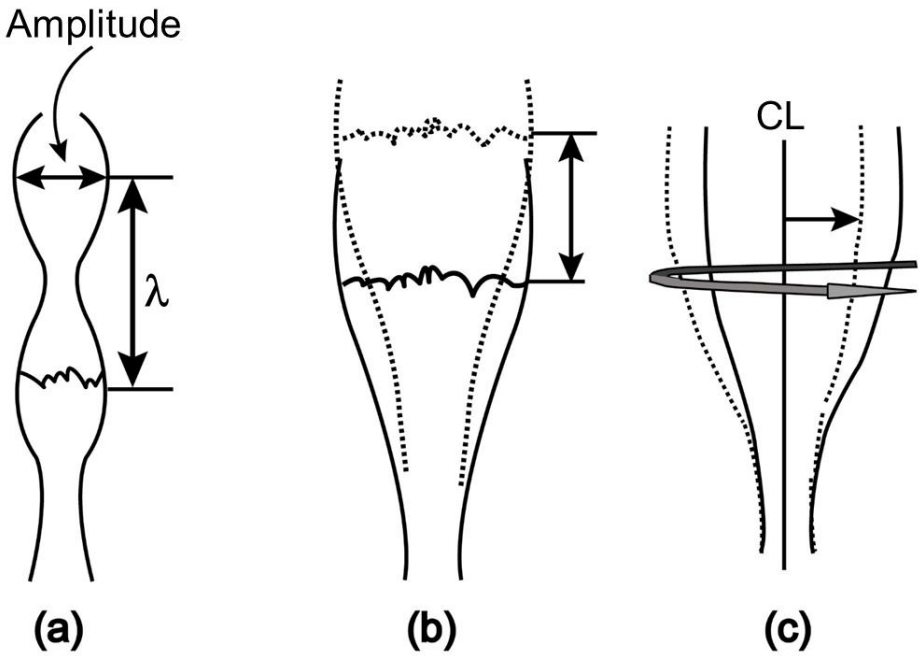

Figure 1.2 Schematic views of typical bubble instabilities: (a) draw resonance, (b) FLH instability and (c) helicoidal instability.

The bubble instability of polypropylene is attributed to its inherent low melt strength as a result of its highly linear chains and relatively narrower molecular weight distribution. Rheological modification is necessary to impart strain hardening property for producing superior quality film[26-30]. Strain hardening, which is defined as the transient viscosity rise above the linear viscoelastic curve at a constant strain rate under extensional flow, is critical for establishing the high melt strength required during film blowing process. One common approach that produces melt strain hardening for linear polypropylene is to introduce tree type branching network. It is well established that branched polypropylene exhibits strong strain hardening

behavior[31, 32]. Therefore, blow films from blends of linear PP and branched PP have been reported to show improved bubble stability, thickness uniformity and maximum solid output. Others have reported the addition of an ethylene copolymer, such as an ethylene/propylene copolymer to control the film bubble, since ethylene homopolymers and copolymers process well for blown films[33].

However, both the addition of branched PP and ethylene copolymer could alter mechanical properties of the blown films negatively. Branched polymers generally have fewer entanglements than linear polymers for a given molecular weight, resulting in low tensile strength and elongation to break of the blown films[24]. On the other hand, addition of an ethylene copolymer lowers the stiffness of polypropylene films. This drives the need for higher performing polypropylene blown films that can provide both processing stabilities as well as fitness for use in the final product. Therefore, this research primarily focuses on the development of polypropylene based nanocomposites that are suitable for blown film application by the use of organically modified montmorillonite nanoclays as additives, long chain polymeric compatibilizers and reactive silane coupling agents.

1.2 Structure Development of Blown Films

The morphology of semicrystalline polymers such as polyethylene (PE) and polypropylene (PP) has been described as mixtures of crystalline and amorphous region. In the crystalline phase, the polymer chains folded back and forth regularly and form ordered region called lamellae with crystal axes labeled as *a* (*a** for polypropylene), *b*, and *c*. The lamellae are connected by a highly disordered amorphous domain containing entangled network of tie chains. Polymers can crystallize upon cooling from the melt. Under a quiescent or low stresses state, spherulite, which is a spheriform aggregate of chain-folded lamellar primary crystallites, is

formed, leading to an isotropic configuration. On the other hand, in the film blowing process, polymer melts are simultaneously stretched along both machine direction (MD) and transverse direction (TD). The stresses applied during bubble growth can organize polymer chains within both crystalline and amorphous phases and lead to the formation of stacked lamellar structure with various degrees of polymer chain orientation, as shown in Figure 1.3. While films with uniaxial orientation consisted a stacked lamellae structure with the lamellar normal parallel to the MD, the morphology of biaxially orientated films appeared to contain lamellar stacks in all directions within the film plane. Different techniques, such as microscopy, X-ray pole figure, birefringence and Fourier transform infrared spectroscopy have been used to determine the crystalline orientation in blown films[34-36]. Since the physical properties of semicrystalline blown film products, such as tensile strength, impact toughness, and clarity, vary significantly depending on the molecular orientation and crystalline structure, one needs to develop understanding to control the film morphology towards the establishment of process/structure/property relationships.

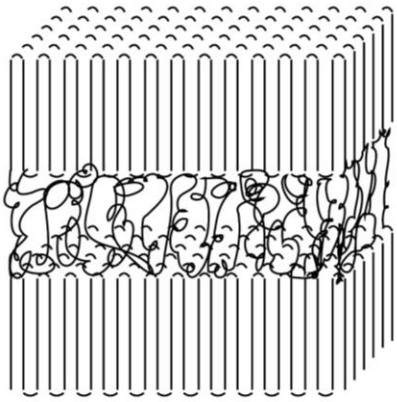

Figure 1.3 Schematic view of stacked lamellar structure.

In developing the stack lamellar structure during the film blowing process, polymer chains first orient along the machine direction as a result of drawing stress. The extended chains then act as nuclei that initialize the growth of lamellar stacks via chain folding perpendicular to the drawing direction[37]. On one hand, depending on the molecular structure, polymers with sufficiently long relaxation time, which allows crystallization to happen before the nuclei relax, are necessary for the formation of lamellar stacks with MD chain orientation[38]. Several studies have reported that blown film from branched polymer (PE and PP) show a row-nucleated, uniaxial lamellae stacking morphology while a spherulite-like superstructure is observed for films from linear polymer, which is attributed to their differences in polymer relaxation time[8, 37, 38]. The presence of a high molecular weight component, even a small amount, can also enhance the formation of the row-nucleated structure due to the preservation of the nucleating sites. Somani et al.[39] studied the flow-induced orientation of isotactic polypropylene (iPP) with same number average molecular weight but different molecular weight distribution. The results showed that iPP containing long chain species exhibited shorter evolution time of nuclei site, which was responsible for a higher degree of crystal orientation of the sample. Drongelen et al.[40] in the study of structural development of low-density polyethylene blown films reported that combining PE of a moderate Mw with a relatively low content of ultra-high molecular weight PE led to highest overall orientation level in blown film. On the other hand, since stacked lamellar structure primarily develops during the crystallization process that occurs between the relaxation of initial chain orientation and the consolidation of blown films, it can also be facilitated by a fast polymer crystallization rate. A real-time study of nonisothermal crystallization kinetics during film blowing of PE and PP has revealed that the crystalline orientation along MD increased with decreasing crystallization halftime[41]. Overall, it is

expected that blown films of certain molecular orientations and crystalline structures can be achieved by modifying polymer compositions in terms of the relaxation time and crystallization rate.

In addition to the properties of the resin, changes in blown film process parameters – die gap, nip speed, internal bubble air volume, frost line height, etc., as shown in Figure 1.4 – can also influence bubble geometry and as a result, structure of the films[42-44]. It is known that during film blowing process, polymers exited the dies are subjected to biaxial stretching: The film is stretched or pulled in the cross direction to reach the ultimate diameter of the bubble. At the same time, it is being pulled in the machine direction by the movement of the downstream equipment. As a result, the polymer chains become oriented along machine and/or transverse directions depending on the applied stresses level at freeze line. The amount of polymer stretching along the TD is indicated by a quantity called blow-up ratio (BUR),

$$BUR = \frac{D_b}{D_{die}} \tag{1.1}$$

where D_b and D_{die} are diameters of the bubble and the die, respectively. A blow-up ratio greater than 1 indicates the bubble has been blown to a diameter greater than that of the die orifice. The amount stretching along MD is characterized by a quantity called take-up ratio (TUR), which is the ratio of film velocity above the frost line (v_f) to linear average velocity of the melt at the die exit (v),

$$TUR = \frac{v_f}{v} \tag{1.2}$$

The film velocity is equivalent to the nip speed and is established by the control system. Experimentally, it can be determined by marking the film and tracking the mark. By varying processing conditions such as the film line speed, output rate, air pressure and frost line height,

the BUR and TUR may be adjusted to obtain blow films with various polymer chain orientation and crystalline structure[45]. Work done by Choi et al.[46] and Shimomura et al.[47] presented a series of high density polyethylene and polypropylene blown films, which ranged from uniaxial to equal biaxial orientation. The results showed that increasing BUR tended to produce a shift of chain alignment toward the transverse direction of the film. This was attributed to the increased stress levels exerted on polymer chains along the transverse direction for larger BUR values. Kwack and Han[48] in the study of crystalline structure development of PE blown film expressed the stresses at freeze line along machine and transverse directions (S_{11F} and S_{33F}) in terms of the tension at the take-up device, take-up ratio, blow-up ratio, and the pressure difference. They concluded that the biaxial stress ratio, S_{11F}/S_{33F} provided an indication of the balance of stretching, and so orientation, between machine and traverse directions. When the stress ratio was greater than unity, S_{11F} was found to play a dominant role in influencing the crystalline axes' orientation.

The importance of process parameters may also be reflected indirectly from their effects on modifying the chain relaxation and crystallization behaviors. Since the relaxation time and rate of crystallization increase with decreasing melt temperature, it is certainly expected that how much orientation can be maintained is strongly dependent on how fast and how early the oriented melt is quenched. For example, a lower quench height, which can be achieved by a higher air flow rate or a faster line speed, allows the oriented polymer melt to relax slower and crystallize faster, and results in blown films with stronger crystalline orientation. This dependence of chain relaxation and crystallization behaviors on process conditions have been reported to be more sensitive for polymers with narrow molecular weight distribution[42].

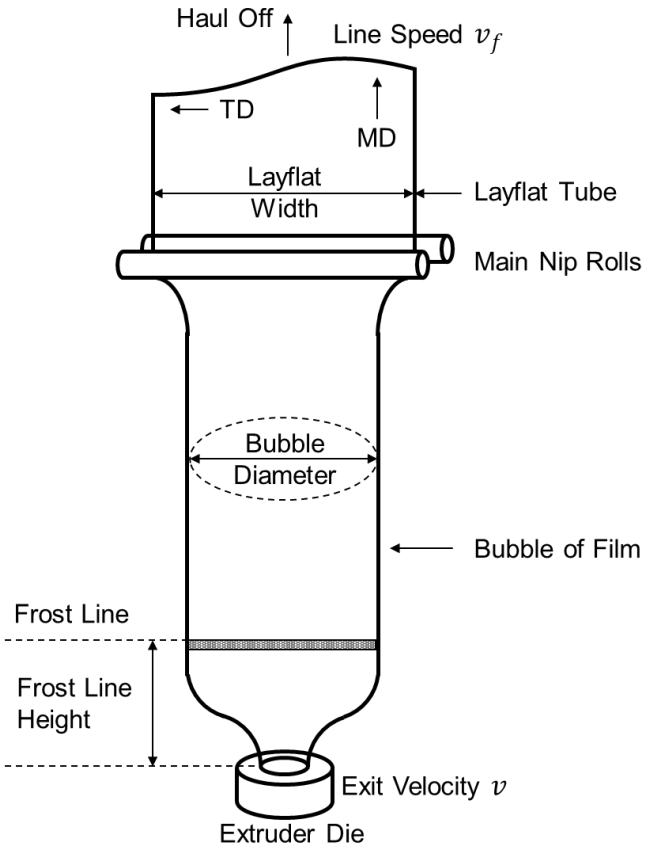

Figure 1.4 Processing parameters of blown film extrusion.

Post-processing by annealing can also modify the morphology of blown films, particularly the crystalline structure[49, 50]. As annealing allows polymer chains to rearrange locally, it can remove some structural defects of the film, and create secondary lamellae aligned in the direction of applied tensions. Accordingly, both the crystallinity and the crystalline orientation increase as a result of annealing, depending on the annealing temperature and time.

1.3 Structure-Property Relationships of Blown Films

A number of studies have been reported in recent years concerning the interrelations between structure and property of blown films that are helpful for blown-film manufacturers.

That is, we can describe and predict the physical properties of the films that will result when a certain structure is imparted by controlling polymer composition and process condition.

It is well established that the mechanical response of oriented blown films is anisotropic along machine and transverse directions. Zhang et al.[37] studied the microstructure of various polyethylene blown films and showed that differences in tensile and tear strengths between MD and TD could be associated with the crystalline lamellar structure formed in the film process: A higher crystalline orientation led to larger anisotropy as evaluated by the ratio of MD to TD properties. Similar results have been reported in polypropylene blown films where in-plane anisotropy of tensile modulus and tear resistance were evaluated as a function of crystalline orientation[11].

Compared to films with spherulitic structure, oriented blown films display significantly enhanced tensile modulus, yield stress and tensile strength, which is attributed to the alignment of crystalline lamellae and polymer chains in the amorphous phase. The tensile deformation of films with lamellar stacks oriented perpendicular to MD has been considered based on a "laminated composite" model, where the film is viewed as a composite with a hard crystalline phase and a soft amorphous phase stacked along the MD[4, 51-53]. For deformations along the MD, both phases are stretched in an iso-stress pattern. Therefore, the modulus is dominated by that of the weak component, or the amorphous phase, which is further affected by the extent of chain orientation and the amount of tie chains. Beyond the stretching limit of tie chains, the film yields as a result of non-recoverable plastic deformation of the crystalline phase possibly via crystallographic slip. Upon further stretching, strain hardening occurs due to uniaxially oriented fiber network structure of the crystals. On the other hand, the deformation along TD is considered as in an iso-strain pattern, where the stresses are distributed primarily among the rigid

lamellae. Therefore, the modulus, which is dominated by that of the crystalline phase, is higher than films with spherulitic structure. Meanwhile, due to the low deformability of crystalline lamellae, oriented films yield at a very small strain along TD. While PE films can be stretched further to a large strain by the pull-out of chains from lamellae perpendicular to the lamellar normal, oriented PP films in general break quickly after the yield point.

Tear resistance, as another important property for the blown films, has been investigated for various materials. For high density polyethylene (HDPE), linear low density polyethylene (LLDPE) and polypropylene (PP), machine direction oriented blown films exhibit a higher tear resistance value along TD than that along MD, while the opposite is true for low density polyethylene (LDPE)[37]. This is because in the former case the stacked lamellar structure makes it easy for the tear to propagate along the interlamellar region in the machine direction while the chain alignment, on the other hand, creates strong resistance for the film to be torn along TD[54]. This anisotropy in tear strength disappears when lamellae become randomly aligned in the plane of films, while an enhancement of orientation in crystalline and amorphous phases leads to a lower the tear resistance along MD and a higher tear resistance along TD. Good correlations have been reported between tear strength and in-plane anisotropy of *a* axis of LLDPE films[55]. The MD tear strength decreases, while TD tear strength increases, when *a* axis is more aligned in the MD. Krishnaswamy and Sukhadia[56] in the study of LLDPE blown films reported that MD and TD tear resistances depended on deformations in the interlamellar region and the stresses borne along the lamellar long axes, respectively. They found that MD tear resistance of the film was higher when the non-crystalline chains were closer to equi-biaxial in the plane of the film. The TD tear resistance was observed to be high when the crystalline lamellae were minimally curved and oriented closer to the film TD. In LDPE films, the adjacent

lamellae are interlocked along the transverse direction as a result of the twisted growth, which leads to higher tear strength in MD compared to that in TD.

The crystalline phase orientation has been reported to also enhance impact, barrier, and optical properties of blown films. From the viewpoint of the control of higher-order structure formation in film processing, the most important factors are considered to be the improvement of physical properties while maintaining a balance between the machine and transverse directions.

1.4 Polymer Nanocomposites

Polymer nanocomposite is commonly defined as a combination of a polymer matrix and additives with at least one of the dimensions in the nanometer range. Over the past three decades, there has been a strong interest in the development of polymer nanocomposites in automotive, packaging, and electronic applications, owing to the capability of nanoparticles in significantly enhancing physical properties of polymeric materials, such as barrier resistance, flame retardancy, wear resistance, as well as mechanical, thermal, electrical and magnetic properties. The leading nanofillers in research and commercial programs include layered silicate nanoclays, nanosilicas, polyhedral oligomeric silsesquioxanes, carbon nanotubes, and graphite platelets. Compared to traditional micro-sized particles, nanoparticles possess larger surface area to volume ratios, which allow for the property reinforcement to be achieved at very low filler concentrations without a significant increasing of material density and opacity.

The area of polymer nanocomposites emerged with the recognition that exfoliated clays could yield significant mechanical property advantages as a modification of nylon 6 by Toyota Motor Co. in the late 1980s[57-60]. Since then, various studies and analyses have been reported on polymer-layered silicate nanocomposites. One of the most common layered silicates used in

polymer nanocomposites belongs to the structural family called 2:1 phyllosilicates, such as montmorillonite. It consists of two-dimensional layers made up of two tetrahedrally coordinated silicon atoms fused to an edge-shared octahedral sheet of either aluminum or magnesium hydroxide. The thickness of one layer is around 1 nm and its lateral dimensions may vary from 30 nm to several microns, which result in a particularly high aspect ratio. These silicate layers have the tendency to stack together as tactoid via Van der Waals forces. Also, the interlayer spacing is filled with alkali and alkaline earth cations, which counterbalance negative charges within the layers generated by isomorphic substitution. A typical interlayer dimension is approximately 1 nm for dehydrated Na^+ montmorillonite.

The properties of polymer-clay nanocomposites depend strongly on the state of nanoclay dispersion in the polymer matrix, which has been characterized by various techniques, such as X-ray diffraction (XRD), Transmission Electron Microscopy (TEM) and so on[61]. Generally, three main morphologies of polymer-layered silicate nanocomposites can be obtained, which are aggregation, intercalation and exfoliation: Nanocomposite with clay aggregation is predominant with micro-tactoid structure; Clay intercalation is a well-ordered multilayer structure with polymer chains inserting between the galleries, leading to expansion of inter-platelet spacing. For exfoliated structure, adjacent nanolayers completely separate from each other and form a disordered morphology in the polymer matrix. Exfoliation of nanoclay results in an enormous increase of interfacial areas between the polymer matrix and dispersed silicate layers, which is desired to achieve strong reinforcement of properties.

The process of nanoclay exfoliation in polymer matrix during melt compounding has been discussed by a “peeling off” mechanism[62, 63]. Initially, clay nanolayers are broken apart from each other by shear stress and become smaller stacks of tactiods. The second step of

nanoclay exfoliation involves diffusion of polymer chains into galleries, thus creating a peeling angle that benefits the transfer of shear stress. This is more likely to occur in the later stage rather than at the beginning of delamination because fewer clay nanolayers are more flexible and more easily to bend than stacks of tactoids, which reduces the resistance to intercalation. Since polymer chains inside clay galleries suffer deformation from its coil state, the segments tend to relax and gain entropy by pushing out adjacent clay layers, which also assists the delamination process. The final separation of individual layered silicates from tactoids occurs when attractive force between adjacent nanoclays can be overcome during exfoliation. According to this mechanism, a greater degree of exfoliation is expected in a highly viscous flow. Fornes et al.[63] in the study of nanoclay dispersion in nylon 6 of three different molecular weight reported that nanocomposites based on the higher molecular weight polyamides yielded a higher degree of clay exfoliation, which was attributed to the high shear stress generated during processing. Meanwhile, in order for the applied shear stress to be effectively transferred to clay nanolayers, strong polymer-clay affinity is required. This is because, in the absence of attractive interaction, polymer chains tend to slip over surfaces of silicate layers without applying shear forces.

In order to achieve better delamination of clay nanolayers, it is well established that the galleries of clay tactoids have to be intercalated with cationic surfactants including primary, secondary, tertiary, and quaternary alkylammonium or alkylphosphonium cations through ion exchange reaction[64]. Depending on the cation-exchange capacity, the surfactant content usually varies from 35% to 45%. The long organic chains of such surfactants, with positively charged ends, are tethered to the surface of the negatively charged silicate layers, which enlarges the interlayer spacing by 1-2 nm. The gallery expansion of nanoclays weakens the attractive interactions, mainly van der Waals forces, between two adjacent nanoplatelets[65]. It also makes

it easier for polymer chains to diffuse between the layers and eventually separate them. On the other hand, the present of surfactants lower the surface energy of the silicate surface and enhances its miscibility with hydrophobic polymers.

The effectiveness of surfactants in improving state of nanoclay dispersion as well as physical properties of nanocomposites depends strongly on the functionality, packing density, and length of the organic modifiers. It has been reported that alky tails with more than 10 carbons are necessary to promote exfoliation of nanoclay[66, 67]. Fornes et al.[68, 69] in the study of nylon 6-organoclay nanocomposites compared the role of the number alkyl groups attached to the nitrogen of the surfactant on the organoclay. Well-exfoliated morphology was obtained for the nanocomposite prepared with one alky tail quaternary cation modified organoclay. This was attributed to a balance between increased gallery spacing and favorable interactions between the nylon and the clay surface since polymer intercalation was difficult without alkyl group on the surfactant and two alkyl groups on the quaternary cation strongly reduced polymer-clay affinity. This is opposite to the case of polyolefin nanocomposites, where alkylammonium cations with more alkyl tails have been reported to result in higher extent of clay exfoliation due to the improved miscibility between aliphatic modifier and hydrophobic polyolefins.

Besides surfactant modification of nanoclays, polymeric compatibilizer is also necessary for the preparation of nanocomposites when polyolefins are the matrix[70]. One of the most commonly used compatibilizers is maleic anhydride grafted polyethylene or polypropylene. The maleic anhydride groups and carboxylic acid groups after hydrolysis can form hydrogen bonds with faces and edges of nanoclay, and therefore reduce the interfacial tension between nanoclay and polymer matrix, which in this case is a blend of neat polyolefin and the compatibilizer. Main

factors that determine the effects of compatibilizer on morphology and properties of nanocomposites include maleic anhydride content, compatibilizer to clay ratio, and molecular weight of compatibilizers[71-74].

1.5 Polymer Nanocomposites Blown Films

Blown films based on polyolefins have been commercially available for several years. However, the inherent limits of physical properties due to the organic hydrocarbon nature of polymeric materials have put bounds to the areas of applications. For example, polyethylene films have poor gas barrier properties such as oxygen and carbon dioxide with relatively low stiffness and tensile strength. These drawbacks can be overcome by the development of nanocomposites. Incorporation of a small quantity of organoclay enables simultaneous enhancements of the mechanical properties and barrier, as well as the thermal resistance of plastic films.

Because of the rigidity of nanoclay, nanocomposite films displays higher tensile modulus along machine and transverse directions compared to blown films prepared with polymeric materials only[75-78]. On the other hand, either improvement or deterioration of tensile strength has been reported in the literature depending on the nanoclay dispersion and its interaction strength with the polymer matrix. Without the use of compatibilizer, Kashyap and Ghosh[79] reported a decrease in the tensile strengths of polypropylene-clay nanocomposite blown films. The opposite effect has been reported by others in some compatibilized polyolefin nanocomposite systems[80, 81]. But the enhancement of strength generally correlates with a drastic sacrifice of elongation to break value of the film, especially along the transverse direction. The large surface area and impermeability to gas of nanoclays can also improve barrier properties of blown films, as the dispersed silicate layers in polymer matrix create tortuous path

for gas to pass through[82-84]. Though many studies have reported on various properties of nanocomposite blown films, few have been conducted to investigate the effect of nanoclay addition on the process/structure/properties relationships.

As mentioned earlier, melt strain hardening is an important parameter that controls processability of polymer melts during blown film process. The benefit of adding nanoclay in blown film application is also attributed to its capability of imparting strain hardening behavior for various polymers[85-87]. Okamoto and coworkers[88] dispersed stearylammonium ion modified montmorillonite into maleic anhydride grafted polypropylene and observed a strong tendency of strain induced hardening under uniaxial extensional test while the matrix polymer did not exhibit this property. This feature has been applied in foaming of polypropylene, which, similar to film blowing, is also governed by extensional flow[89, 90]. There have also been several attempts in the literature to explain the possible causes of strain hardening behavior in different systems[91, 92].

1.6 Research Objectives

This research is motivated by the needs to develop high performing polypropylene blown films that can provide both processing stabilities as well as end-use properties by the development of organoclay nanocomposites. Although several studies have demonstrated the build-up of strain hardening behavior for linear PP with the incorporation of organoclay and a polymeric compatibilizer, due to insufficient polymer-clay interactions, mainly hydrogen bonding, a high concentration of compatibilizer is required to obtain acceptable strain hardening level as well as nanoparticle dispersion. This will bring down some essential properties of the final products when compared to the bulk polymer that is of high molecular weight. In the present work, a reactive silane coupling agent, aminoalkyldimethoxysilane, was introduced to

treat the organoclay so that the weaker force of polymer-particle attraction was replaced with stronger chemical bonds. The objectives of this research were:

(1) To study the morphology and rheology in dynamic shear and uniaxial extensional flow of the melt-compounded state of polypropylene-layered silicate nanocomposites with different modes of polymer-particle interactions at different interactive sites.

(2) To further evaluate the applicability of polypropylene-clay nanocomposites in blown film process by investigating the stability of microstructure and rheology in dynamic shear and uniaxial extensional flow upon reprocessing. A masterbatch additive was also developed for restoring the rheological properties of reprocessed nanocomposites.

(3) To prepare blown films from polypropylene-clay nanocomposites with low compatibilizer to clay ratio that exhibited improved processability and mechanical properties compared to films from neat polypropylene.

(4) To develop a viscoelastic model based on nanocomposite systems with different modes of polymer-particle coupling and investigate the underlying mechanism of enhanced frequency-dependent dynamic moduli at low frequency regimes as well as strain hardening behavior of nanofilled entangled polymer melts.

CHAPTER 2

POLYPROPYLENE/CLAY NANOCOMPOSITES PREPARATION AND CHARACTERIZATION

2.1 Material

Two different polypropylene were used as matrix of nanocomposites: Profax 6523 from Basell, was a homopolymer with melt flow index of 4 g/10 min (230°C/2.16kg); The film grade polymer PPC300.4 from Spartan Polymers Inc, was a propylene-ethylene block copolymer with 12 to 15 wt% ethylene and had a melt flow index of 0.45 g/10 min (230°C/2.16kg). The latter, due to its high melt viscosity, was used for the preparation of polypropylene based blown films. Maleic anhydride grafted PP (PP-g-MA) was used as compatibilizer: Exxelor 1015 (Mw = 122,000, MA content = 0.42%) from ExxonMobil was a copolymer with a melting temperature of 145°C.

The nanoclays used in this study were organically modified montmorillonite clay from Nanocor. Two different organoclays were used for preparing PP/clay nanocomposites -- I.44P which has a quaternary onium ion surfactant with two C-18 tails and I.30P which has a primary onium ion surfactant with a single C-18 tail.

Silane coupling agents were used in this study that allows the modification of polymer-particle interactions in the nanocomposites. Two different silanes used for this study were:

(1) N-(2-aminoethyl)-3-aminopropylmethyldimethoxysilane (aminoalkyldimethoxy silane)

(2) Octyltrimethoxy silane

The chemical structures of the two silanes have been presented in Figure 2.1.

(a)

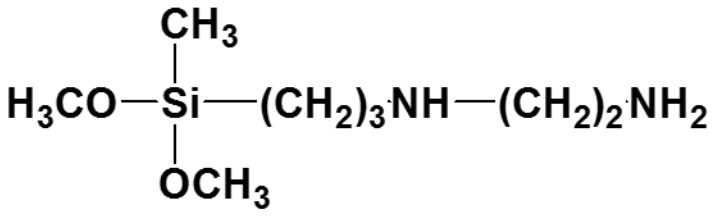

(b)

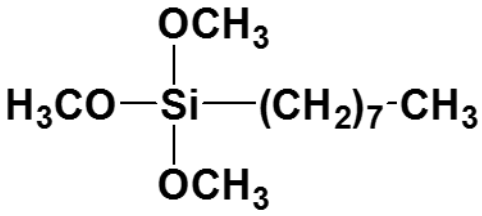

Figure 2.1 Chemical structure of silane coupling agents (a) aminoalkyldimethoxy silane and (b) phenyltrimethoxy silane.

2.2 Nanocomposites Preparation

Several methods of nanocomposite preparation have been utilized resulting in both intercalated and exfoliated nanostructure: *In situ* polymerization method where the layered silicate is swollen within the liquid monomer or a monomer solution allows the formation of polymer between galleries of clay particles and has produced intercalated polystyrene, nylon-6 nanocomposites etc.[93-97]; Intercalated of polymer from solution involves mixing polymer and organoclay in a solvent system where the polymer is soluble and the layered silicate is swellable[98-100]. The polymer intercalates and displaces the solvent between the clay layers and results in intercalated structure; Melt method compounds polymer and organoclay under

strong shear above the melting point of the polymer[62, 63, 101, 102]. This method has great advantages because of the absence of solvent and its compatibility with current industrial processes, such as extrusion and injection molding.

The nanocomposites for the scope of this research were prepared by melt mixing technique. Both batch and continuous mixing process have been used. Before compounding, the PP-g-MA and organoclays were dried overnight in a vacuum oven to minimize the possible moisture induced degradation during mixing. For batch process, a 75 cc volume Banbury batch mixer from C.W. Brabander Instuments, Inc with counter-rotating screws and pneumatic feed ram was used. Polypropylene, maleic anhydride grafted PP and clay were mixed for 10 minutes at 180°C with continuous nitrogen purge. For preparing two-component nanocomposites containing only PP-g-MA and organoclay, the temperature during compounding was maintained at 165°C, which was well above the melting point of the PP-g-MA (145°C) used in this study. To avoid starve mixing, materials with a total amount of 47 g were added, which generated high shear forces to maximize clay particle dispersion and exfoliation. The mixed materials were removed from the mixer chamber with a spatula. The collected compounds were compression molded by a hydraulic press and were used for various characterizations.

For continuous process, nanocomposites were prepared in a Leistritz, co-rotating twin-screw extruder (diameter = 27 mm, L/D = 48) with a screw speed of 250 rpm and barrel temperature of 190°C. A two-step process involving adding masterbatches to bulk polymer in a "let-down" operation was used. This processing protocol has been reported to result in nanocomposites with better clay dispersion, even for small values of compatibilizer to clay ratio[103-107]. The masterbatch has a large loading of the organoclay (20 to 30 wt%) combined with polymer compatibilizer that is of low molecular weight. In this research, 20 wt% of neat

PPC300 was also included for masterbatch preparation in order to build up high torque values for better mixing. The masterbatch was then let down with the use of bulk PP to nanocomposites with desirable clay content. The extruder output was held constant at 2.5 kg/h. Both PPC300 and nanocomposites were then blown into 1 mil thick films with a blow-up ratio (final tube diameter/die diameter) of 3.2 at a low frost line height.

2.3 Compression Molding

A Wabash hydraulic press was used to prepare samples for rheological studies and structural characterizations. The polymer pellets or chunks were placed in a 1.5 mm thick square mold. The mold filled with the material was covered on both sides with polyimide release films and this was then placed in between two thick steel plates. This mold assembly was placed in between the pre-heated plates of a compression molding machine at 200°C for 15 mins, which allowed the materials to melt completely. The melt was subjected to a pressure of 1 tons for 5 mins followed by 5 tons for 5 mins and then cooled down to room temperature with cooling water while maintaining the pressure of 5 tons. The samples were then carefully removed from the mold and examined for any defects (voids, cracks, merging boundaries and foreign particles). A lower temperature of 175°C was used for compression molding of PP-g-MA as well as the two-component nanocomposites.

2.4 Silane Treatment of Organoclays

Two different silane treatment processes were used for this research: a wet process and a dry process. The wet process for grafting reaction was carried out in a methanol/water mixture (80/20 by volume). 15 g of organoclay and 4.5 g of silane were added in a glass beaker with 700 ml of the solvent mixture. After 6 hours of stirring at room temperature, the clay suspension was

filtered and rinsed for 3 times using the same solvent to remove any unreacted silane. The resulting precipitate was left in an oven at 80°C with a vacuum of 500 mm Hg for 24 hours. The treated clay was then powdered in a mortar and pestle. The dry process was carried out by Malvern Minerals Co.: the organoclay was exposed to 1 wt% refluxed silane vapor. In both processes, the organoclay after silane treatment was sieved with a No. 200 sieve.

2.5 X-Ray Diffraction

X-ray powder diffraction (XRD) technique is primarily used for phase identification of a crystalline material. The interaction of incident rays with the sample produces a diffracted ray when conditions satisfy Bragg's Law of diffraction

$$n\lambda = 2dsin(\theta) \tag{2.1}$$

where d is the spacing between diffracting planes, θ is the incident angle, n is any integer, and λ is the wavelength of the beam. This law relates the wavelength of x-ray to the diffraction angle and the lattice spacing in a crystalline sample. By scanning the sample through a range of 2θ angles, the information on unit cell dimension of the powdered material is attained.

Due to its easiness and availability, XRD is most commonly used to probe the structure of clay particles. Montmorillonite clay has a layer-by-layer structure with its basal spacing of the (001) plane of about 0.96 nm[108]. The organic treatment by various alkyl ammonium surfactants as well as silane coupling agents can lead to intercalation of the organic molecules inside the clay galleries, resulting in an increase of d-spacing. This layer expansion results in the appearance of a new basal reflection at a lower 2θ value corresponding to the larger gallery height.

In this study, a Bruker Davinci diffractometer operating at 40 kV, 40 mA with Ni-filtered Cu Kα radiation source was used to characterize the interlayer distance between stacked clay platelets. A proper slit (1.2 mm) on mounted on the detector side was selected based on the resolution and intensity of the diffraction peak of interest. Note that variation in the width of the receiving slit generally affects the peak height and width as well as the ability to resolve peaks. To obtain XRD pattern of clay samples, the clay powder was compacted on a glass disc and tested over a 2θ range of 0.4-10° with equal increments of 0.02°. The *d*-spacing of organoclay was then calculated using Equation 2.1.

2.6 BET Surface Area Measurement

The BET theory, proposed by Brunauer, Emmett and Teller in 1938[109], explains the physical adsorption of gas molecules on a solid surface and can be further used as an important analysis technique for the measurement of the specific surface area of a material. This theory refers to multi-layer adsorption, and usually adopts non-corrosive gasses as adsorbates to determine the surface area data.

In this study, A Micrometrics (Gemini V) surface area and pore size analyzer was used to determine the specific surface area of various organoclays, using nitrogen as the adsorbent gas. Around 1.5 g of the clay sample was degassed at 120ºC with nitrogen as the purge gas for 24 hours before the test. The sample was then weighed accurately and subjected to the BET surface area analysis following the adsorption procedure. Helium gas was used to estimate the free volume in the sample tube followed by the adsorption of nitrogen gas, under liquid nitrogen temperature, to calculate the total volume. This information was then used to estimate the specific surface area of organoclays.

2.7 Thermogravimetric Analysis

The organic content and thermal stability of organoclay are usually studied by thermogravimetric analysis (TGA). The organoclay at high temperature undergoes weight loss due to the formation of volatile products after degradation of organic components. The weight loss is then monitored as a function of temperature under controlled atmosphere as an indication of its organic content and thermal stability.

A TA Instruments Q500 apparatus was used in this research to evaluate the weight loss of various organoclays with increasing temperature. The analysis was performed by heating about 10 mg of clay powder from room temperature to 800°C using a high resolution ramp under a nitrogen atmosphere. The high resolution ramp varies the heating/cooling rate of the furnace in response to changes in the rate of decomposition of the sample to improve weight change resolution.

2.8 Transmission Electron Microscopy

Transmission Electron Microscopy (TEM) is a microscopy technique that allows a beam of electrons to transmit through an ultra-thin specimen and interact with the specimen as it passes through it. The interaction of the electrons transmitted through the specimen produces images with resolution below 0.5 Ångströms. The contrast under the bright field imaging mode, which is most commonly used for TEM analysis, is formed directly by occlusion and absorption of electrons in the sample. Thicker regions of the sample or regions with a higher atomic number will appear dark, whilst regions with no sample in the beam path will appear bright. In the case of PP/clay nanocomposites, the dispersed silicate layers showed up as dark lines in bright PP matrix. This technique has been widely used to describe the state of dispersion and exfoliation of

clay particles in various matrix[61, 110]. The main limitation of TEM is that the volume probed is very small and may not be representative of the nanocomposite in its whole.

In order to prepare the specimen for TEM imaging, the ultra-microtoming technique was used for this study with a PTXL ultra-microtome (RMC, Boeckeler Instruments) connected to a CRX cryo unit. A small rectangular piece cut out of a compression molded disc was mounted on the ultra-microtome and maintained at -120°C with liquid nitrogen in order to provide enough rigidity for smooth sectioning so as to maintain structure of the sample, since the glass transition temperature of polypropylene is below 0°C. A section of 90 nm thick was prepared by ultra-microtoming and collected on a 200 mesh copper grid. TEM micrographs of various nanocomposites were obtained with a JEOL 100CX instrument at 200KeV acceleration voltage. A quantitative analysis of particle dispersions was also performed on TEM images taken at different magnifications. The curved length of silicate layers and their average thickness were measured manually with the use of ImageJ software. The number average thickness of all particles in each system was calculated.

TEM analysis was also applied to blown films of nanocomposites to characterize the clay particle orientation. The specimen was prepared by first immersing the thin film in an epoxy resin and ultra-microtomed along the TD-ND plane under cryo condition after the resin had solidified.

2.9 Rheology

Rheology is the science of how materials deform and flow under stress. It has been used as a semi-quantitative tool to investigate the structure-property relationship of polymer for many

years[111-114]. In the present research, the rheological properties of PP/clay nanocomposite melts of various compositions were studied under both shear and extensional flow.

2.9.1 Shear Rheology

The linear viscoelastic properties of PP and its nanocomposite was studied by oscillatory shear experiment. A parallel plate geometry was used, where one of the plates is stationary and the other one is mobile so that simple shear flow was applied to the test material in-between. In a controlled strain experiment, the sample was subjected to a homogeneous deformation at a sinusoidally varying shear strain (γ) represented as

$$\gamma(t) = \gamma_0 sin(\omega t) \tag{2.2}$$

The resulting stress is also sinusoidal and can be written in terms of the stress amplitude, τ_0, and the phase shift, δ, usually called the loss angle, as follows

$$\tau(t) = \tau_0 \sin(\omega t + \delta) \tag{2.3}$$

The dynamic test results are usually reported in terms of the storage and loss moduli *G'* and *G"* as functions of frequency

$$\tau(t) = \gamma_0[\mathrm{G}'(\omega)\sin(\omega t) + G"(\omega)cos(\omega t)] \tag{2.4}$$

where *G'* and *G"* are calculated from an amplitude ratio $G_d \equiv \tau_0/\gamma_0$ and δ as follows

$$G' = G_d \cos(\delta) \tag{2.5}$$

$$G" = G_d \sin(\delta) \tag{2.6}$$

Dynamic shear tests were carried out on a TA Instruments AR2000 Rheometer with parallel plates of diameter of 40mm. Compression molded disc was tested over a frequency range from 0.01 to 100 rad/s under a fixed strain of 1% in most cases. This was within the linear

viscoelastic regime of various PP and PP/clay nanocomposites as confirmed by oscillatory strain sweeps where the G' and η' were monitored as a function of strain at a fixed frequency. The strain at which the chosen viscoelastic property decreases indicates the onset of nonlinearity. An oscillatory time sweep was also carried out for 1 hour at a frequency of 1 rad/s and a strain of 1% to ensure good stability of each material. A constant value of storage modulus within 5% over time was considered as stable. The applied temperatures for shear test varied based on different polymer matrix and were specified in relevant chapters. To minimize thermal degradation, a continuous purge of nitrogen was maintained during all tests. The collected data were also checked to ensure that the corresponding torque values were above the acceptable lower torque-sensing limit of the transducer. For the oscillatory frequency sweep of PP-g-MA alone, a 5% strain, which was within the linear viscoelastic regime, was used so that the torque signal is enlarged to obtain more reliable results.

2.9.2 Extensional Rheology

Extensional rheology is of particular importance as it governs the flow behavior of polymers in many processing operations such as fiber spinning, film blowing, blow molding, thermoforming etc.. Because of the presence of shear stresses at stationary boundaries, homogeneous extensional flows are difficult to generate. In this work, polymer melts are subjected to uniaxial extensional flow to study its extensional rheological behavior.

The uniaxial extensional viscosity of PP and its nanocomposites was measured using an extensional viscosity fixture (EVF) on a TA-ARES instrument. Test specimens with dimensions of 18 mm x 10 mm x 0.75 mm were compression molded following the above mentioned procedure. A Sentmanat Extension Rheometer (SER-2) fixture was also used to perform uniaxial extensional stretching for PPC300 and its nanocomposites with the dimensions of specimens

being 24 mm x 10 mm x 0.75 mm. Both designs involve elongating the sample within a confined spacing with the use of rotating drums that wind up the sample, as shown in Figure 2.2(a). Under uniaxial extensional flow, material is stretched very rapidly along one direction while the free surfaces of the sample are under a uniform normal stress, usually one atmosphere of compression. Therefore, uniaxial extension leads to a reduction in both width and thickness of the specimen.

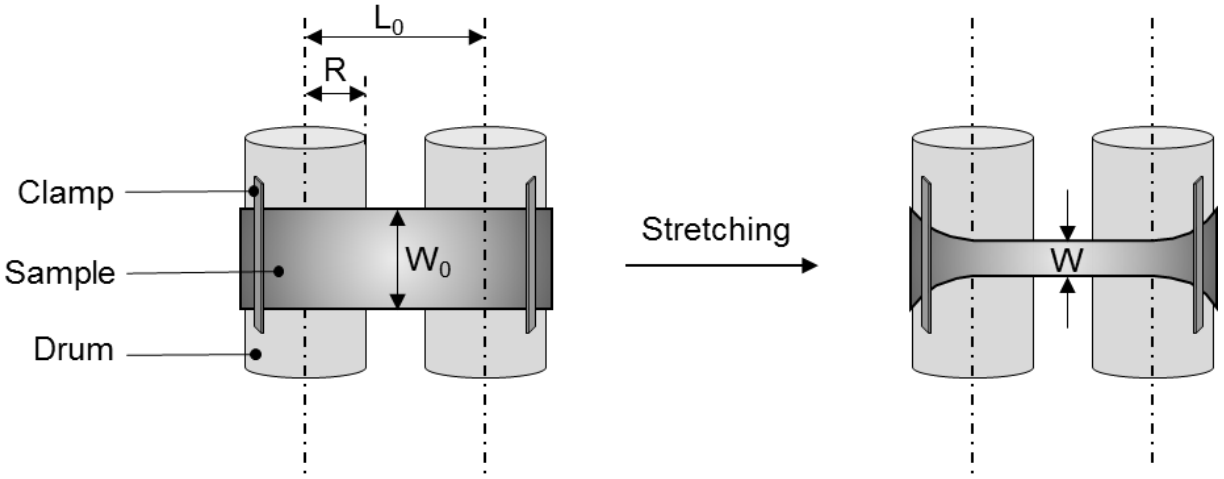

Figure 2.2 Schematic of the uniaxial extension with EVF/SER fixture.

Since the force measuring cylinder is fixed in space, it can be directly coupled to the torque transducer of the rheometer. The extensional force at the sample derived from the measured torque is used to calculate the extensional stress ($\sigma_E(t)$) as follows

$$\sigma_E(t) = \frac{F_S(t)}{A_S(t)} \tag{2.7}$$

where $F_s(t)$ is the extensional force and $A_s(t)$ is the sample area. The extensional strain rate is given based on the drum rotational rate as follows

$$\dot{\varepsilon} = \frac{2\Omega R}{L_0} \tag{2.8}$$

where Ω is the angular rotation speed of the motor, R is the radium of drum and L_0 is the stretch zone gap length. Based on the extensional stress and extensional strain rate, the uniaxial extensional viscosity is calculated as follows

$$\eta_E(t) = \frac{\sigma_E(t)}{\dot{\varepsilon}} \tag{2.9}$$

The extensional viscosity measurements were made for PP and its nanocomposites at four strain rates (0.1, 0.5, 1.0 and 2.0s^{-1}) over Hencky strains up to 3. Since these tests are very sensitive to the sample condition, care was taken so that the test specimens are free of any voids or inhomogeneities. In order to ensure that the specimen was uniformly stretched in the central portion during the test, the state of the stretched specimen was also inspected immediately after the test, so as to observe any sagging of the polymer melt due to gravity effect and any non-uniform stretching.

2.10 Characterization of Blown Films

2.10.1 Film Thickness Uniformity

Film thickness uniformity is an important concern for blown film manufacturers as a large thickness distribution causes several problems. For example, it is generally difficult to prepare thin film when the thickness distribution is large. It also results in great variation in the physical properties. The thickness of blown films in this study was recorded at different positions across the circumference of the film with a TMI digital micrometer. Eighteen positions were measured for each film at a distance of 1.5 cm and the standard deviation (SD) value was calculated for each material to evaluate the thickness uniformity.

2.10.2 Mechanical Properties

Tensile properties of the blown films at both machined direction (MD) and transverse direction (TD) were characterized with an Instron Universal Testing Machine model 5565, based on ASTM-882. The tensile characteristics were measured at 500 mm/min crosshead speed with initial gauge length of 50mm. For tensile modulus determination, a crosshead speed of 25 min/min and a specimen gage length of 250 mm were used. This length is conducted in order to minimize the effects of grip slippage on test results. 1% secant modulus was then evaluated by dividing the corresponding stress by the designated strain (1%).

The tear resistance of blown films along both MD and TD was tested based on ASTM D1922 with Elmendorf Tearing Tester equipped with a standard 1600-gf pendulum. This test method is proposed to determine the average force in gram to propagate tearing through a specified length of plastic film after the tear has been started. Test specimens were cut using a die, as shown in Figure 2.3, to form a constant radius testing length. For specimen with low tear resistance, multiple specimens sandwiched together were used in order to bring the scale reading above 10. The tear resistance was calculated as

$$Average\ tear\ resistance\ (g) = \frac{16 \times average\ scale\ reading}{n} \tag{2.10}$$

where n is the number of specimens.

Because of the thickness non-uniformity as will be discussed below, the film samples used for mechanical test were selectively cut to have a mean thickness of 25 μm. Measurements on five different specimens were averaged for each compound.

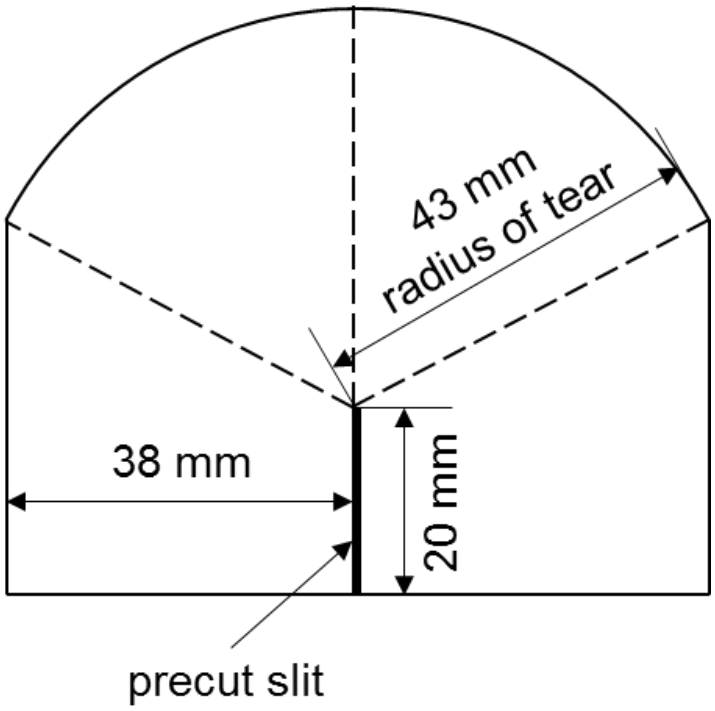

Figure 2.3 Die or template for constant-radius test specimen.

2.10.3 Prism Coupler

Birefringence is the optical property of a material having a refractive index that depends on the polarization and propagation direction of light. Since a polymer molecular chain has a polarizability anisotropy originated from its three-dimensional chemical structure, it exhibits birefringence when the polymer molecular chains are oriented by stress. Therefore, birefringence has been used to measure polymer orientation in blown films[55, 56, 115, 116]. The birefringence is described by

$$\Delta n = n_{/\!/} - n_{\perp} \tag{2.11}$$

where $n_{/\!/}$ and $n_{\perp}$ are the refractive indices for light polarized parallel and perpendicular to the orientation direction.

The refractive indices of blown film along MD, TD and normal direction (ND) were measured using a Metricon Prism Coupler Model 2010/M with an accuracy of $\pm$ 0.0005. The film was brought into contact with the base of a prism by means of a pneumatically-operated coupling head. A polarized laser beam with a wavelength of either 632.8 nm, was directed through the prism, striking the base of the prism at the coupling spot and is normally totally reflected at the prism base onto a photodetector, as shown in Figure 2.4. At a certain value of the incidence angle, which depended on the refractive index of the specimen, a sharp drop in the intensity of the light reflected from the base of the prism occurred and created a "knee" in the reflectance curve. The refractive index of the film was then derived from the light propagation constant determined by the knee location and the index of the prism. By changing the polarization state of the laser, index anisotropy (birefringence) can be measured in directions both along and perpendicular to the blown film surface.

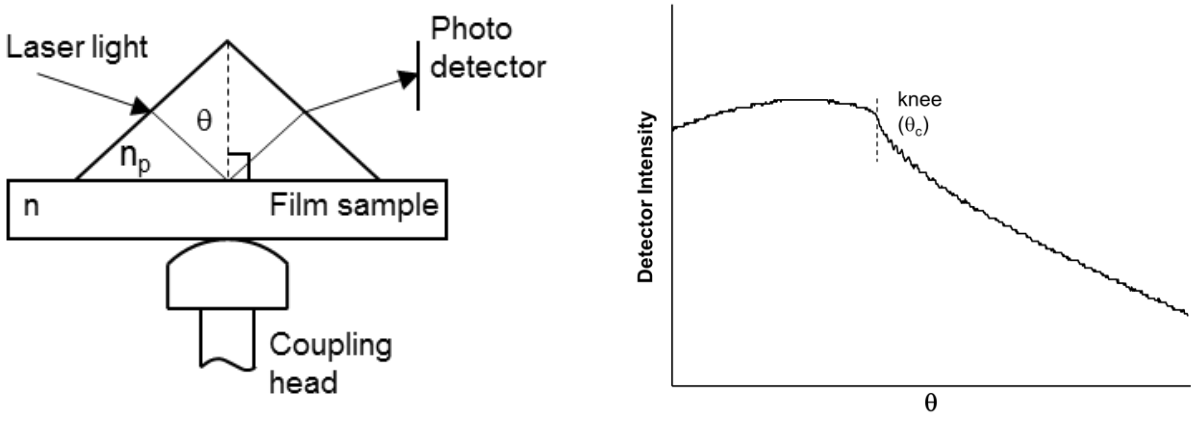

Figure 2.4 Measurement principle of Prism Coupler for blown film.

2.10.4 Scanning Electron Microscopy

A scanning electron microscope (SEM) is a type of electron microscope that produces topographical information of a sample surface by scanning it with a focused beam of electrons. Electrons are liberated from an emission source and accelerated in a high electrical field gradient. Within the high vacuum column, these so-called primary electrons are focused and deflected by electronic lenses to produce a narrow scan beam that bombards the object. As a result, secondary electrons are emitted from each spot on the object. The angle and velocity of these secondary electrons relate to the surface structure of the object. A detector catches the secondary electrons and produces an electronic signal. This signal is amplified and transformed to a video scan-image that can be seen on a monitor or to a digital image that can be saved and processed further

For traditional SEM, a Thermionic Emitter is used to generate electrons. By heat up a filament with electrical current, the electrons can escape from the filament when the heat is enough to overcome the work function of the filament material. Thermionic sources have relative low brightness, evaporation of cathode material and thermal drift during operation. In comparison, Field Emission SEM emits electron by placing the filament in a huge electrical potential. It generally produces clearer, less electrostatically distorted images with spatial resolution down to 1.5 nanometers. As a result, the crystalline morphology of semi-crystalline polymer can be directly observed by FESEM without the need for chemical treatment on the samples.

In the present study, the crystal structure and orientation of layered silicates in MD-TD plane of blown films were characterized with ZEISS FESEM at an accelerating voltage of 20 kV.

Samples were prepared for viewing by sputtering with a layer of 1 nm tungsten to avoid any accumulation of electron on the sample, called charging of the sample.

CHAPTER 3

PROCESSING POLYPROPYLENE NANOCOMPOSITES WITH SILYLATED ORGNAOCLAYS: COUPLING AT EDGES VERSUS GALLERY FACES

3.1 Introduction

Polymer nanocomposites with layered silicates have two different types of interface sites: at edges and faces of the nanolayers[117]. The edge sites have hydroxyl groups and the sites on the gallery faces have oxygen atoms along with exchangeable cations in the galleries. For example, sodium montmorillonite is organically modified by exchanging the sodium ions from the galleries with organophilic onium ion surfactants carrying one or two alkyl tails each with 18 carbons typically[66, 118]. When the matrix polymer is nonpolar such as polypropylene (PP), some amount of functionalized polypropylene such as polypropylene grafted with maleic anhydride (PP-g-MA) is added to promote polymer-particle interactions – typically in the form of hydrogen bonding between the anhydride and the groups on the nanolayer surfaces. The polymer-particle interface at either site may be strengthened further by means of silane coupling agents[119-122] that interact with the nanolayer sites at one end and with the functionalized polymeric compatibilizer at the other end. The use of silane coupling agents can also lead to improved dispersion[123] and improved mechanical properties[124-127].

The properties and effects of silanes are determined by their molecular structures, generally represented as shown in Figure 3.1 below. The silicon at the center is linked through a spacer R to an organofunctional group Y at one end and directly to hydrolyzable groups such as alkoxy groups at the other end. The alkoxy groups hydrolyze to hydroxyl groups and react with the hydroxyl groups at the edges of the clay to form Al−O−Si bonds or they may form hydrogen

bonds with the active sites on the gallery faces. The organofunctional group Y interacts with the polymeric compatibilizer either by hydrogen bonding or by forming a covalent bond. Depending upon the molecular structure of the silane coupling agents, it can end up either inside the layered clay galleries[118, 122, 128] resulting in an increase in the basal spacing or react mainly with the edge hydroxyl groups[129, 130]. Shanmugharaj et al.[128] studied the influence of dispersing medium used during the silylation procedure, on the grafting of montmorillonite clays and reported that with increasing solvent surface energy, the possibility of intercalation of silane molecules within the clay galleries increases. The presence of silane molecules within the clay galleries could provide greater interaction between the polymer and the clay, resulting in better dispersion and improved mechanical properties.

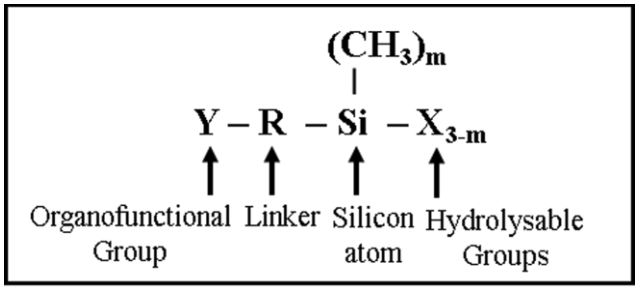

Figure 3.1 Schematic of the structure of silane coupling agents.

The objective of the work presented here was to investigate the morphology and rheology in dynamic shear and uniaxial extensional flow of the melt-compounded state of polypropylene-layered-silicate nanocomposites with different modes of polymer−particle coupling at different interface sites. The melt rheology of polymer−clay nanocomposites is sensitive to the loading and the state of dispersion as well as the orientation distribution of nanolayers[71, 119, 131-137]. Low frequency linear viscoelastic moduli have been used by Durmus et al.[138] and Vermant et al.[112] to quantify the degree of dispersion of layered silicates in polymer melts. High aspect

ratio nanolayers have also been shown to modify the extensional flow behavior of the polymer melts in some cases[88, 90, 139], imparting strain hardening to the transient uniaxial extensional viscosity where the matrix polymer did not exhibit this property. The opposite effect has been reported by others[86, 91, 140-142] of reduced strain hardening after adding the same high aspect ratio nanoparticles to a matrix polymer that displayed strain hardening by itself; the cause of the varied effects remains unclear. The results presented in this paper reveal that silane coupling at the edges alone or silane penetration into the galleries give rise to different effects on the morphology and melt rheology, particularly on strain hardening in extensional flow of the nanocomposite melts.

3.2 Experimental Details

3.2.1 Materials

The polypropylene matrix used in this study was Profax 6523 from Basell. Maleic anhydride grafted PP, PO1015 from ExxonMobil, was a random copolymer of propylene and ethylene and was used as compatibilizer. Two different organically modified montmorillonites from Nanocor were used -- I.44P which has a quaternary onium ion surfactant with two C-18 tails and I.30P which has a primary onium ion surfactant with a single C-18 tail. Two different silanes were used for this study: N-(2-aminoethyl)-3-aminopropylmethyldimethoxysilane (aminoalkyldimethoxy) silane and octyltrimethoxy silane.

The selection of aminoalkyl silane as coupling agent was based on the fact that amines present on the silane treated clays can react with the anhydride group of the PP-g-MA[143-146], forming an amide or imide linkage. Lu et al.[146] investigated the reaction between PP-g-MA and amines by melt mixing them in various proportions in an extruder. The study suggested that

the reaction between the two was very fast and was completed within 90s, which was supported by FTIR analysis. Song and Baker[147] studied the reaction between different amines (primary, secondary and tertiary amines) and anhydride group in polymeric systems and reported rapid formation of the imide linkage between the polymer and the amines. Octyltrimethoxy silane, on the other hand, was used to cover the silicate layers with non-polar alkyl chains so that an enhancement of the compatibility between clay particles and the bulk polypropylene was obtained. At the same time, the interaction between PP-g-MA and organoclay was weakened after silylation with octylsilane. The methoxy groups of all the silanes get hydrolyzed in presence of moisture and may then react at the nanolayers edges to form Al-O-Si bonds[129] or participate in hydrogen bonding with the oxygen atoms at the gallery face sites. The silane treated clays were then used to prepare nanocomposites with 85 wt% linear PP, 12 wt% PO 1015 as the compatibilizer and 3 wt% of nanoclay, the details of which are presented in Table 3.1.

Table 3.1 Constituents in different nanocomposites.

Composite	85 wt%	12 wt%	3 wt%
PPNC1	Polypropylene (Profax 6523)	Maleic anhydride grafted PP (PO1015)	I.44P
PPNC2			Amino silane treated I.44P
PPNC3			I.30P
PPNC4			Amino silane treated I.30P
PPNC5			Octyl silane treated I.44P

3.2.2 Processing and Characterization

Silane treatment of organoclays was carried out based on the wet process in a methanol/water mixture as described in Chapter 2. The non-treated or treated organoclay were used to prepared PP nanocomposite with PP-g-MA as compatibilizer by melt mixing for 10 min in a Brabender batch mixer at 180°C with continuous nitrogen purge. Before compounding. The

PP-g-MA and organoclays were dried overnight in a vacuum oven before usage. Polymer matrix containing PP and PP-g-MA with a weight ratio of 85:12 was also prepared under the same processing condition.

The clay powder was characterized for XRD, BET and TGA analysis to study the effect of silane treatment on its interlayer spacing, surface area and organic content, respectively. Compression molding by a hydraulic press was used to make composite specimens for TEM analysis and rheological characterizations. Dynamic shear tests were carried out on a TA Instruments AR2000 rheometer with parallel plates of diameter 40 mm over a frequency range from 0.01 to 100 rad/s at 180 °C under nitrogen flow. A fixed strain of 1% was used in all cases, which was confirmed by a strain sweep to be within the linear viscoelastic regime of each material. The melt extensional viscosity of the nanocomposites was measured using an extensional viscosity fixture (EVF) on a TA-ARES instrument. The extensional viscosity measurements were made for the nanocomposites at 180 °C and at four strain rates (0.1, 0.5, 1.0, and 2.0 s−1) over Hencky strains up to 3. To verify that the samples were stable during these tests and that the strain hardening was not caused by a continuously changing structure of the nanocomposite, dynamic time sweep tests were conducted on these samples. The dynamic shear storage modulus of these nanocomposite melts remained unchanged over a period of 1 h, confirming that the samples were stable over an hour. The details of all the preparation and characterization procedures were provided in Chapter 2.

3.3 Results and Discussion

3.3.1 Characterization of Organoclays

The two chosen organoclays have different aspect ratios to start with: they were determined to be 68 for I.44P and 56 for I.30P[148]. The cationic surfactant is also different in the two clays as noted previously. The proportion of cationic surfactant was determined from ash content measurements to be 40 wt % in I.44P and 30 wt % in I.30P. This is consistent with greater packing of the quaternary onium ion surfactant with two alkyl tails in the galleries of I.44P. The primary onium ion surfactant ($R\text{-}NH_3^+$) in I.30P tends to be perpendicular to the gallery faces and the protons in the headgroup can form hydrogen bonds with the oxygen atoms on the gallery faces[65]. The quaternary onium ion surfactant with two C-18 tails has a higher interlayer packing density and cannot form hydrogen bonds to the gallery faces.

The *d*-spacing from XRD scans of the clays and BET surface area measurements recorded before and after silanization have been tabulated in Table 3.2. The *d*-spacing of both aminosilane and octylsilane treated I.44P was about the same as that of the I.44P organoclay without silane treatment. It follows then that the silane reaction occurs at the edges alone of the I.44P. The *d*-spacing for the aminosilane treated I.30P organoclay was greater than that of the untreated I.30P, and this indicates that the amino silane molecules have reacted at both the faces and edges of the nanolayers in I.30P.

The BET surface area of sodium montmorillonite clays is in the range of 43 to 50 m^2/g[149-151]. The BET surface area of each of the organoclays, I.30P and I.44P, was found to be about 10 m^2/g after surfactant treatment. When the I.44P was further treated with aminosilane coupling agents, there was no significant drop in the BET surface area, indicating that the silanol

groups have reacted mainly with the hydroxyl groups at the edges of the nanolayers. However, there was a significant drop in the BET surface area of the silylated I.30P, indicating that silane coupling has occurred both at the edges and the faces of the clay nanolayers. This may be explained by the fact that the primary onium ion surfactant ($R\text{-}NH_3^+$) in I.30P tends to be perpendicular to the gallery faces with more room for penetration by other molecules such as silanes[65].

Table 3.2 BET Area and *d*-spacing of organoclays with and without silane treatment.

Coupling Agent	**I.44P (dialkyl quaternary onium ion surfactant)**		**I.30P (alkyl primary onium ion surfactant)**	
	BET Area (m^2/g)	*d*-spacing (nm)	BET Area (m^2/g)	*d*-spacing (nm)
None	9.8	2.58	9.5	2.34
Dimethoxy aminosilane	9.1	2.54	3.8	3.21
Trimethoxy octyl silane		2.47		

The linkages and interactions arising from silane treatment at the edges and faces are illustrated in Figure 3.2. The silanol groups react with the hydroxyl groups at the edges forming a covalent bond (Al-O-Si) with the clay[129]; the amine end of aminosilane was available for reaction with the functionalized polypropylene which may have an anhydride group or an acid group during compounding. Thus, the coupling between the edges of aminosilane treated clay and the polymeric compatibilizer will be made up entirely of covalent bonds. The replacement of hydroxyl groups at the edges of clay particles with octyl tails of the octylsilane increases its compatibility with the bulk polypropylene and reduces its reactivity with the functionalized polypropylene. The silanol groups in the galley can form only hydrogen bonds with the oxygen

atoms on the faces and these will be looser than the hydrogen bonds holding the primary onium ion surfactant at the faces as shown in Figure 3.1(b).

(a) Silane at edge

(b) Silane in interlayer gallery

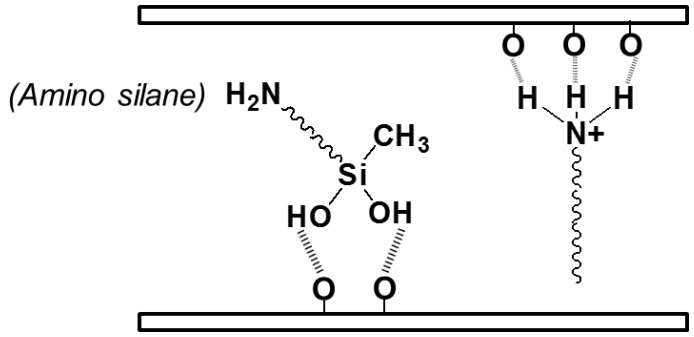

Figure 3.2 Reactions and interactions of hydrolyzed silanes (a) at the edge and (b) at the gallery faces.

The TGA profiles of the I.44P clay before and after silane treatment presented in Figure 3.3(a) are very close except for the small amount of surfactant lost in the solvent based silane treatment process. But in the case of the I.30P clay, Figure 3.3(b) reveals that the silane that penetrated the galleries was removed from the galleries at a lower temperature indicating much looser bonds to the gallery faces for the silane than for the primary onium ion surfactant in the I.30P, as highlighted also in Figure 3.1(b).

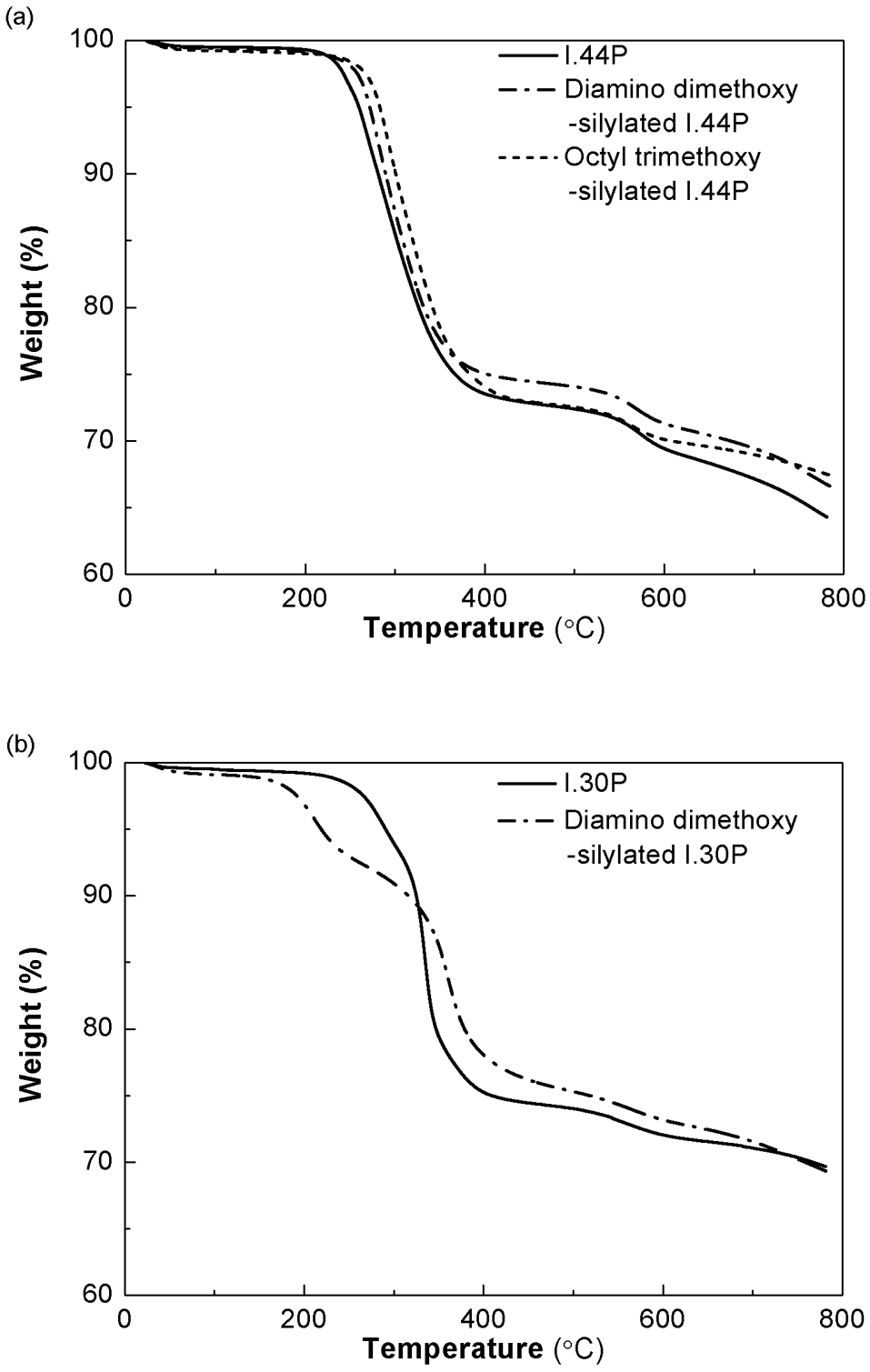

Figure 3.3 TGA profiles before and after silane treatment of different organoclays.

3.3.2 Dispersion and Structure of Polymer Nanocomposites

TEM micrographs of the five composites presented in Figure 3.4 allow us to compare the changes in degree of dispersion due to silane treatment of the organoclays. It should be noted again here that the average length of the nanolayers in I.44P is 25% greater than that in I.30P. Without silane coupling, the polymeric compatibilizer forms mostly hydrogen bonds at faces and edges of the nanoclay, and this level of interaction leads to poor dispersion as seen from Figure 3.4(a) and (c). It appears that the dispersion was noticeably improved by aminosilane treatment. Much thinner nanoparticles may be seen in Figure 3.4(d), for the case where the silane penetrates the galleries. Octylsilane treatment of I.44P led to more uniformly dispersed clay tactoids in the polymer matrix as seen from Figure 4(e), which was attributed to the reduced surface energy difference between the nanoclay and the polymer matrix. The variation in state of particle dispersion can also be seen from the values of mean stack thickness tabulated in Table 3. The mean thickness was 6.5 nm in the I.30P composite and 5.2 nm in the composite with silane treated I.30P. In the case of the I.44P composites, the mean thickness was reduced from 16 to 11 and 12 nm after silylation with aminosilane and octylsilane, respectively. This indicates that the presence of aminoalkyl silane in the interlayer galleries leads to much better dispersion of the nanolayers in the polymer.

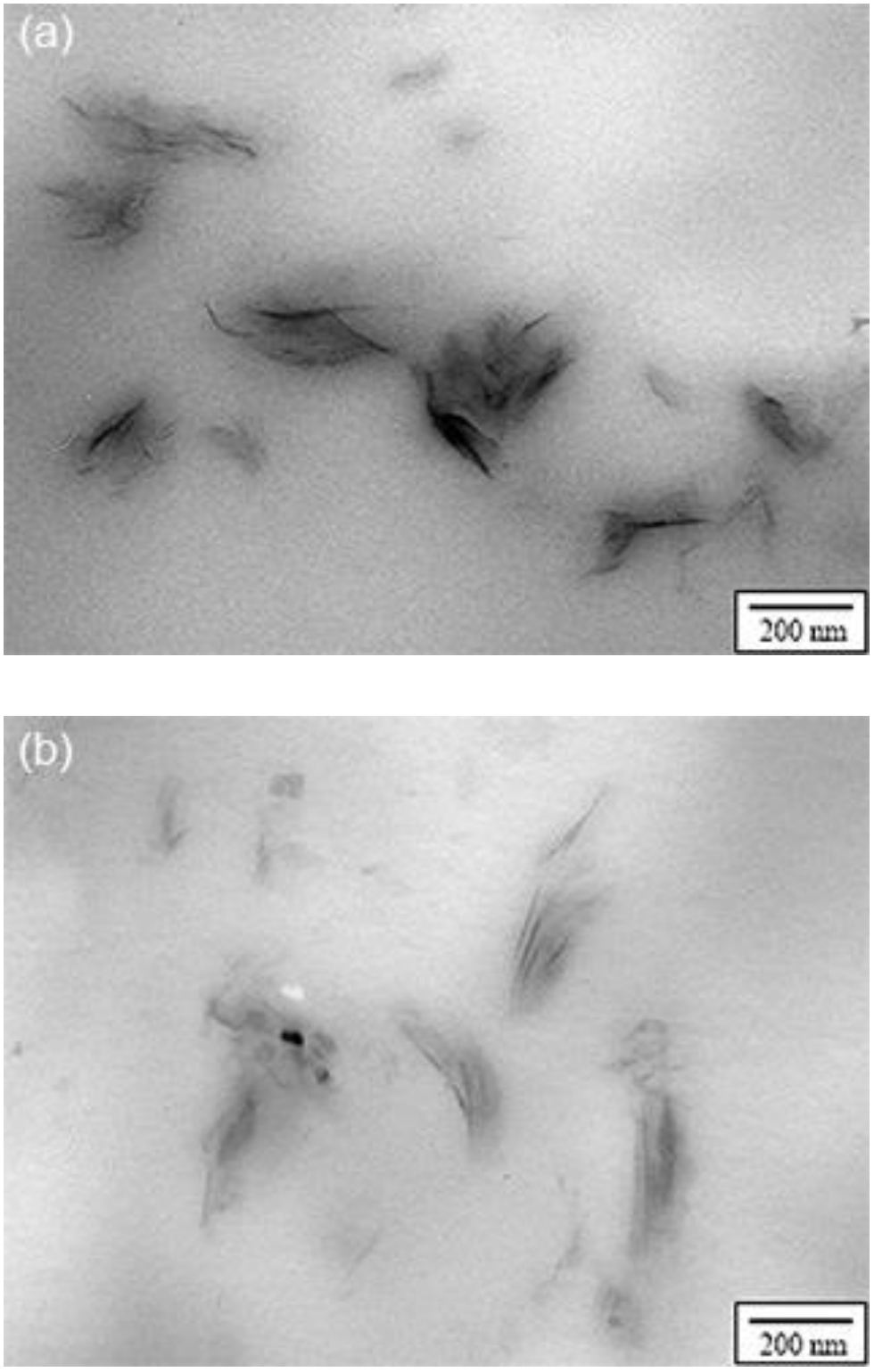

Figure 3.4 TEM micrographs of nanocomposites prepared with various organoclays: (a) I.44P, (b) aminosilane treated I.44P, (c) I.30P, (d) aminosilane treated I.30P and (e) octylsilane treated I.44P.

Figure 3.4 (cont'd)

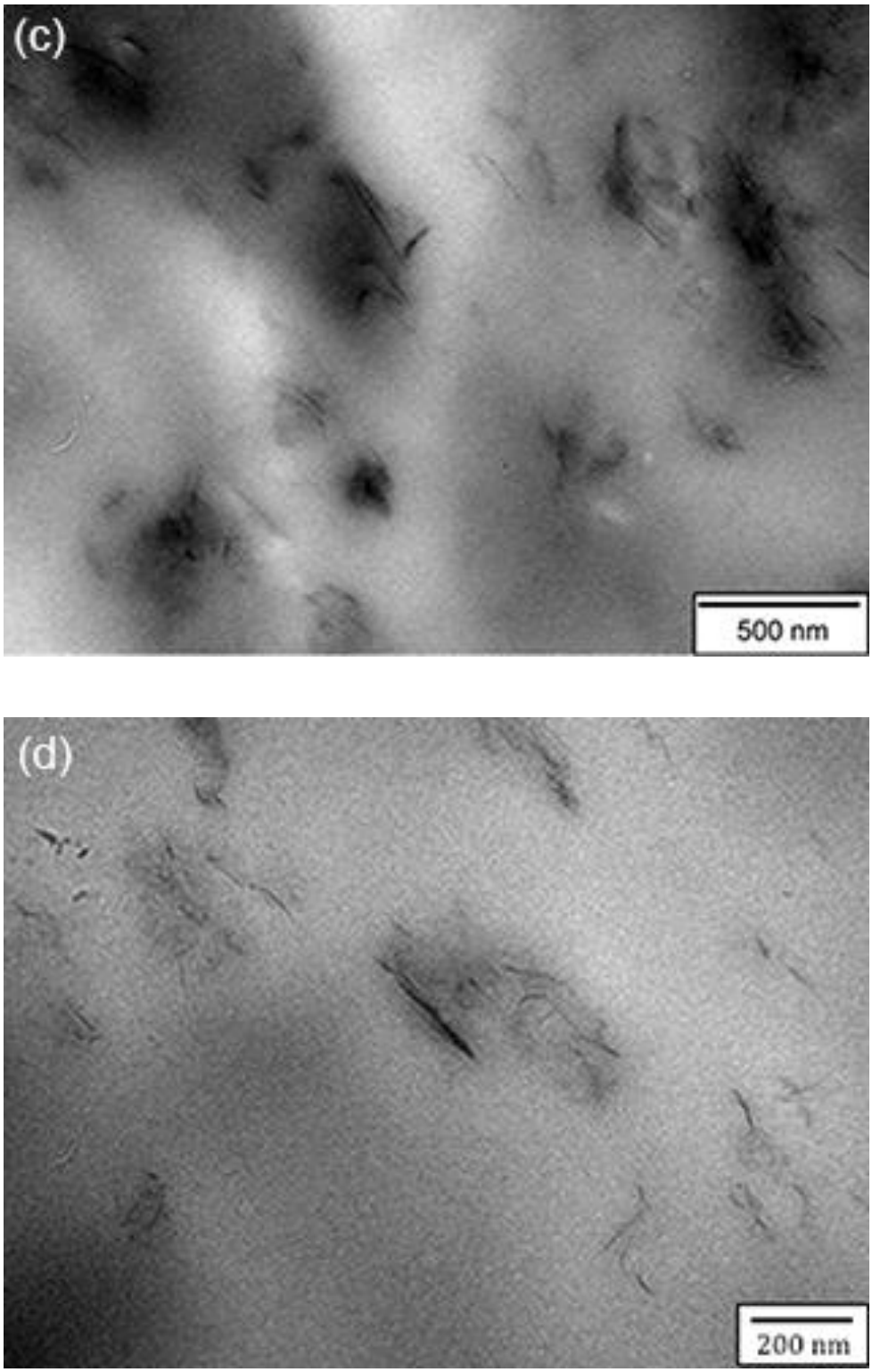

Figure 3.4 (cont'd)

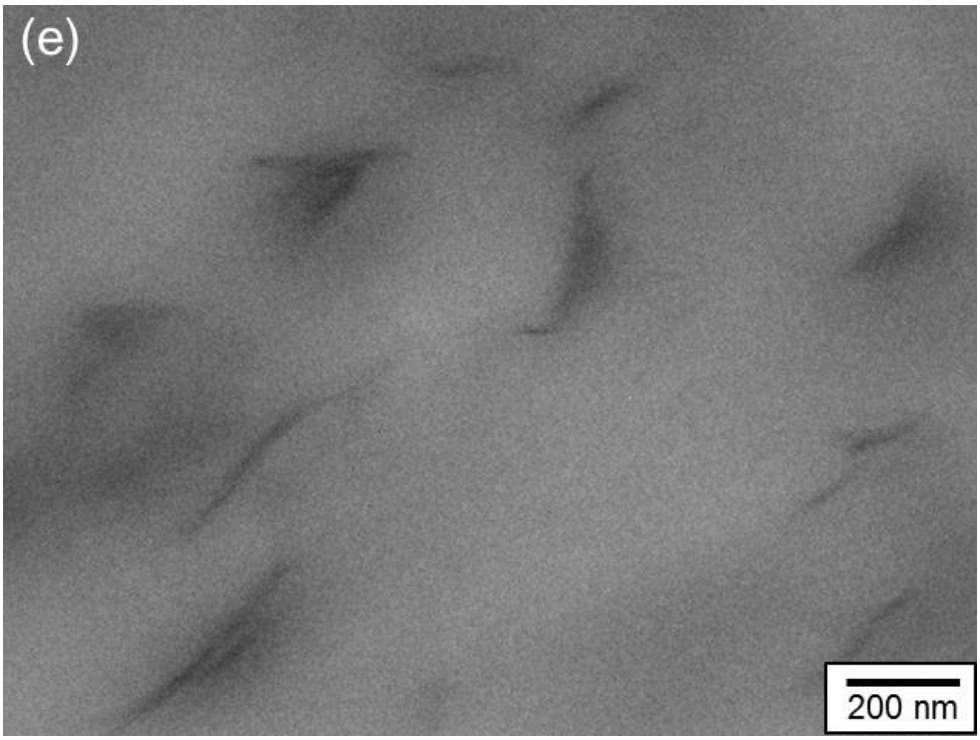

Table 3.3 Estimated mean thickness for various nanocomposites.

Compound	Mean thickness (nm) in original compound
PPNC1	15.9
PPNC2	10.9
PPNC3	6.5
PPNC4	4.1
PPNC5	12.1

3.3.3 Dynamic Shear Rheology of Nanocomposite Melts

The effect of particle surface treatment on the polymer-particle interactions can be gauged from the dynamic shear storage modulus at low frequencies because this reflects the extent of bridging between particles through entangled polymers[135, 152, 153]. The frequency-

dependent dynamic shear storage modulus and dynamic viscosity at 180 °C have been plotted in Figure 3.5 for PPNC1, PPNC2 and PPNC5 and in Figure 3.6 for PPNC3 and PPNC4. The low frequency storage modulus was lower for the composite melt with silane-treated organoclay in all cases. With the same silane coupling agent, this effect was seen to a greater extent in both dynamic shear modulus and dynamic shear viscosity with the I.30P nanocomposites where coupling occurred at both faces and edges of the nanolayers. This is because the potential for bridging through particle-attached chains entangled with other chains was reduced. In the absence of silane treatment, functionalized polymer chains could interact directly with each site on the clay surface. But the aminosilane reduced the amount of polymer attachments as each amine end could tie up two sites on the clay surface. Similarly, less particle attached chains were presented in PPNC5, as the octylsilane lowered the reactivity between nanoclay and functionalized polymer chains.

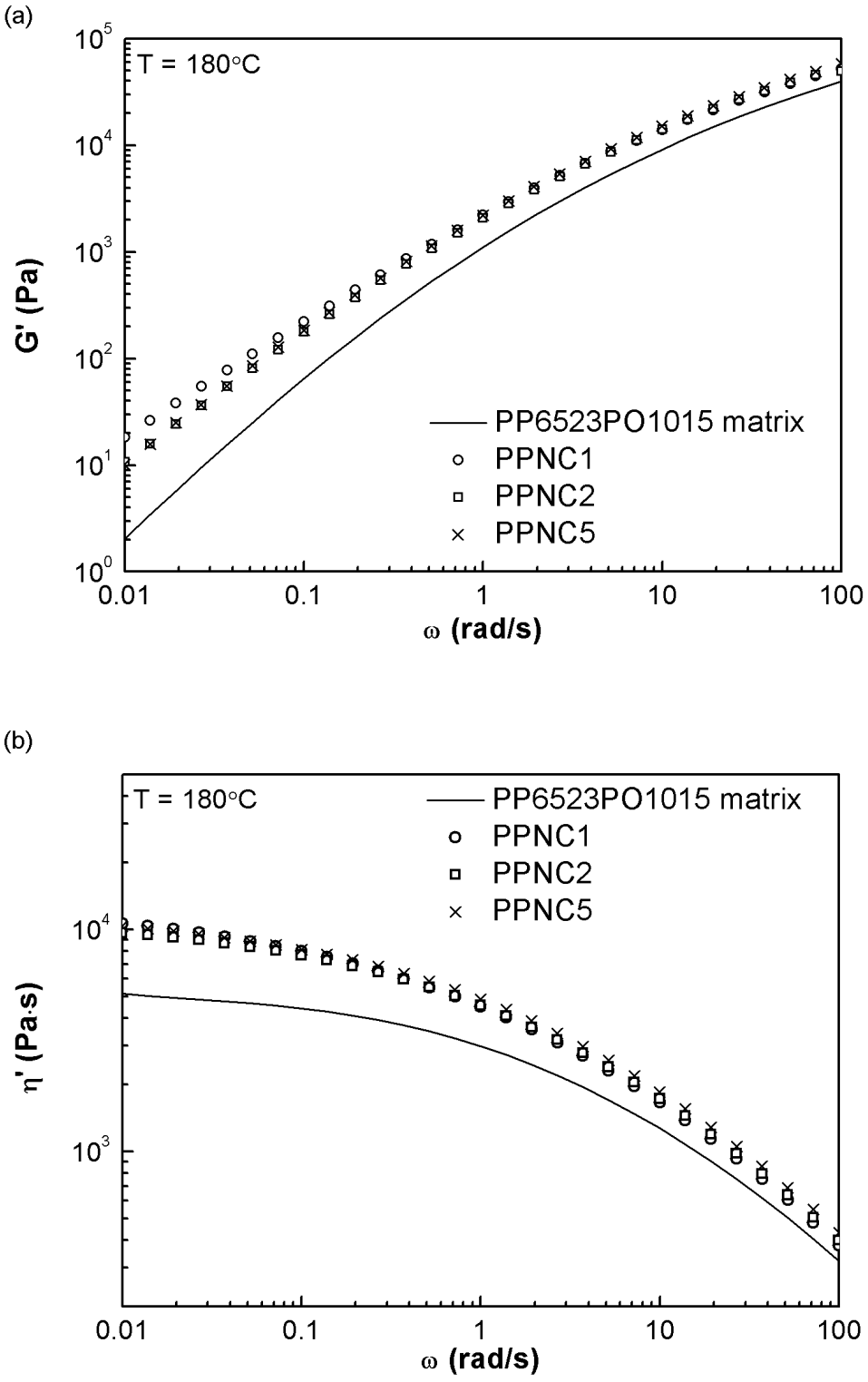

Figure 3.5 (a) Storage modulus and (b) dynamic viscosity of PP/PP-g-MA matrix and nanocomposites with I.44P and aminosilane and octylsilane treated I.44P organoclay.

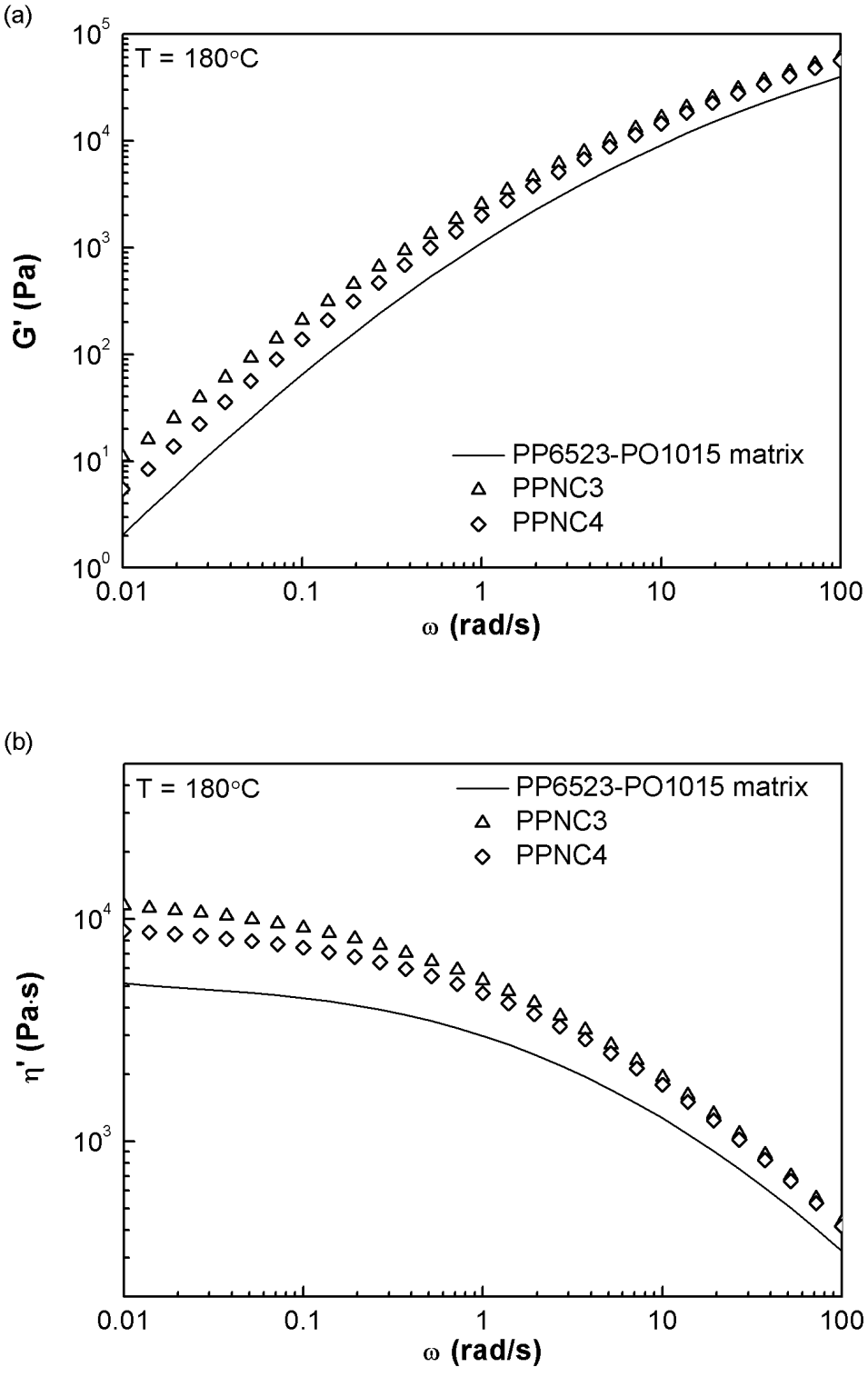

Figure 3.6 (a) Storage modulus and (b) dynamic viscosity of PP/PP-g-MA matrix and nanocomposites with I.30P and aminosilane treated I.30P organoclay.

3.3.4 Transient Uniaxial Extensional Viscosity

The imparting of strain hardening in uniaxial extensional flow to a linear polypropylene that does not display any strain hardening, by adding nanoparticles of high aspect ratio, is an important rheological effect for processing operations. This is obtained only when the polymer compatibilizer molecular weight is sufficiently high, and this is true for the one chosen in this study. The effect of silane treatment on the uniaxial extensional viscosity transients is addressed here. First, the stability of the composites was tested by carrying out a time sweep over an hour on each of them and on the matrix blend of polypropylene and compatibilizer. The results are presented in Figure 3.7. It is apparent that the dynamic storage modulus variation over an hour was less than 5% for all the melts.

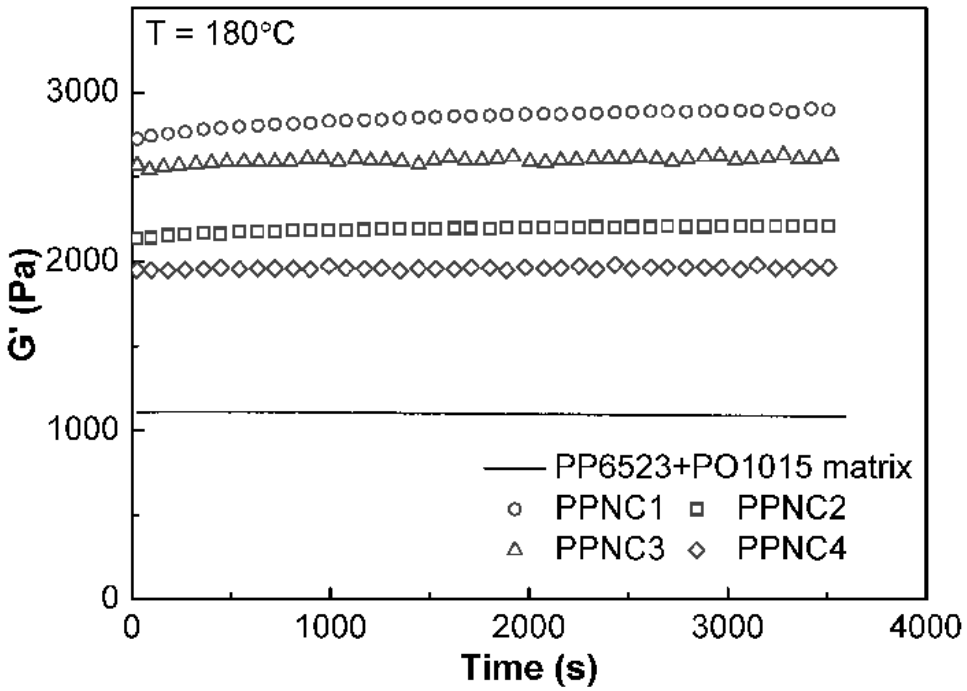

Figure 3.7 Time sweeps of storage modulus at 1 rad/s for various nanocomposite melts and for the matrix polymer blend.

The uniaxial extensional viscosity transients at strain rates ranging from 0.1 s^{-1} to 2 s^{-1} are plotted for the five nanocomposite melts in Figure 3.8. Each of these runs was carried out with a maximum specified Hencky strain of 3. It can be seen that all nanocomposites, expect for PPNC5, displayed distinct strain hardening behavior, as evidenced by the upward deviation of the extensional viscosity with increased strain. The lack of strain hardening in PPNC5 indicates the importance of attractive polymer-clay interaction rather than particle dispersion in inducing this behavior. The extent of strain hardening of other nanocomposites was quantified at each strain rate by estimating a strain hardening ratio χ between the actual value of extensional viscosity and the value on the baseline curve corresponding to linear viscoelastic behavior, with a fixed strain. The baseline curve or linear viscoelastic "envelope" was obtained by extrapolating viscosity data from strains between 0.1 and 0.4 to higher strains. The maximum value χ_{max} of this ratio was evaluated at the highest strain before the stretched strand breaks or deforms nonuniformly; this was about 2.3 for PPNC1, PPNC2, and PPNC3 and 3 for PPNC4, that is, until the end of the run. Plots of the maximum strain hardening ratio against strain rate have been presented in Figure 3.9 for the four melts. As seen from this figure, the maximum strain hardening ratio was raised from below 2 to near 3 by the presence of aminoalkyltrimethoxysilane coupling both in PPNC2 and in PPNC4 and more so in PPNC4. The maximum ratio was higher than 2 over the entire range of strain rates for PPNC4 where silane coupling was present at both faces and edges. In this case, the silane with the reacted polymer compatibilizer was loosely attached to the face sites by the silanol groups as shown in Figure 3.1 and this provided a slower relaxing entanglement network involving the site-attached chains and the free polypropylene chains[154]. This is the likely cause for the remarkable strain hardening exhibited by the PPNC4 nanocomposite melt.

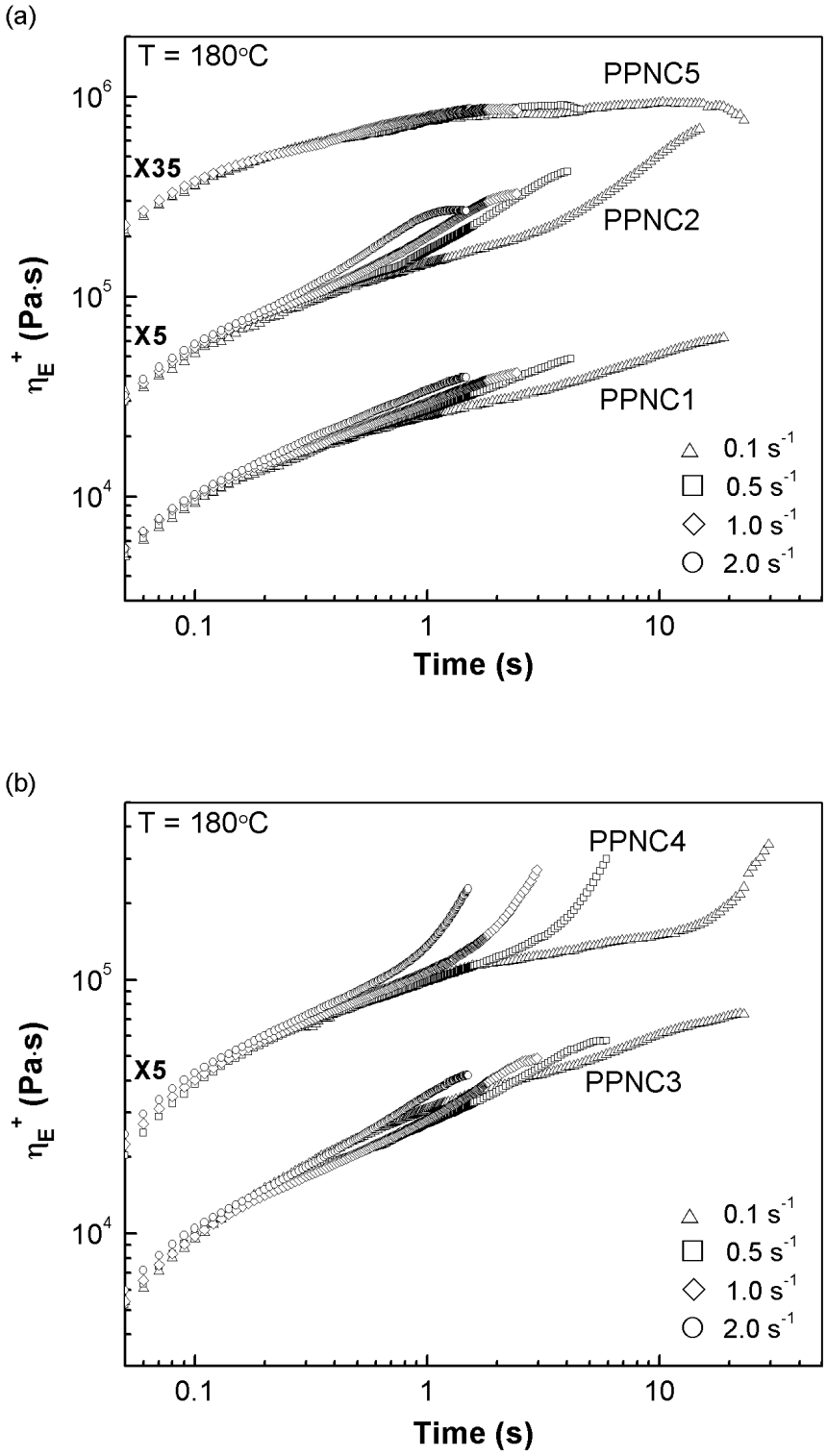

Figure 3.8 Uniaxial extensional viscosity transients (η_e) at several strain rates for as compounded nanocomposite melts.

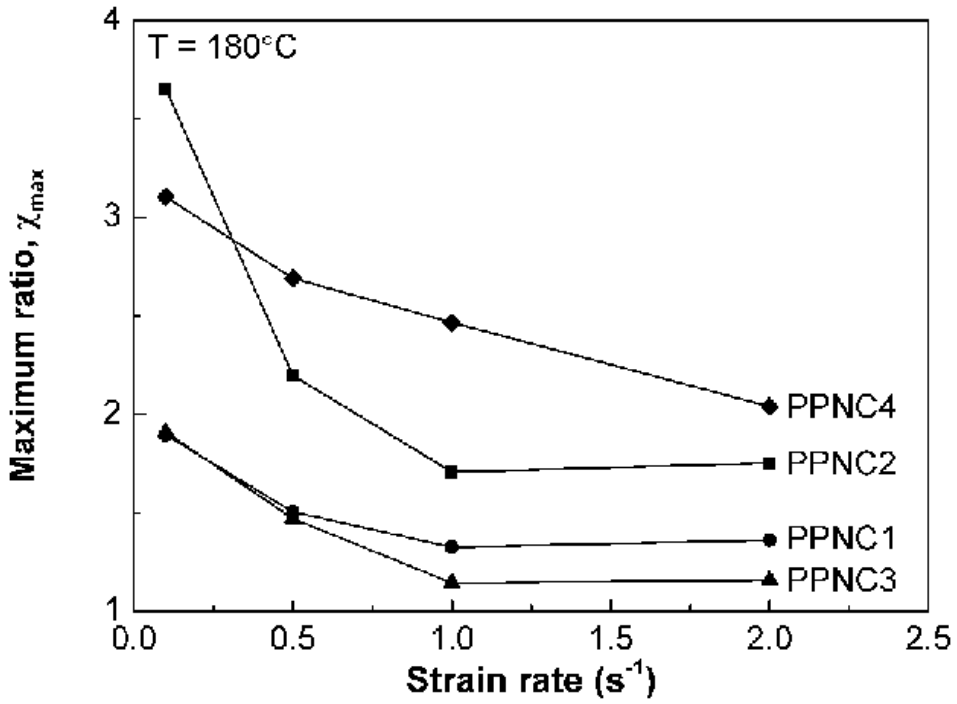

Figure 3.9 Maximum strain hardening ratio for the four melts at 180°C; this corresponds at all strain rates to a strain of 2.3 for PPNC1, PPNC2, and PPNC3 and to a strain of 3 for PPNC4.

3.4 Conclusions

Two different organically modified layered silicates were treated with aminoalkyldimethoxysilane and octyltrimethoxysilane in a methanol−water mixture; in the case of organoclay with the greater interlayer packing of surfactant, the silanols reacted only at the nanolayer edges while in the other case, the silanes entered the interlayer galleries and loosely attached to faces of nanoclays via hydrogen bonds. In nanocomposites prepared with 3 wt % of the organoclay, the aminosilane enhanced polymer-clay interactions by reactively coupling to polymeric compatibilizer (PP-g-MA) while the octylsilane weakened polymer-clay interactions. The effect of silane coupling in all cases was noticeably improved dispersion with thinner stacks. The low frequency dynamic storage modulus of the nanocomposites with silane coupling was lower The uniaxial extensional viscosity of nanocomposites melts with aminosilane coupling

displayed greater strain hardening behavior compared to that of the nanocomposites with non-silylated organoclay, especially in the case of coupling at faces and edges. No strain hardening was obtained in nanocomposite prepared with octylsilane treated nanoclay. These results demonstrate the potential for rheology modification by means of coupling agents with long chain polymeric compatibilizers in processing polypropylene clay nanocomposites.

CHAPTER 4

PROCESSING OF RECYCLED POLYPROPYLENE - CLAY NANOCOMPOSITES

4.1 Introduction

Polymer-layered silicate nanocomposites have attracted great attention due to the extraordinary capacity of nanoclays in tuning both processability and end-use properties of polymeric materials. The recycling and post-processing of these materials have also become increasingly important due to its potentially economic and environmental benefits. One important aspect of recycling nanocomposites is the microstructure changes induced by reprocessing, since the effects of nanoclay on reinforcing polymer matrix depend strongly on the state of clay dispersion. Russo et al.[155] reported that reprocessing of nylon 6-organoclay nanocomposites could degrade or improve dispersion depending on the flow conditions: the use of single screw extruders led to re-aggregation or restacking of particles but the use of twin screw extruders led to further delamination[155]. This difference was caused by the high shear stress obtained in the latter case that broke up clay aggregates during reprocessing. In polyolefin-layered silicate nanocomposites, the increased polarity of matrix due to thermo-oxidative degradation can also be responsible for the improvement of particle dispersion upon reprocessing[155-161].

However, a better dispersion of nanoclay in the nanocomposite does not necessarily increase the performance of the functional properties such as the thermal and mechanical properties due to the negative effect of degradation. Polymer matrix is prone to degrade during reprocessing via thermo-oxidative and mechanical chain scission, which reduces both processability and end-use properties of these materials. Incarnato et al.[162] observed that the

weight-average molecular weight and shear viscosity of polypropylene by itself decreased progressively with the number of reprocessing cycles. As a consequence of degradation, the smaller fragments of polymer chains do not contribute effectively to the mechanical properties[163]. In polymer-clay nanocomposites, the degree of polymer degradation may be affected by the presence of organoclays. Fornes et al.[164] reported a higher level of aging and color changes in nylon 6-clay nanocomposites compared to that of neat nylon 6, which was attributed to the occurrence of chemical reactions between the decomposed species of surfactants and the polymer matrix [134, 164, 165].

This study focused on the degradation of PP-organoclay nanocomposites (PPNC1, PPNC2, PPNC3 and PPNC4) subjected to reprocessing in a capillary rheometer. The neat PP was also reprocessed to illustrate the degradation of polymer molecular structure via rheological characterization. Results presented in the following sections show that penetration of silane coupling agent into the clay gallery leads to far greater degradation of structure and rheology in reprocessed polypropylene-clay nanocomposites. Although several studies have been carried out with regard to reprocessing of polymer nanocomposites, few have been conducted on restoring or boosting properties of these materials. In this work, a new masterbatch additive was developed and tested for boosting the rheological properties of reprocessed PP, and PP-organoclay nanocomposites.

4.2 Experimental Details

4.2.1 Materials

Linear polypropylene (PP6523) and various PP/clay nanocomposites (PPNC1, PPNC2, PPNC3 and PPNC4) prepared using unsilylated and silylated I.44P and I.30P nanoclays, characterized in Chapter 3 were used to study the effect of additional reprocessing on the morphology and rheology. To prepare masterbatch additive for restoring rheological properties of recycled compounds, maleic anhydride grafted PP (Exxelor PO1015 from ExxonMobil) and aminoalkyldimethoxy silane treated I.44P organoclay were used.

4.2.2 Processing and Characterization

Extruded or recycled polypropylene was prepared by reprocessing PP6523 through a single screw extruder (C.W. Brabender Inc.) at 220°C. After each extrusion cycle, the material was granulated and re-extruded. This sequence was repeated for three times. The reprocessing of nanocomposites was conducted by extrusion PPNC1, PPNC2, PPNC3 and PPNC4 through a capillary die of 1 mm diameter and L/D = 30 at 180 °C and a shear rate of 500 s^{-1} in a Dynisco LCR6000 capillary rheometer. The shear rate was chosen to allow sufficient residence time in the die. The compounded materials were first granulated in a mini granulator. The granules were carefully fed into the rheometer and packed for 6 min to melt. The extruded strands were collected for characterization.

A masterbatch was prepared by melt mixing PO1015 PP-g-MA and aminosilane treated I.44P organoclay with a ratio of 2:1 by weight in a Brabender batch mixer at 180 °C for 10 min with a continuous nitrogen purge. The silane treatment in the previously reported work was carried out by a wet process in a methanol-water mixture and resulted in coupling only edges of

I.44P. In this study, an alternative vapor phase treatment process, which has been reported in the literature[166], was exploited, leading to penetration of silanes in the interlayer galleries without sacrificing the thermostability. The treated clay was sieved with a No. 200 sieve before use. The extruded or reprocessed PP or PPNC was then compounded in the batch mixer with 15 wt% of this masterbatch additive following the same compounding procedure.

The dispersion of organoclay in extruded PP nanocomposites was assessed by transmission electron microscope. Various materials were also characterized for the linear viscoelasticity in shear and transient uniaxial extensional viscosity of the melts at 180 °C. The details of the characterization techniques are presented in Chapter 2.

4.3 Results and Discussion

4.3.1 Dispersion and Structure of Reprocessed Nanocomposites

Figure 4.1 shows the TEM micrographs of reprocessed nanocomposites after extrusion at 500 s^{-1}. Estimates of the average thickness of nanolayer stacks in and reprocessed nanocomposites have been tabulated in Table 4.1. Compared to the compounded nanocomposites in Chapter 3, it is readily seen that reprocessing has improved the morphology of nanocomposites for PPNC1 and PPNC3 that have no silane treatment. The thickness of nanolayer stacks was significantly reduced upon reprocessing. This may be attributed to the additional shear in reprocessing which broke up larger clay stacks[155]. However, reprocessing affects the morphology of PPNC2 and PPNC4 quite differently.

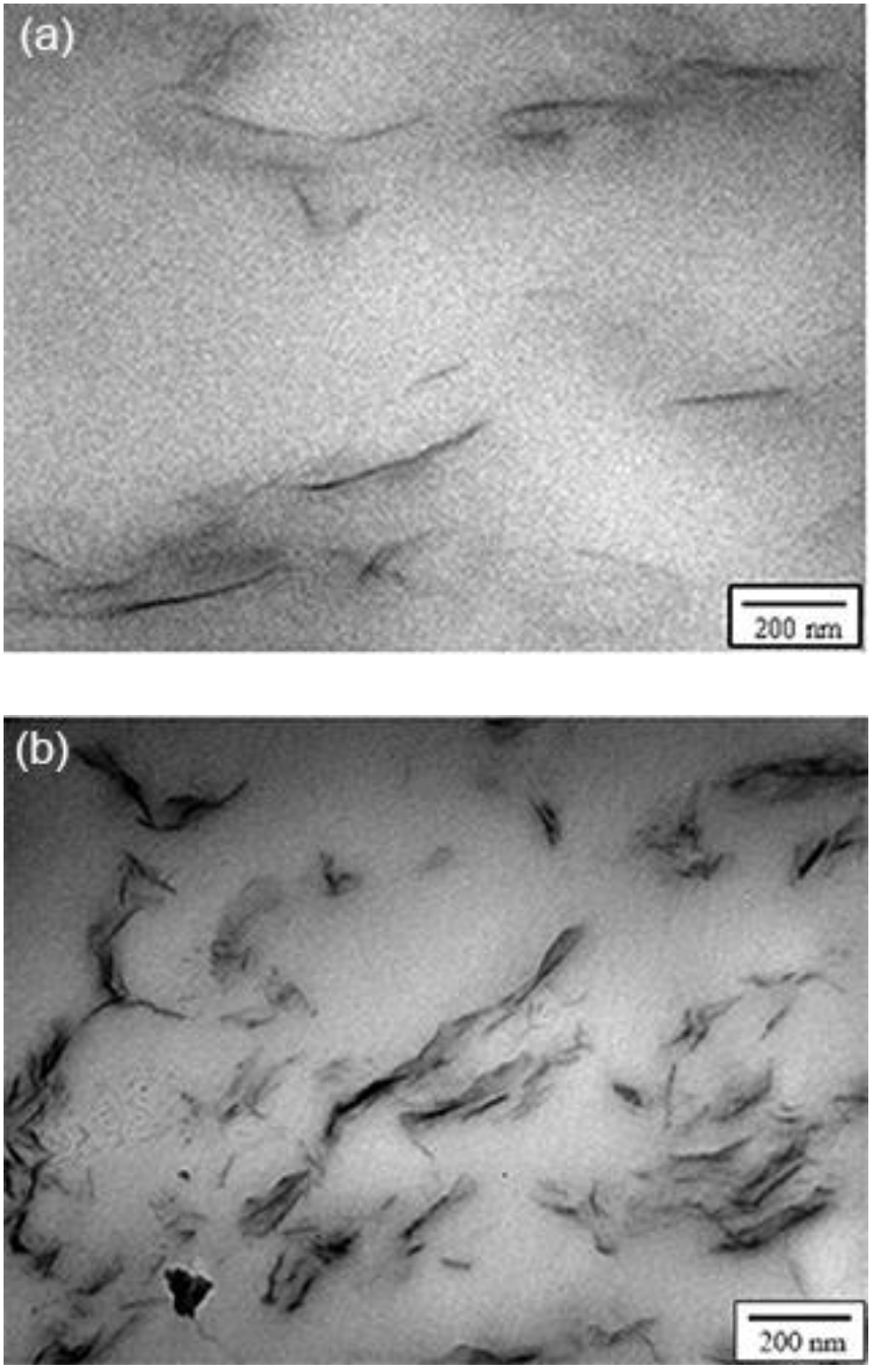

Figure 4.1 TEM micrographs of reprocessed (extruded) nanocomposites with various organoclays: (a) I.44P, (b) silylated I.44P, (c) I.30P, (d) silylated I.30P.

Figure 4.1 (cont'd)

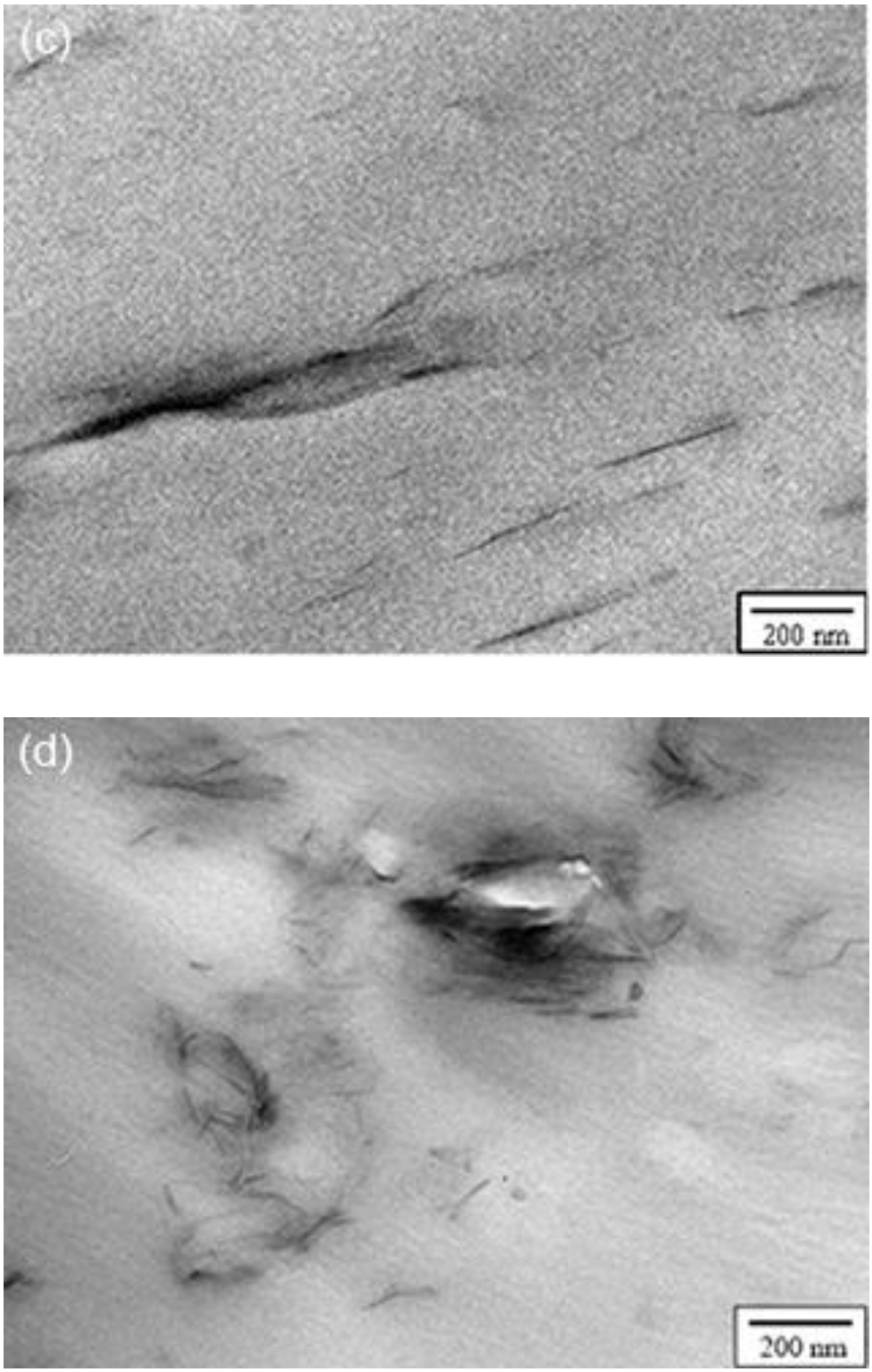

The morphology of PPNC2 was improved upon reprocessing with the mean thickness reduced from 10.9 to 7 nm but the morphology of PPNC4 was degraded upon reprocessing with the mean thickness going up from 4.2 to 6.6 nm. In the case of PPNC2, the silane was covalently bonded to the edge site and there was no silane at the gallery faces as shown in Figure 3.2(a). But in PPNC4, the silanes at the gallery faces were more loosely attached although the polymer compatibilizer was covalently bonded to the silane the same way (see Figure 3.2(b)); this leads to loss of the polymer compatibilizer from the gallery. This was also seen in the TGA profile, Figure 3.3(b), for PPNC4 where the thermal stability was lowered by silane treatment at the faces.

Table 4.1 Estimated mean thickness for nanocomposites after reprocessing.

Compound	Mean thickness (nm) in reprocessed nanocomposite
PPNC1	6.9
PPNC2	7.0
PPNC3	5.1
PPNC4	6.6

4.3.2 Dynamic Shear Rheology of Reprocessed Polypropylene and Nanocomposites

The dynamic shear rheology curves for neat polypropylene and recycled polypropylene from the third cycle of extrusion have been presented in Figure 4.2. Extrusion of virgin polymer melt led to the reduction of storage modulus and dynamic viscosity along all frequencies, which was attributed to severe thermal and shear induced polymer degradation during reprocessing.

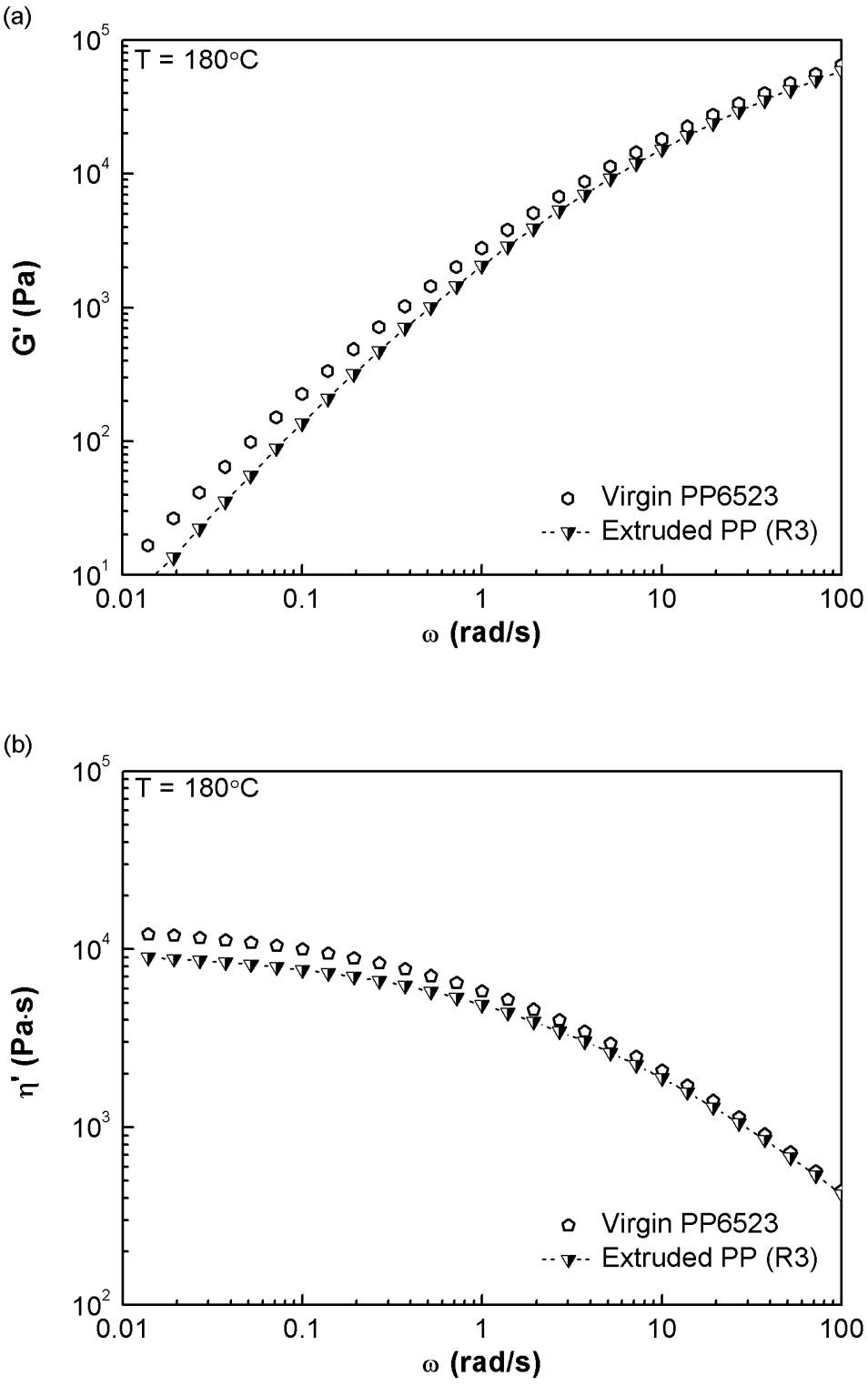

Figure 4.2 (a) Storage modulus and (b) dynamic viscosity of neat polypropylene and recycled polypropylene generated from the third cycle of extrusion.

The effects of reprocessing on the dynamic shear moduli and dynamic shear viscosity for PPNC1 and PPNC2 may be seen from Figure 4.3. The low frequency storage modulus was elevated after reprocessing and this is consistent with the improved dispersion of nanoparticles upon reprocessing in the two cases. There was some degradation of the polymer matrix upon reprocessing and this lowered the dynamic viscosity at the high frequency end by about 25% in both cases. Figure 4.4 presents a comparison of dynamic moduli before and after reprocessing for PPNC3 and PPNC4. The effect of reprocessing with silane here was to lower the dynamic shear storage modulus which is consistent with the poorer dispersion seen for this case. More specifically, the extent of bridging through site-attached polymer chains entangling with other free chains was reduced considerably. Furthermore, the dynamic viscosity curve for PPNC4 after reprocessing dropped by a factor of 4. This was largely due to the degradation of structure because the matrix viscosity dropped only by 25%, as estimated from the high frequency value and the average particle aspect ratio. The dynamic viscosity curve for PPNC3 after reprocessing was closest to the original curve indicating the least degradation of matrix for that case; this is related to the stability of the primary onium ion surfactant in the organoclay.

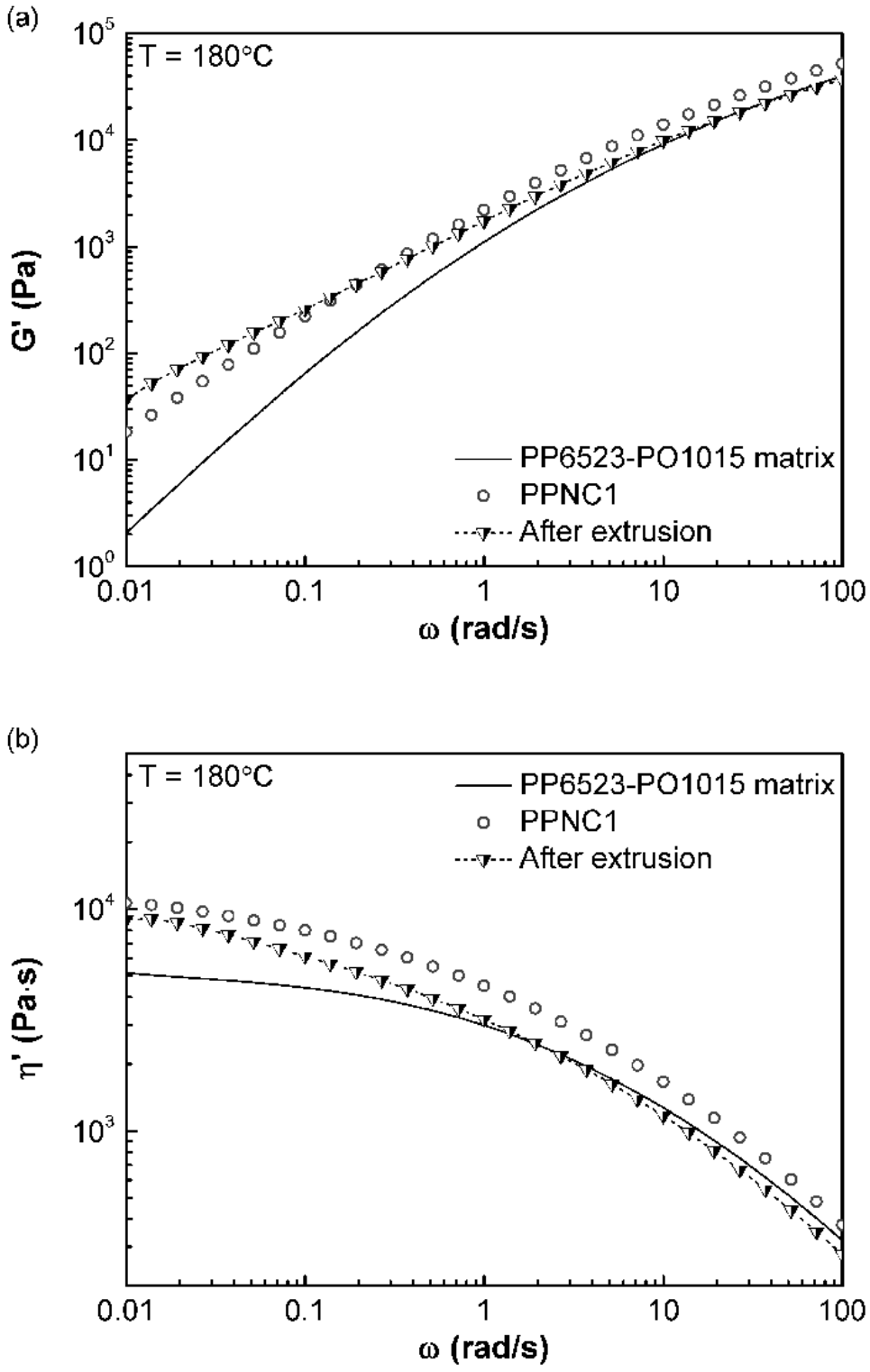

Figure 4.3 Storage modulus and dynamic viscosity of nanocomposites prepared with I.44P and silylated I.44P organoclay before extrusion and after extrusion.

Figure 4.3 (cont'd)

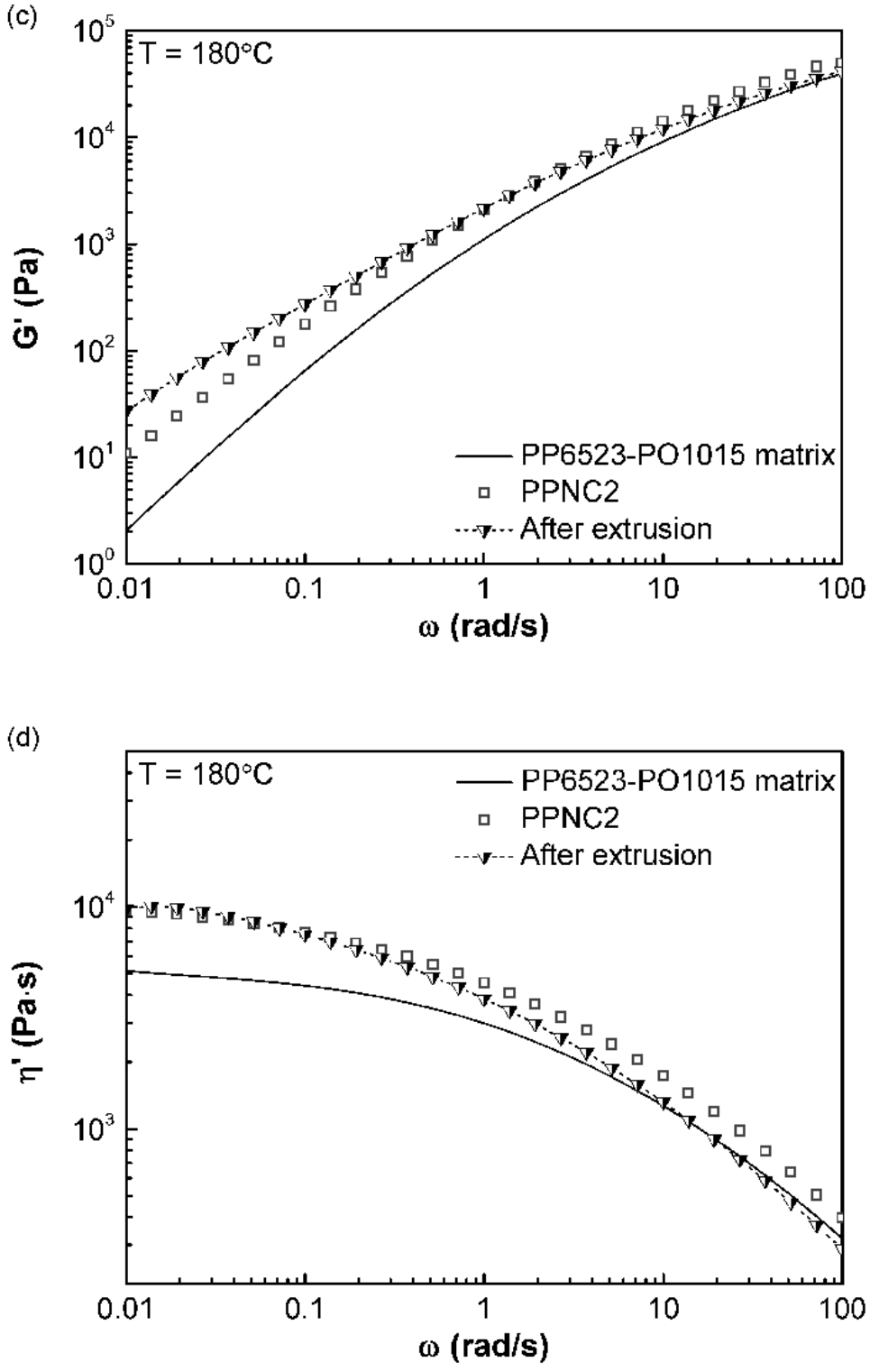

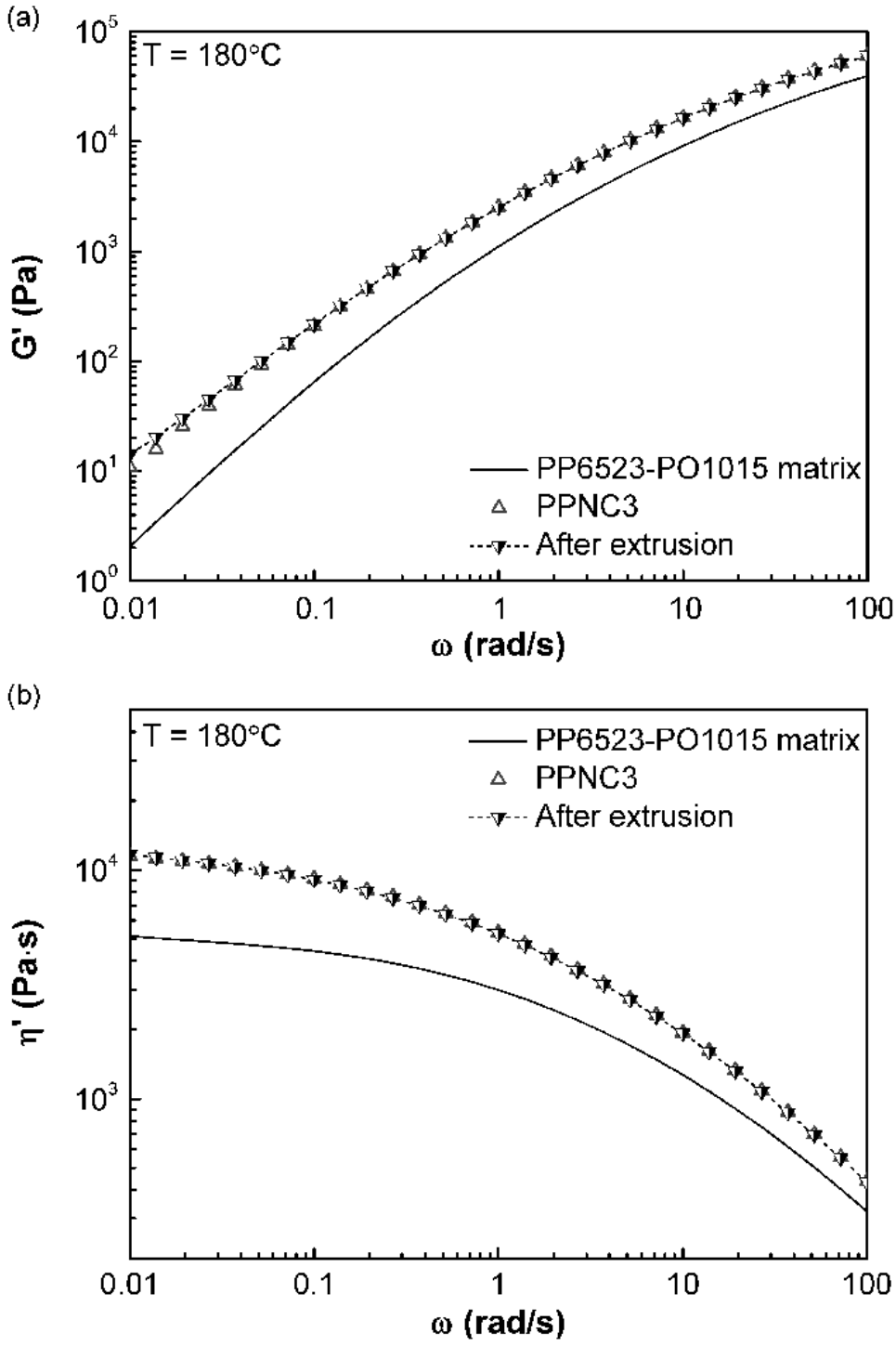

Figure 4.4 Storage modulus and dynamic viscosity of nanocomposites prepared with I.30P and silylated-I.30P organoclay before and after extrusion.

Figure 4.4 (cont'd)

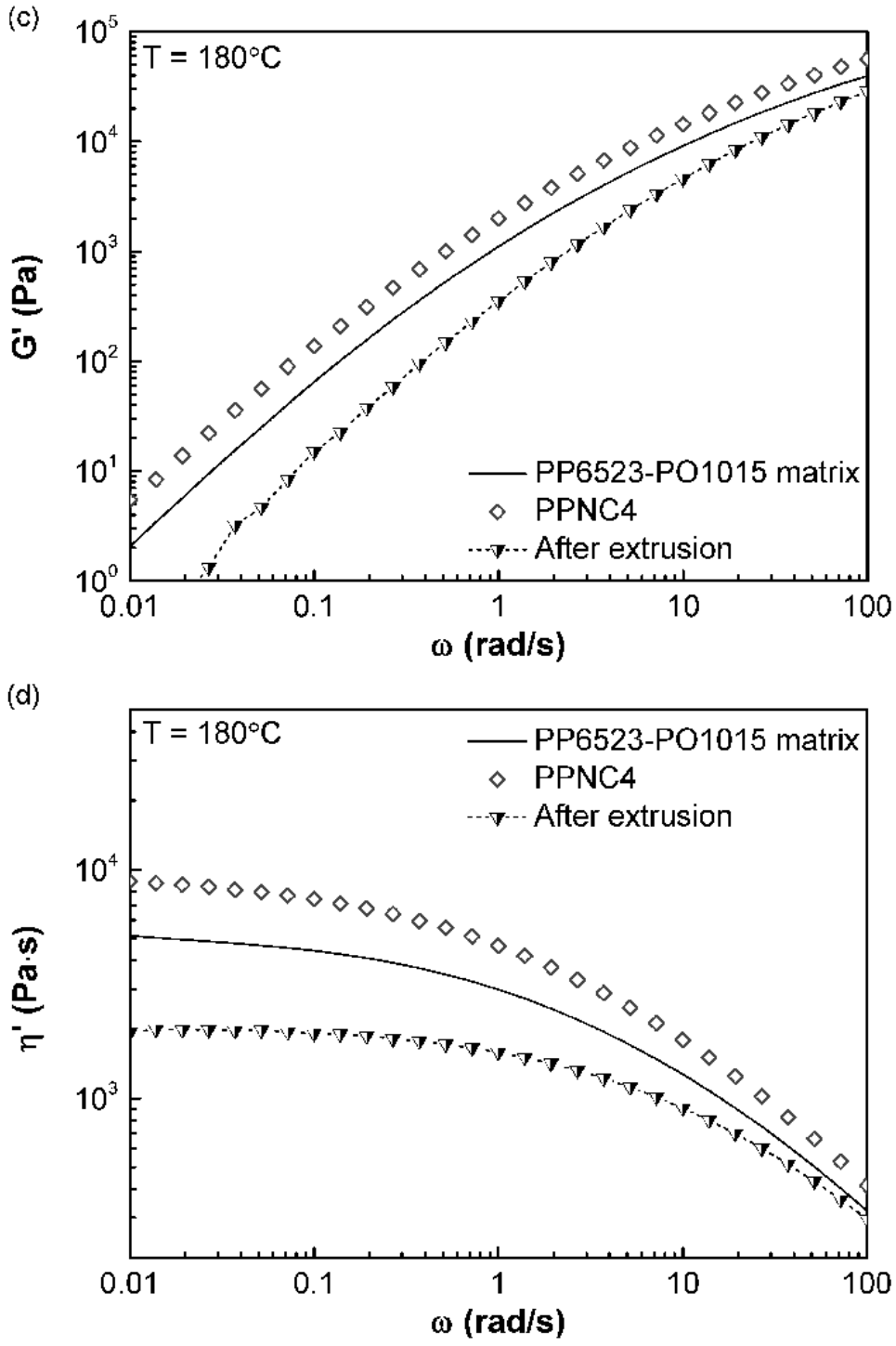

4.3.3 Transient Uniaxial Extensional Viscosity of Reprocessed Polypropylene and Nanocomposites

Figure 4.5 presents the uniaxial extensional viscosity transients of neat polypropylene before and after extrusion. Linear PP does not exhibit strain hardening behavior under uniaxial extensional flow. The extensional viscosity characterized under different strain rates all reached a steady state value. For reprocessed PP, a lower steady state extensional viscosity was obtained as a result of polymer degradation.

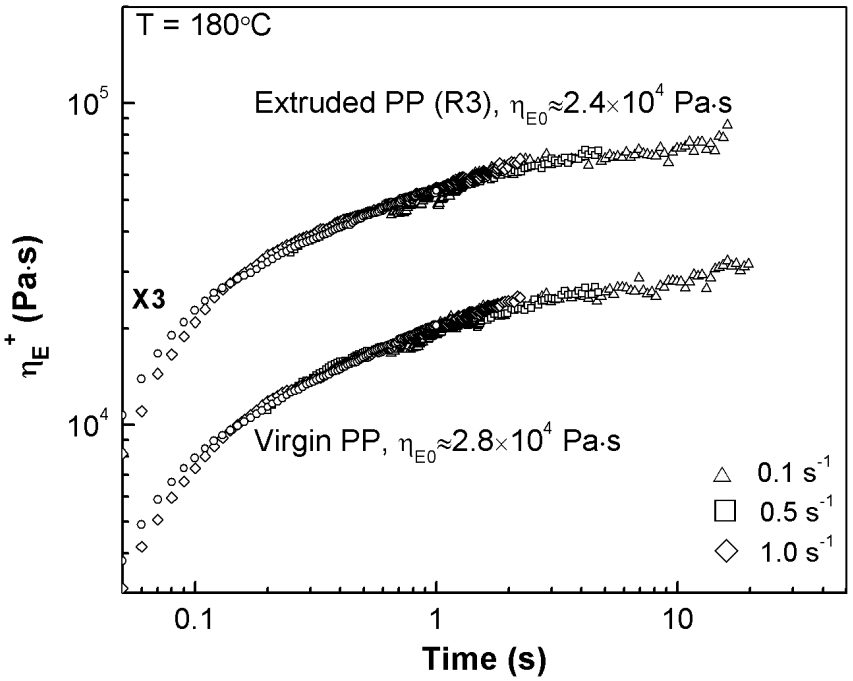

Figure 4.5 Uniaxial extensional viscosity transients (η_E^+) of neat polypropylene and recycled polypropylene generated from the third cycle of extrusion.

The effects of reprocessing on the extensional viscosity of nanocomposites have been presented in Figure 4.6 for PPNC1 and PPNC2 and in Figure 4.7 for PPNC3 and PPNC4. There was a drop of 15% to 30% in the maximum extensional viscosity magnitudes for PPNC1, PPNC2, and PPNC3 after reprocessing. This may be attributed to some loss of entanglements

both among free chains and between the free chains and particle-attached chains. The drop in extensional viscosity magnitudes was much more drastic for PPNC 4, between 70% and 90%. The strands of reprocessed PPNC4 broke at lower strains, and this was due to the degraded morphology.

The maximum strain hardening ratio χ_{max} dropped after reprocessing by about 0.5 over most strain rates for PPNC2 while the strain hardening ratio for PPNC4 dropped from near 3 to near 1 over most of the range. By contrast, the maximum strain hardening ratio was nearly unchanged for the other two nanocomposites without silane coupling. In the case of PPNC4, this effect may be attributed to a great reduction upon reprocessing, in the fraction of compatibilizer chains loosely attached to the face sites through the silanes; thus the slower relaxing entanglement network was lost. This led to loss of the strain hardening effect in the nanocomposite.

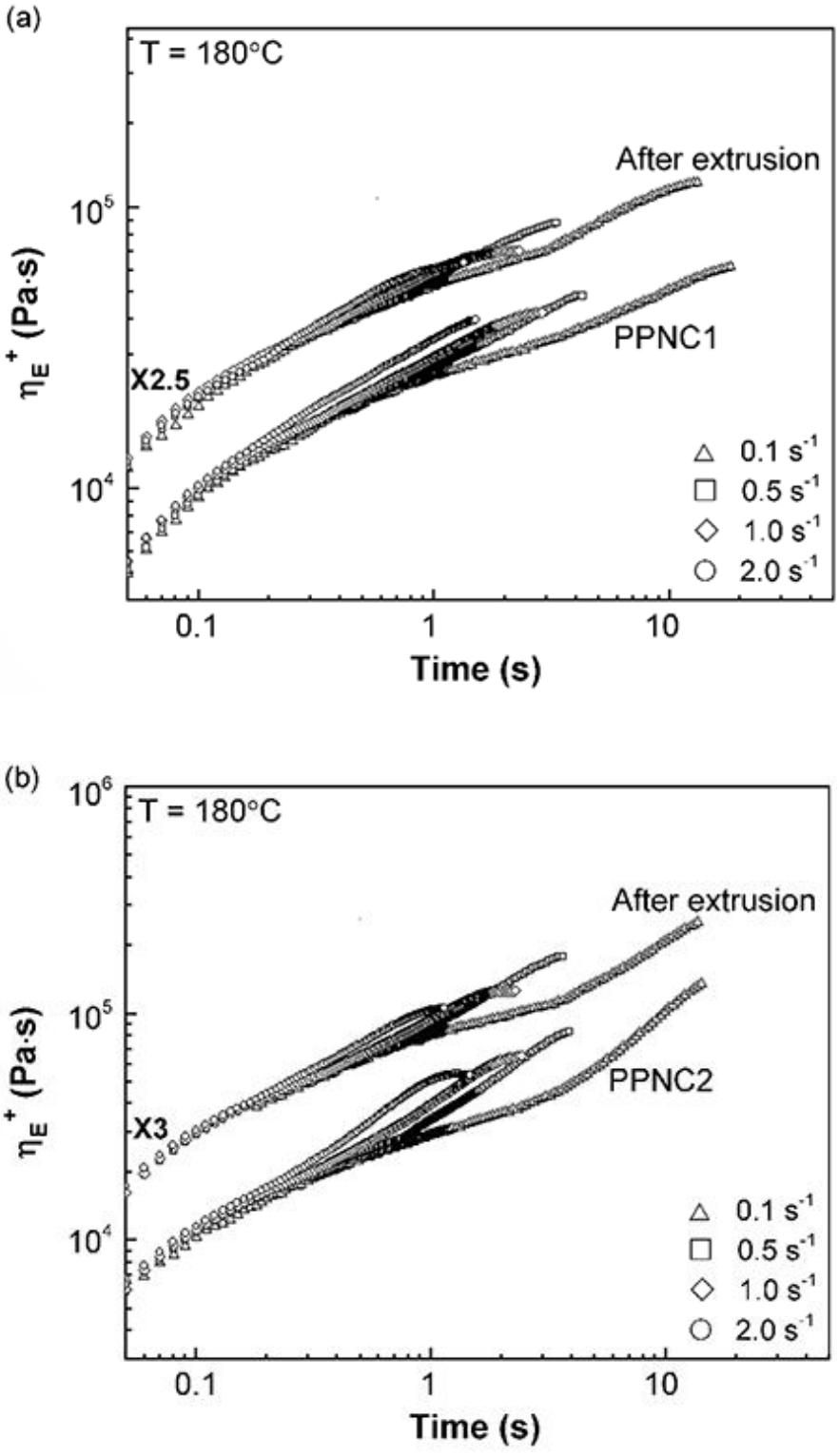

Figure 4.6 Uniaxial extensional viscosity transients (η_e) at several strain rates for nanocomposite melts with I.44P and silylated I.44P before and after extrusion.

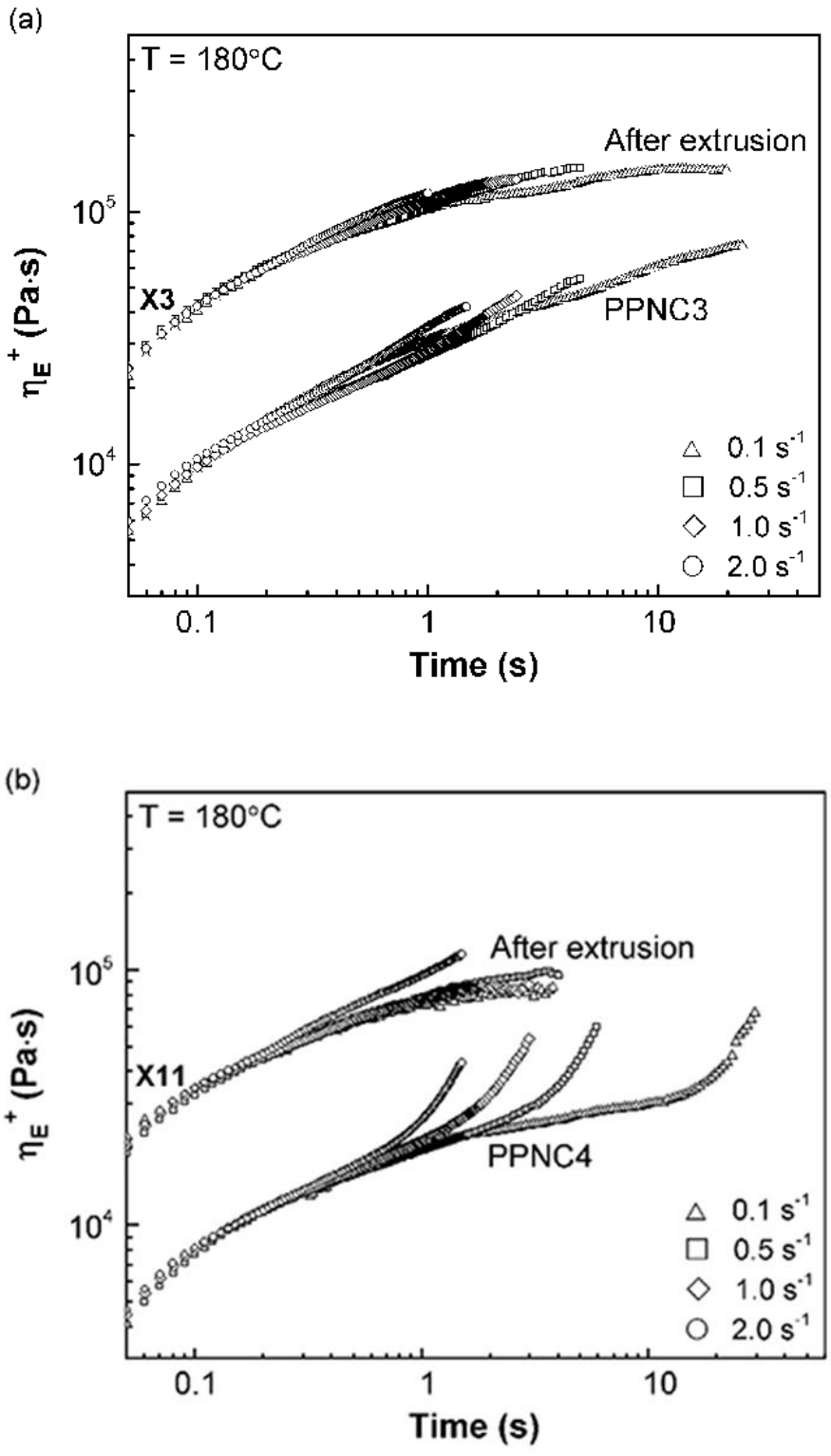

Figure 4.7 Uniaxial extensional viscosity transients (η_e) at several strain rates for nanocomposite melts with I.30P and silylated I.30P before and after extrusion.

4.3.4 Shear and Extensional Rheology of Masterbatch Containing Recycled Compounds

A masterbatch additive was prepared by melt mixing PO1015 PP-g-MA with aminosilane treated I.44P organoclay to boost rheological properties of recycled materials. The silane treatment in this study was carried out by a dry process. The results of XRD characterization for non-silylated and silylated I.44P have been presented in Figure 4.8. As discussed in Chapter 3, *d*-spacing of the aminoalkyldimethoxy silane treated I.44P via wet process was about the same as that of I.44P without silane treatment, indicating that silane reaction occurs at the edges alone of the I.44P. In contrast, the dry process for silane treatment led to an increase of *d*-spacing from 2.54 nm to 2.74 nm. This expanded interlayer spacing after silane treatment of organoclay has been reported as an indication of silane intercalation into the gallery faces of silicate layers[85]. Therefore, the dry process allows silane to functionalize both the edges and faces while in the case of wet process, only edges are modified for I.44P organoclay.

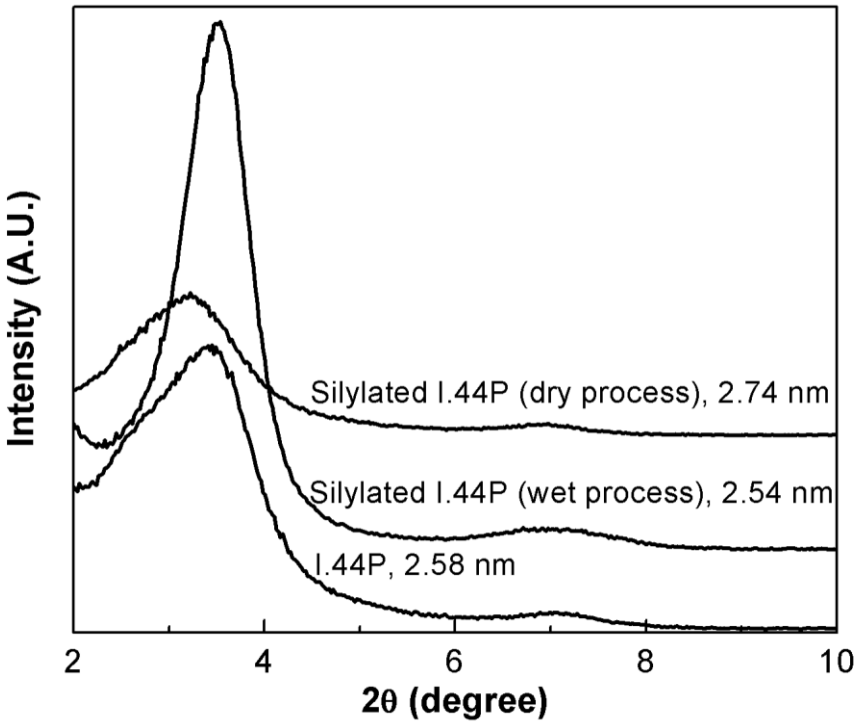

Figure 4.8 XRD patterns of non-silylated and silylated I.44P organoclay by wet process and dry process.

Figure 4.9 displays the TGA profiles of the I.44P and silylated I.44P organoclays obtained via different processes. The mass loss in the region of 200-500°C was due to the decomposition of organic portion of organoclay. The low organic content of organoclay after silane grafting from the wet process was attributed to the washout of some surfactants by the solvent during treatment[167]. For silylated organoclay based on the dry process, the residual mass of organoclay at T = 450 °C decreased from 69.3% for untreated I.44P to 68.2% for dry process silylated I.44P, indicating the presence of around 1 wt% silane after treatment. Meanwhile, there was no mass loss occurring below 220°C. This is in sharp contrast to the poor thermal stability of silylated I.30P, which exhibited a significant lower onset temperature for thermal decomposition as shown in Figure 3.3.

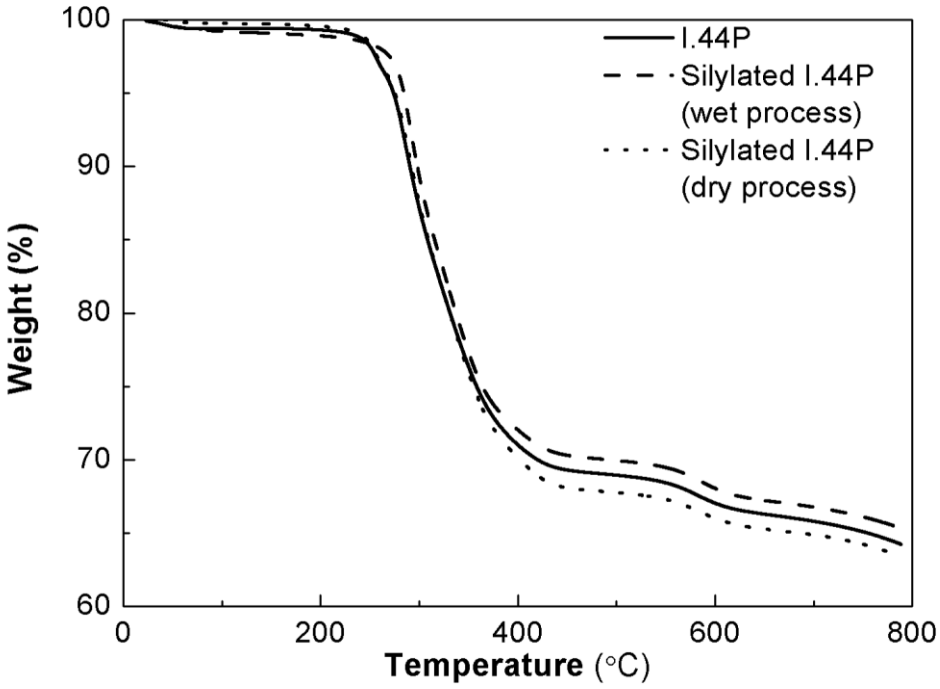

Figure 4.9 TGA of non-silylated and silylated I.44P organoclay by wet process and dry process.

15 wt% of the masterbatch, which composed of PP-g-MA and aminosilane treated I.44P from the dry process, was added to the recycled PP6523 as well as the reprocessed PPNC1 to boost rheological properties of these materials. As shown in Figure 4.10, the storage modulus and dynamic viscosity of recycled PP were elevated significantly with the addition of masterbatch, especially at the low frequencies. In boosted PPNC1, as shown in Figure 4.11, the strong shear thinning behavior in the dynamic viscosity curve and the appearance of a modulus plateau indicate the formation of a silicate network in the nanocomposites, due to the high overall nanoclay content of 8 wt%. The increase of storage modulus and dynamic viscosity at high frequencies for boosted compounds was attributed to the shear amplification effect[168], where the intrinsic strain of the polymer matrix becomes higher than the external strain because of the non-deformed nature of rigid particles.

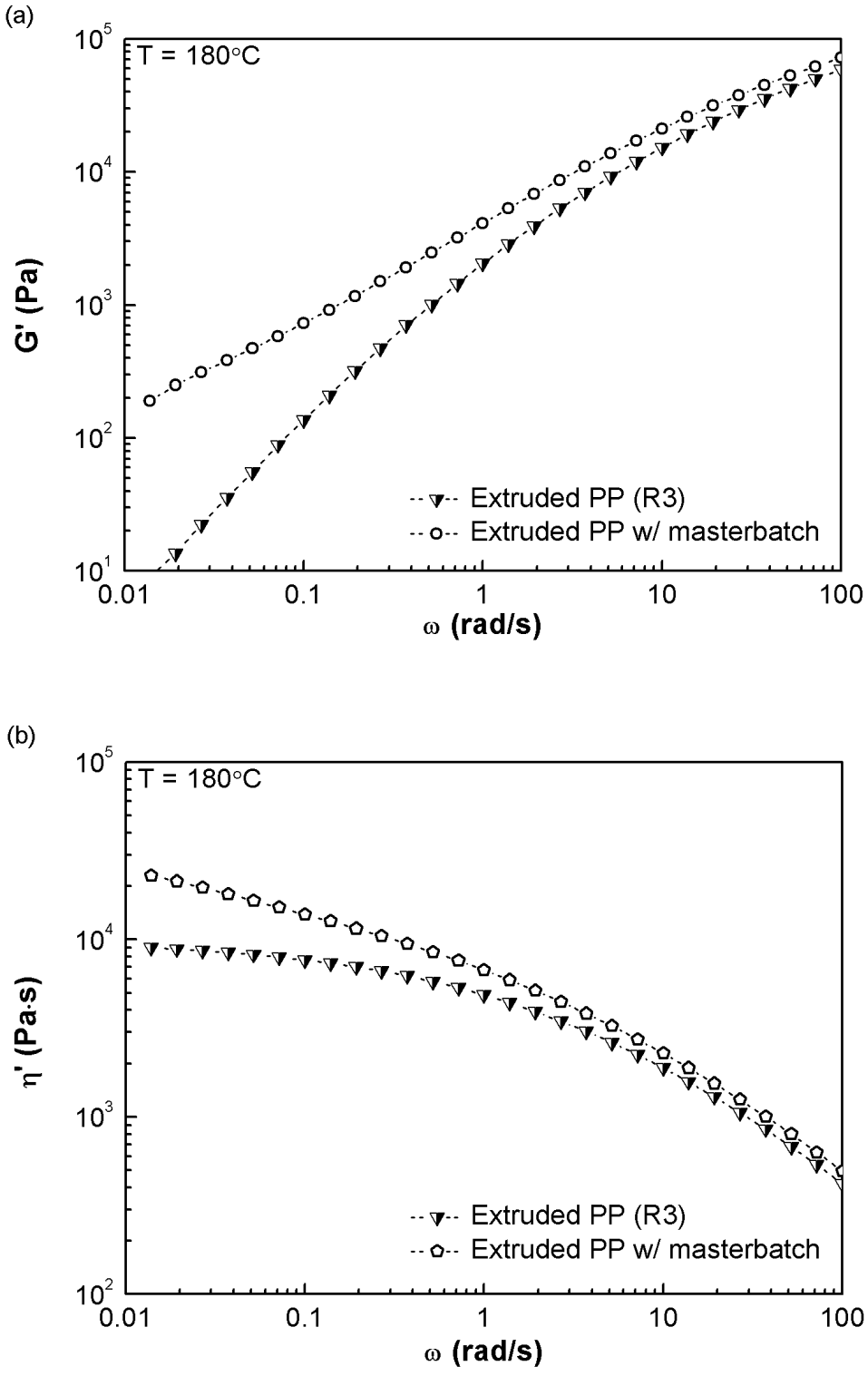

Figure 4.10 Storage modulus and dynamic viscosity of recycled polypropylene, reprocessed PPNC1 and their boosted nanocomposites containing 15 wt% masterbatch additive.

Figure 4.10 (cont'd)

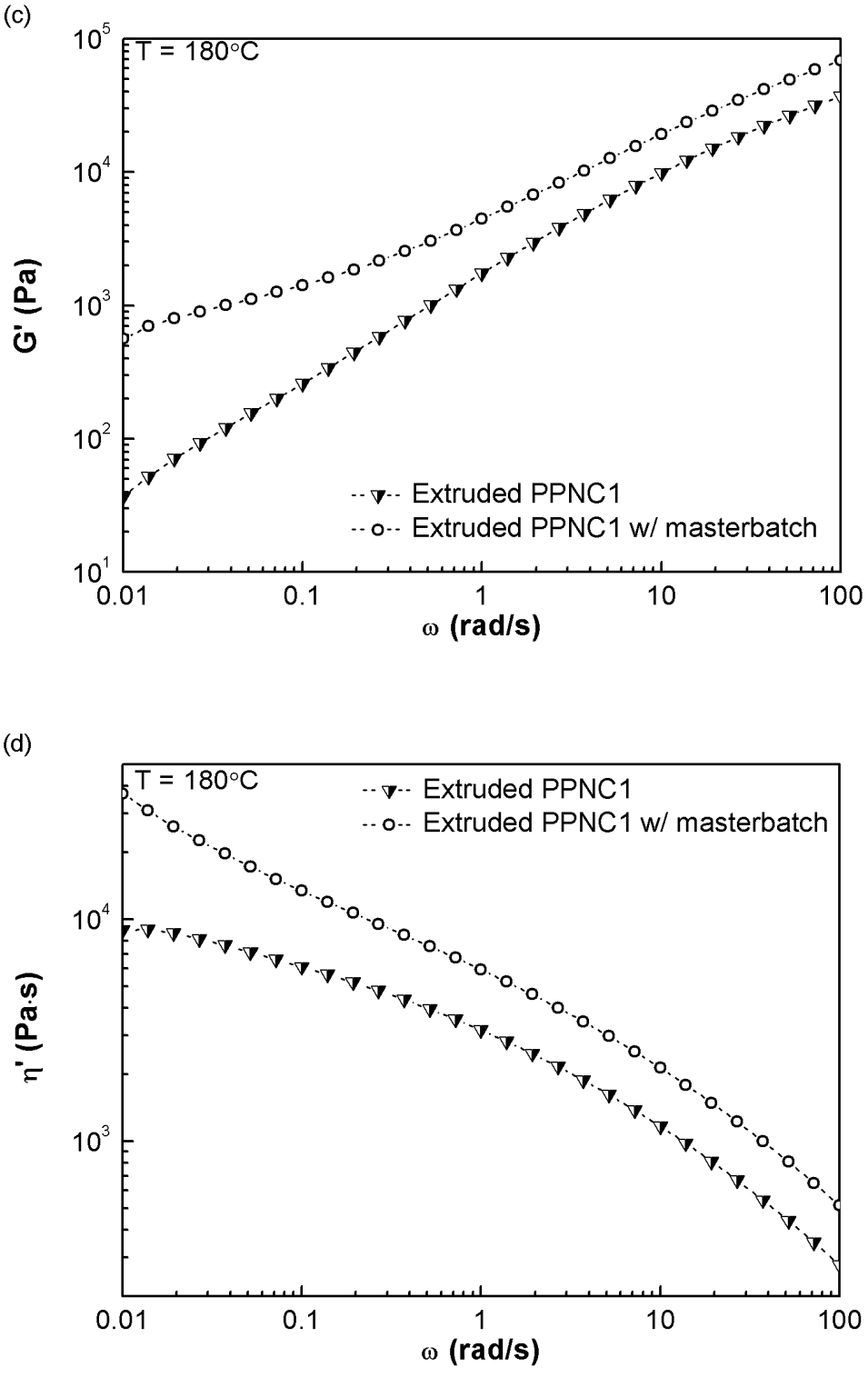

The uniaxial extensional viscosity of boosted PP and PPNC1 has been presented in Figure 4.11. The boosted PP displayed strong strain hardening behavior while the recycled PP melts didn't possess this property. The strain hardening behavior of reprocessed PPNC1 was greatly improved by the incorporation of masterbatch and became even stronger than that of the original nanocomposite. Because of chain scission during reprocessing, the entanglement density of polymer chains was lowered. In boosted compounds, the attractive polymer-particle interactions lead to supplementary entanglements with slower relaxation time formed between particle attached chains and bulk polymer chains[154], which is responsible for the remarkable strain hardening behavior.

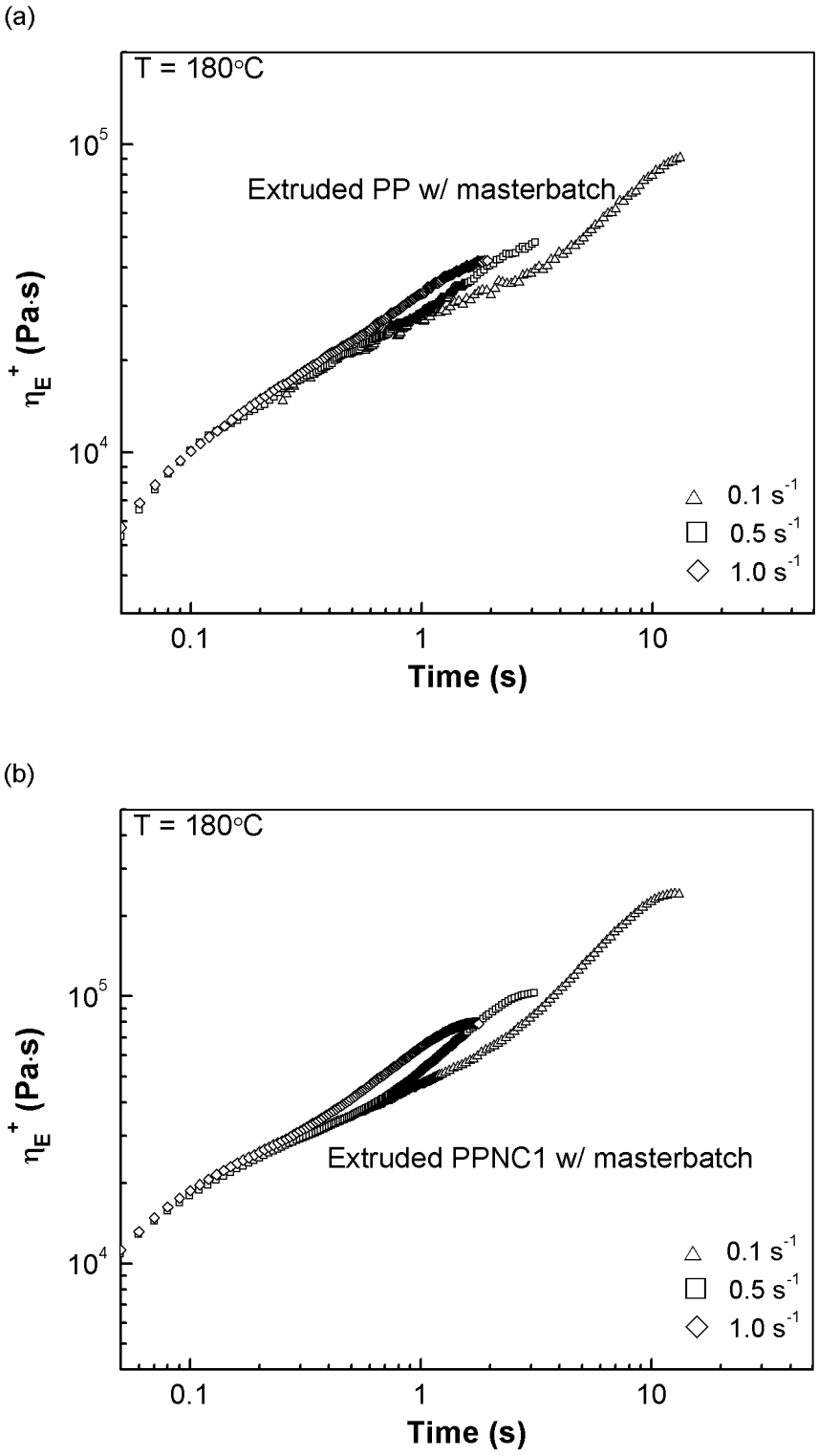

Figure 4.11 Uniaxial extensional viscosity transients (η_E^+) of boosted nanocomposites containing 15 wt% masterbatch additive.

4.4 Conclusions

Reprocessing of linear polypropylene and polypropylene-organoclay nanocomposites by extrusion led to degradation of polymer chains. Some improvements in the state of clay dispersion were obtained in reprocessed nanocomposites prepared with non-silylated organoclays. When the silanes were reactively coupled only to the edge sites of the layered silicates, the nanostructure was stable and the polymer enhanced filler network was strengthened. When the silanes were presented at both gallery faces and edges, the network of entanglements between particle attached chains and free chains was weakened considerably upon reprocessing. Severe degradation of both morphology and strain hardening behavior, as evidenced by the formation of particle agglomerate and 70% to 90% drop in extensional viscosity magnitudes, respectively, were observed. This was caused by the low thermal stability of loosely held silanes from the gallery face sites of I.30, which separated from the nanolayers upon reprocessing along with the bonded compatibilizers.

The incorporation of 1 wt% silane in I.44P through a dry process led to coupling at both edges and gallery faces, without sacrificing the thermal stability of organoclay. When a masterbatch composed of PP-g-MA and the silylated I.44P was prepared and added to the reprocessed PP and I.44P organoclay based nanocomposite, rheology of the resulting compounds in both dynamic shear and uniaxial extensional flows was improved well beyond the original compounds. These improvements may be attributed to additional entanglements between particle attached chains of the additive and the bulk polymer chains.

CHAPTER 5

STRUCTURE AND PROPERTIES OF BLOWN FILMS FROM POLYPROPYLENE-CLAY NANOCOMPOSITES WITH SILANE COUPLING

5.1 Introduction

The film blowing process involves biaxial stretching of the polymer melt under extensional flow and it is important to have sufficient strain hardening for good processability. While molten linear polypropylene exhibits no strain hardening in extensional flows, this property can be obtained by adding long chain branched polypropylene (LCB-PP)[31, 32]. Blown films of the blends have been demonstrated with improved bubble stability, thickness uniformity and maximum solid output[11, 26, 27, 29]. The addition of branched polypropylene could also alter mechanical properties of the blown films. For example, Fang et al.[24] reported a severe drop in tensile strength of blown film along machine direction after incorporating a branched PP of lower molecular weight into linear PP. This was attributed to the reduced density of tie chains for the crystalline structure of the films. A drastic deterioration of elongation to break along the transverse direction of films from the blends was also observed.

The incorporation of organically modified nanoclay in polypropylene has also been used to prepare blown films. This is benefit because of the effect of organoclay on inducing strain hardening behavior[85, 86, 88, 90] as well as modifying the physical properties of the films. The effectiveness of reinforcement by organoclay depends strongly on its dispersion and interactions with polymer matrix. Without the use of compatibilizer, deterioration of mechanical properties has been reported in films blown from polypropylene-clay nanocomposites based on linear isotactic polypropylene as the matrix[79, 169]. On the other hand, blown films from

nanocomposites with strengthened polymer-particle interactions in the presence of maleic anhydride grafted PP have been reported to possess a higher Young's modulus, and tensile strength[81, 170]. But the enhancement of strength generally correlates with a drastic sacrifice of elongation to break value, especially along the transverse direction.

Melt compounding of nanoparticles with polymers can be facilitated by pre-compounding a masterbatch containing a high loading of nanoparticles[171]; the masterbatch can then be added to the bulk polymer in a let-down stage. In the case of polyolefins and organoclay or organically modified montmorillonite, the masterbatch must include a functionalized polyolefin compatibilizer[103, 104]. It has been reported that nanocomposites prepared with the masterbatch led to better clay dispersion, even for small values of compatibilizer to clay ratio. Because of the low molecular weight nature of compatibilizer, this low compatibilizer to clay ratio is essential in achieving enhanced physical properties of the final products. Additional treatment of the organoclay with silane coupling agents[172] leads to improved dispersion[123] and improved mechanical properties[173] and in some cases, enhanced processability in the form of greater strain hardening of the melt in extensional flows[90]. Recent results from our laboratory[85] have shown that when the silane penetrated the interlayer galleries and provided reactive coupling to the polymeric compatibilizer at the faces as well, the uniaxial extensional viscosity displayed a greater extent of strain hardening. The silane treatment in the previously reported work was carried out by a wet process in a methanol-water mixture and could not uniformly provide this penetration of galleries in all cases - particularly the organoclay that had a greater interlayer packing of quaternary onium ion surfactant with two alkyl tails. An alternative vapor phase treatment process has been reported in the literature to provide greater penetration of silane in the interlayer galleries[166].

Hence the objective of the research reported here was to use a solvent-free process for silane treatment of a montmorillonite that was ion exchanged with quaternary onium ion surfactant; to incorporate the resulting product in a masterbatch for preparation of polypropylene nanocomposite blown films, and examine the rheology, film blowing processability, film morphology and mechanical properties. The following sections show that the masterbatch additives formulated here lead to improved rheology and processability for film blowing and also yield films with more uniform thickness as well as greater mechanical properties.

5.2 Experimental Details

5.2.1 Materials

The film grade polymer PPC300.4 from Spartan Polymers Inc. was a propylene-ethylene block copolymer with 12 to 15 wt% ethylene and had a melt flow index of 0.45 g/10 min (230°C/2.16kg). Maleic anhydride grafted PP (Exxelor PO1015 from ExxonMobil) was used as compatibilizer. The organoclay used was Nanomer I.44P from Nanocor, which has a quaternary onium ion surfactant with two C18 tails. The silane coupling agent was aminoalkyldimethoxy silane, from Evonik Industries, which react with the anhydride group of the PP-g-MA to form an amide or imide linkage.

5.2.2 Processing and Characterization

Two different silane treatment processes were used for this study: a wet process and a dry process. Silylated organoclay based on the dry process was used to make the masterbatch for most nanocomposites. The nanocomposites were prepared by melt compounding in a Leistritz, co-rotating twin-screw extruder (diameter = 27 mm, L/D = 48) with a screw speed of 250 rpm at 190°C. A two-step process involving adding masterbatches to bulk polymer in a “let-down”

operation was used. The detailed compositions of various compounds are shown in Table 4.1. Both PPC300 and nanocomposites were blown into 1 mil thick films with a blow-up ratio of 3.2.

Table 5.1 Compositions of different nanocomposites.

Designation		PP C300 (wt%)	PO1015 (wt%)	Silylated I.44P (wt%)
Masterbatch	MB1	20	53.3	26.7
	MB2	20	48	32
Let-down	PPNC6	85	10	5
	PPNC7	76	16	8
	PPNC8	80	12	8

The clay powder was characterized for XRD and TGA analysis to study the effect of silane treatment via different approach on its interlayer spacing and organic content, respectively. Compression molding by a hydraulic press was used to make composite specimens for TEM analysis and rheological characterizations. Dynamic shear tests were carried out on a TA Instruments AR2000 Rheometer with parallel plates of diameter 40mm over a frequency range from 0.01 to 100 rad/s at 200 °C under nitrogen flow. A fixed strain of 1 %, which was confirmed to be within the linear viscoelastic regime, was used in all cases. The melt extensional viscosity of the nanocomposites was measured at 200 °C using a Sentmanat Extensional Rheometric fixture (SER-2) mounted on a TA-ARES instrument and at four strain rates (0.1, 0.5, 1.0, and 2.0 s^{-1}) over Hencky strains up to 3. The test temperature was changed for the Profax 6523 based compounds to 180°C.

The film thickness was recorded at various points across the width of the film with a TMI digital micrometer. Eighteen positions were measured for each film at a distance of 1.5 cm and the standard deviation (SD) value was calculated for each material. Tensile properties of the

blown films at both machined direction (MD) and transverse direction (TD) were evaluated with an Instron Universal Testing Machine model 5565, based on ASTM-882. The tear resistance of blown films was tested based on ASTM D1922 with Elmendorf Tearing Tester. Because of the thickness non-uniformity as will be discussed below, the film samples used for mechanical test were selectively cut to have a mean thickness of 25 mm. Measurements on five different specimens were averaged for each compound. The refractive indices of blown film along MD, TD and normal direction (ND) were measured using a Metricon Prism Coupler Model 2010/M with an accuracy of $\pm$ 0.0005. The birefringence was then calculated as the difference in refractive index between two orthogonal directions. The crystal structure and orientation of layered silicates in blown films were characterized with ZEISS Field Emission Scanning Electron Microscope (FESEM) at an accelerating voltage of 20 kV. Samples were prepared for viewing by sputtering with a layer of 1 nm tungsten. Transmission Electron Micrographs were also obtained for nanocomposite blown films sliced by the TD-ND plane to investigate the particle orientations. The details of all the preparation and characterization procedures were provided in Chapter 2.

5.3 Results and Discussion

In this study, silylated I.44P organoclay from dry process was used as the nanofiller for preparing polypropylene nanocomposites and blown films. The loss of surfactants for silylated I.44P from wet process makes it the less compatible with the polypropylene matrix than the one based on dry process. Also, it has been demonstrated that organoclay with silane functionalization occurring at both faces and edges, as in the case of the silylated I.44P from dry process, led to a better nanocomposite compound in terms of rheological properties and particle dispersion[85].

5.3.1 Characterization of Polypropylene Nanocomposites

The dispersion of silylated clay from dry process in nanocomposites was characterized by TEM and the micrographs have been shown in Figure 5.1. It appears that most clay particles were exfoliated and well dispersed in polymer matrix. The amine functional groups presented on the silane treated clays can react with the anhydride group of the PP-g-MA, forming covalent bonding, and this level of interaction leads to strong particle exfoliations. Also, as seen from Table 4.2, the mean stack thickness of nanolayers was about 5 to 6 nm when a compatibilizer loading to clay ratio of 2:1 was used. This value increased slightly for PPNC8 with the ratio being 3:2. which is consistent with the appearance of thick stacks of organoclay particles as seen in Figure 3(c).

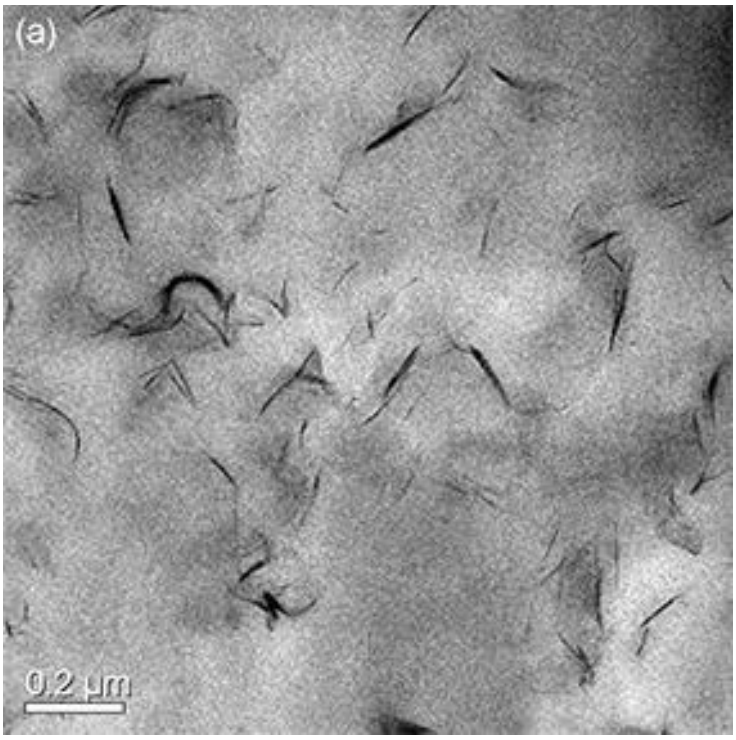

Figure 5.1 TEM micrographs of the extruded compounds: (a) PPNC6 (b) PPNC7 and (c) PPNC8.

Figure 5.1 (cont'd)

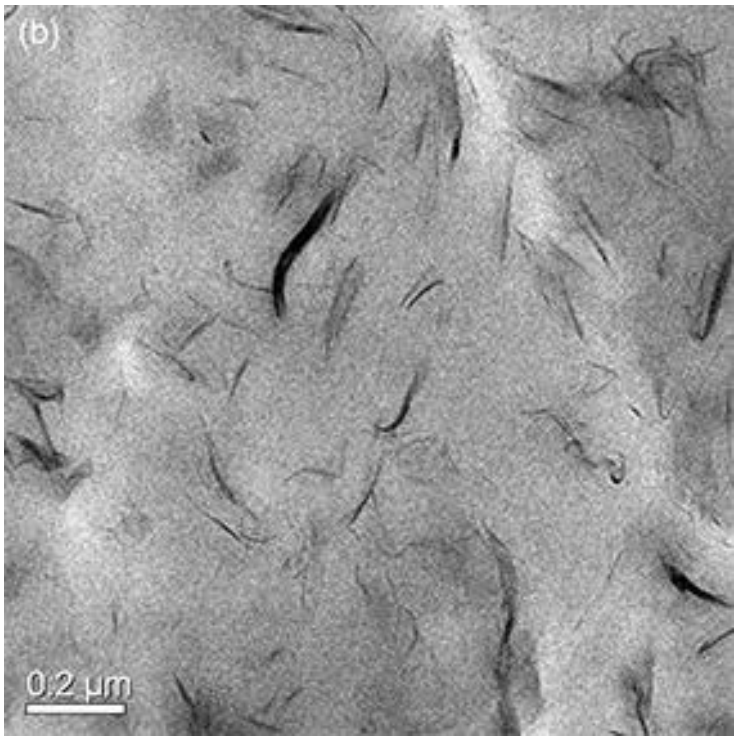

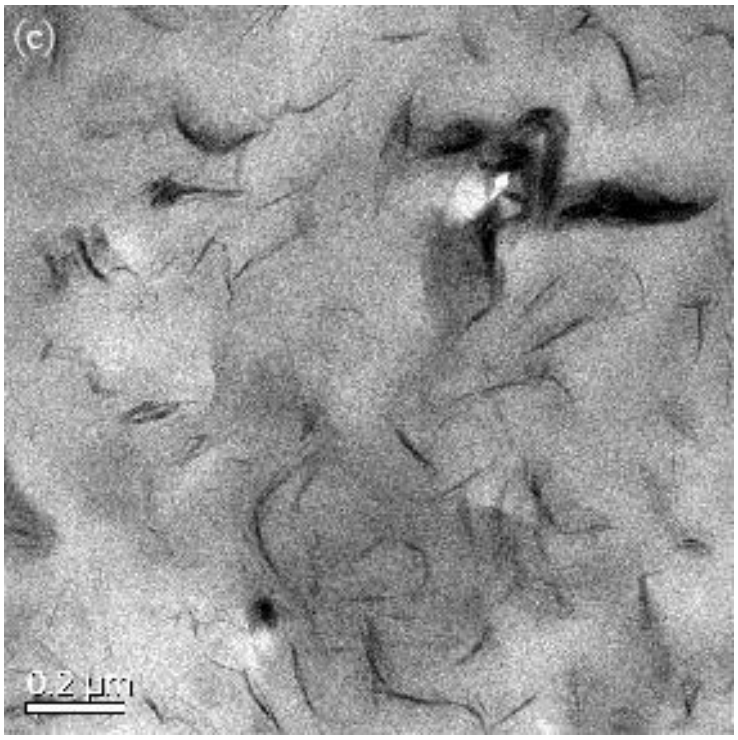

Table 5.2 Estimated mean particle thickness for nanocomposites before and after reprocessing.

Compound	Silylated clay loading	Ratio of PP-g-MA to clay	mean particle thickness (nm)
PPNC6	5 %	2:1	5.2
PPNC7	8 %	2:1	5.8
PPNC8	8%	3:2	6.7

Linear viscoelastic behavior at low frequencies -- especially of the storage modulus curve can be used to infer the effect of the polymer-particle interactions for nanocomposite melts. The frequency-dependent dynamic shear storage modulus and dynamic viscosity for PPC300 and nanocomposites melts have been plotted in Figure 5.2. The nanocomposites displayed increased storage modulus and dynamic viscosity comparing with the PPC300 and more so for the ones with 8 wt% of organoclay. This is a result of retarded chain relaxation and bridging between silicate layers by entangled chains in the bulk as well as attached to nanoclays.

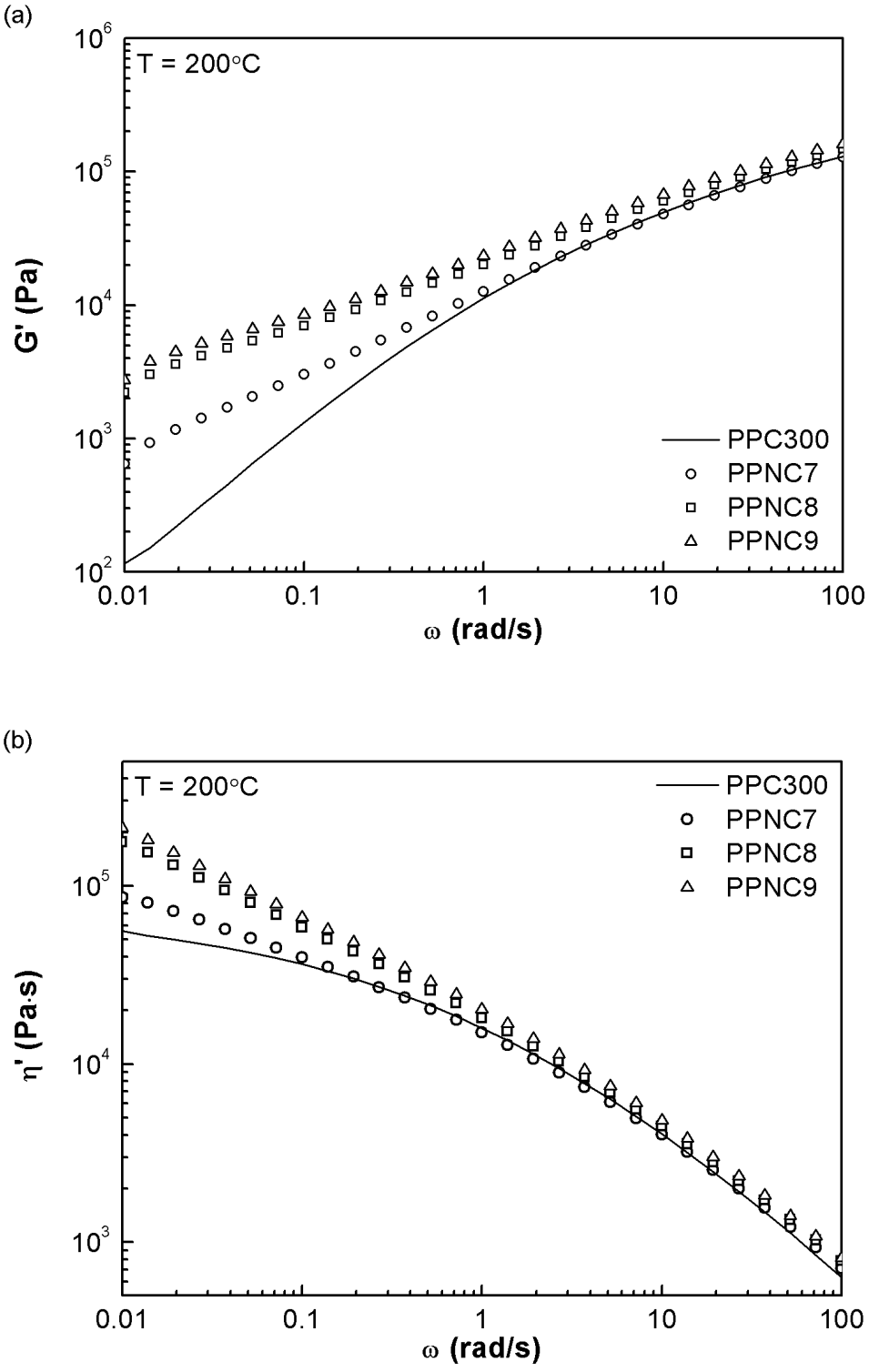

Figure 5.2 (a) Storage modulus curves and (b) dynamic viscosity curves for neat PP C300 and nanocomposites prepared with silylated I.44P by dry process.

The presence of strain hardening in uniaxial extensional flow of molten polymer is an important rheological property for film blowing process. The uniaxial extensional viscosity transients of neat PP and nanocomposite melts at strain rates of 0.5 and 1.0 s^{-1} with a maximum specified Hencky strain of 3 have been presented in Figure 5.3. While the linear PP used in this study didn't display strain hardening, the incorporation of PP-g-MA of high molecular weight and silylated organoclay from dry process led to a strong strain hardening behavior. This is caused by the trapped entanglement network involving the particle-attached compatibilizer chains at surfaces and edges of organoclay and the free polypropylene chains. The strain hardening ratio at maximum strain (χ_{max}) was evaluated between the actual value of extensional viscosity and the value on the baseline curve extrapolated from the initial linear portion. The resulting (χ_{max}) values have been tabulated in Table 3. It is seen that the maximum strain hardening ratio for PPNC6 was around 2.5 at both strain rate. This value decreased when more organoclay was added as in PPNC7. When lower amount of compatibilizer was used, PPNC8 displayed the lowest strain hardening ratio.

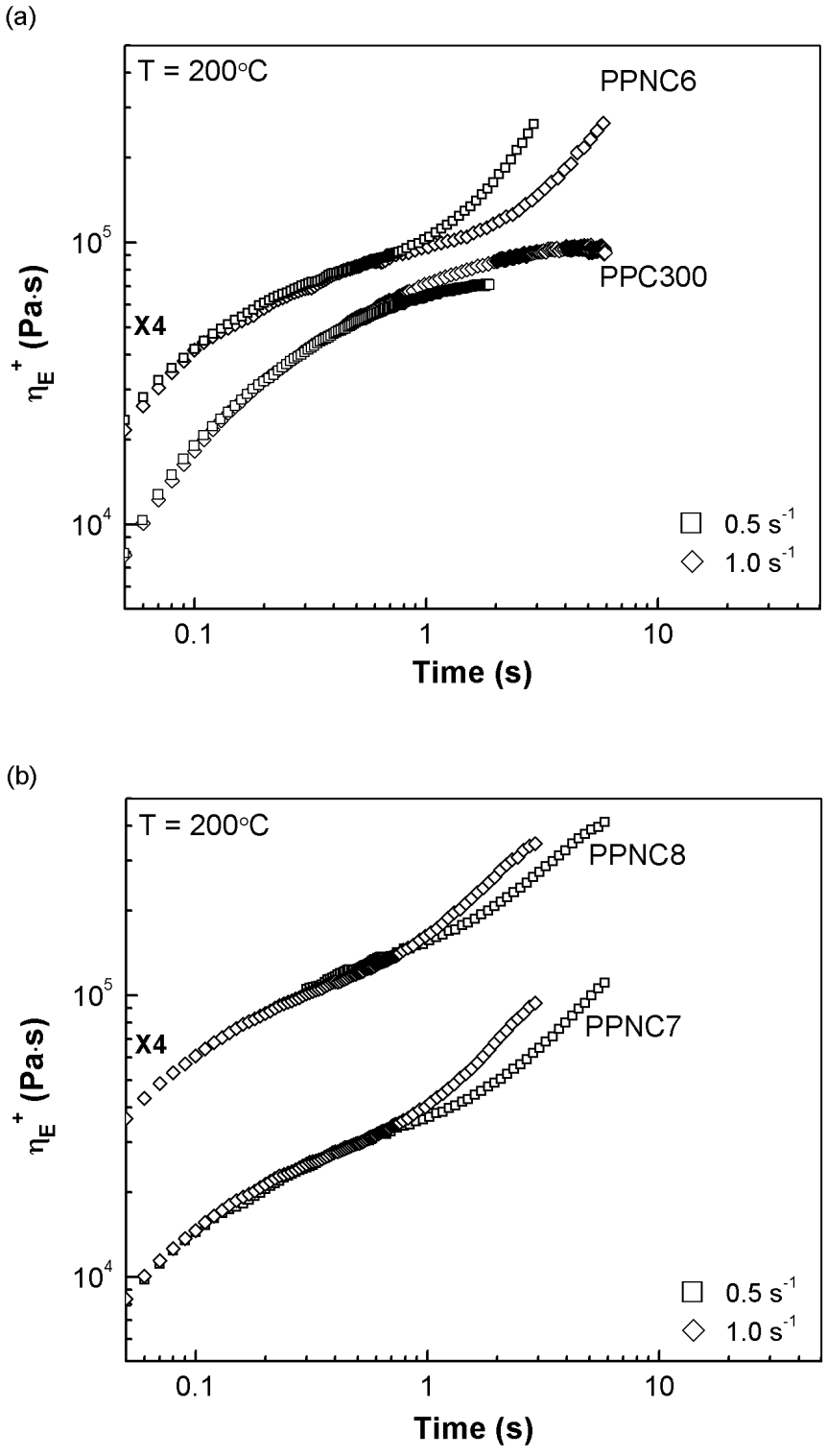

Figure 5.3 Uniaxial extensional viscosity transients (η_E^+) at several strain rates for neat PPC300 and nanocomposites prepared with silylated I.44P.

Table 5.3 Maximum strain hardening ratio at strain of 3 for polymer melts at 200°C

Strain rate (s^{-1})	**Strain hardening parameter @ ε_H = 3.0**			
	PPC300	PPNC6	PPNC7	PPNC8
0.5	NA	2.58	2.08	1.89
1.0	NA	2.55	2.36	2.16

5.3.2 Characterization of Blown films

In Figure 5.4, the film thickness variation is plotted against the positions along the circumference with the standard deviation values displayed in each graph. All nanocomposites films showed improved thickness uniformity comparing with neat PP film. This improvement of blown films homogeneity has been reported to correlate with the presence of strain hardening behavior under uniaxial extensional flow by the so-called "self-healing mechanism"[27]. The thin portion of a stretched film that experiences a large elongation induces a high extent of strain hardening as well as elongation viscosity. As a result, it would exhibit a stronger resistance to further deformation comparing with the thick portion. With the same organoclay content (8 wt%), nanocomposite with higher PP-g-MA to clay ratio (2-1) possessed better thickness uniformity. This is consistent with the comparison of maximum strain hardening ratio shown in Table 2, as strong strain hardening behavior leads to better thickness uniformity of blown films. When the PP-g-MA to clay ratio of 2-1 remained the same, nanocomposite with 5 wt% clay displayed a slightly worse thickness uniformity than the one with 8 wt% clay, as a result of larger η_E ($\dot{\epsilon_0}$;t) values when more clay was added for the latter case.

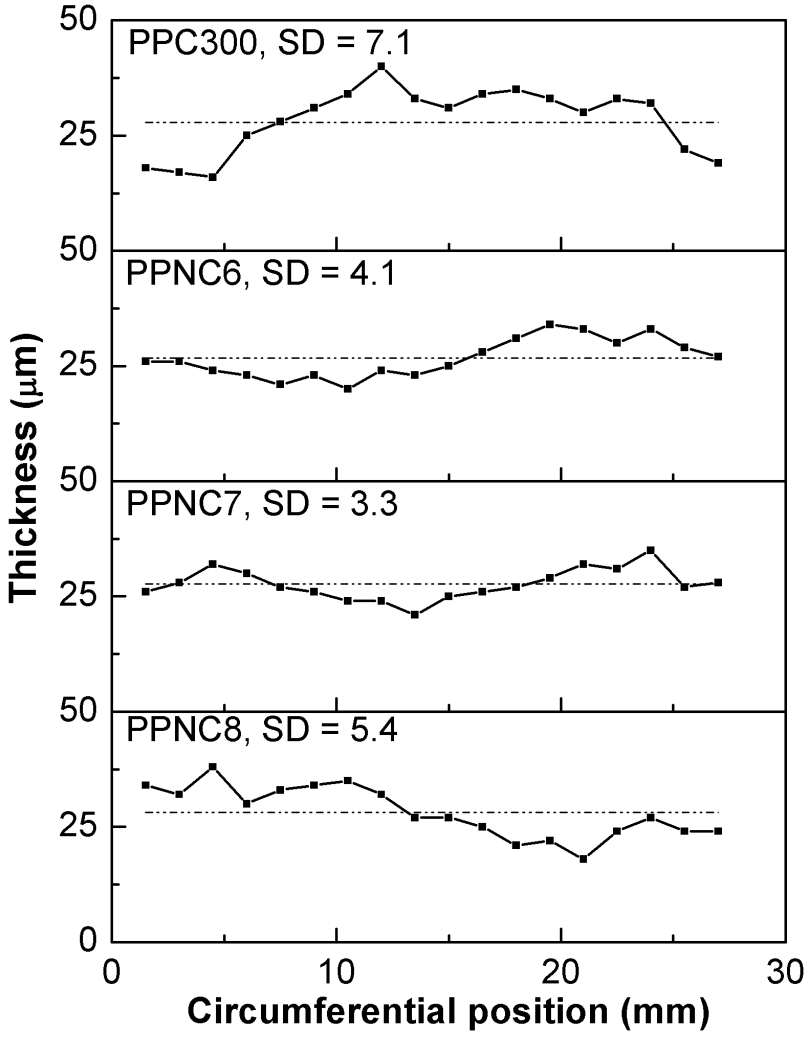

Figure 5.4 Thickness variation in neat PPC300 and nanocomposite blown films. Dash lines represented the mean thickness of each film.

The crystalline structure of isotactic polypropylene (i-PP) exists in a monoclinic α-form with adjusted orthogonal crystal axes labeled, *a**, *b*, and *c*[9, 10]. Under quiescent condition, the crystalline domains of i-PP are typically cross-hatched or comprised of so-call parent and daughter lamellae. In the film blowing process, the crystal structure of polypropylene could be altered. The crystal structure in various blown films in this study was first characterized with

FESEM. The micrographs for PPC300 film under two different magnifications have been presented in Figure 5.5. It can be seen that a majority of the crystal lamellae formed stacks and aligned mostly along MD. More importantly, no noticeable cross-hatching structure was observed. In the film blowing process, polymer chains orient first along the machine direction as a result of drawing stress. The formation of stack lamellar structure has been attributed to the growth of lamellae perpendicular to the drawing direction, from the elongated chains acting as nuclei[37]. Roozemond et al.[174, 175] developed a model to quantify the parent to daughter crystal ratio in polypropylene under flow condition. It was reported that the extensional flow increased the parent to daughter ratio, as a result of the accelerated the growth rate of stacked lamellae as parent crystals while that of the daughter crystal remained the same as under quiescent condition. Hence, the growth of parent crystals dominates under extensional flow, which weakens the formation of cross-hatching structure as in the PPC300 blown film shown in Figure 5.5.

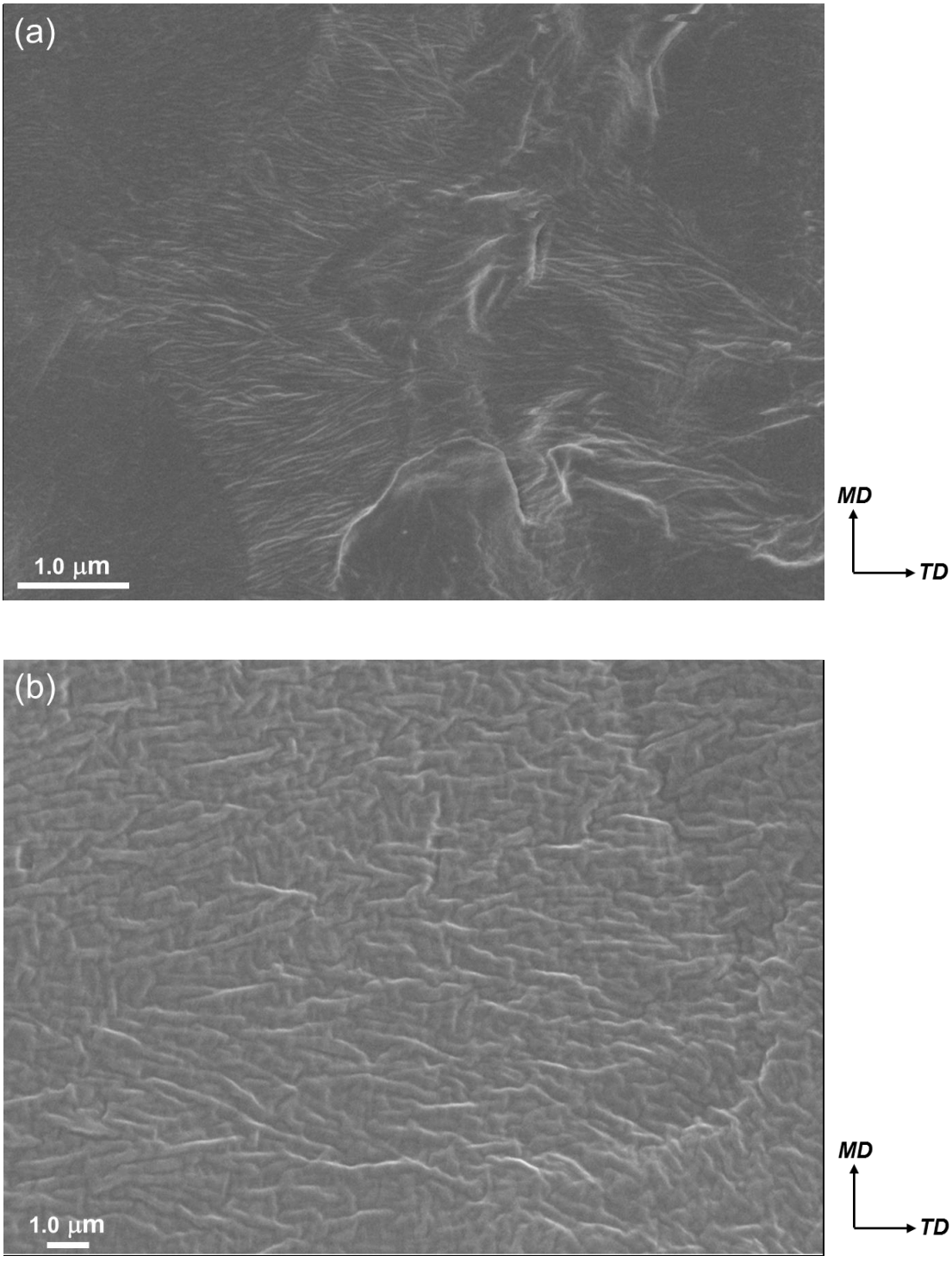

Figure 5.5 Lamellar orientation in PPC300 blown film: (a) low magnification and (b) high magnification.

Next, the crystalline structure of nanocomposite films has been presented in Figure 5.6. In sharp contrast with PPC300 films, blown films from nanocomposites displayed a dominant cross-hatching structure with the lack of lamellar orientation. Since the parent to daughter ratio in polypropylene depends on the relative growth rate between parent crystals and daughter crystal, the existence of cross-hatching structure in nanocomposite films was attributed to the reduced growth rate of the parent crystal in the presence of nanoclay particle. It is known that well dispersed nanoclay layers can act as heterogeneous nuclei. With silane existing at both the faces and edges of our nanoclay, the polypropylene matrix is strongly coupled with the nanolayers, leading to a retarded growth of parent crystals by rearrangement of chains with restricted mobility into lamellae. As a result, growth rate of both parent and daughter crystals become comparable, which eventually the lead to the formation of cross-hatching in nanocomposite films. In order to further illustrate this, the FESEM image of a different nanocomposite film that showed stacked lamellae without cross-hatching structure has been presented in Figure 5.7. The nanocomposite was prepared with the use of I.44P organoclay modified with aminoalkyltrimethoxysilane existing only at the edges and possessed poor particle dispersion. Therefore, this confirms the importance of nanoparticle dispersion and coupling with matrix chains in inducing cross-hatching structure in PP blown films.

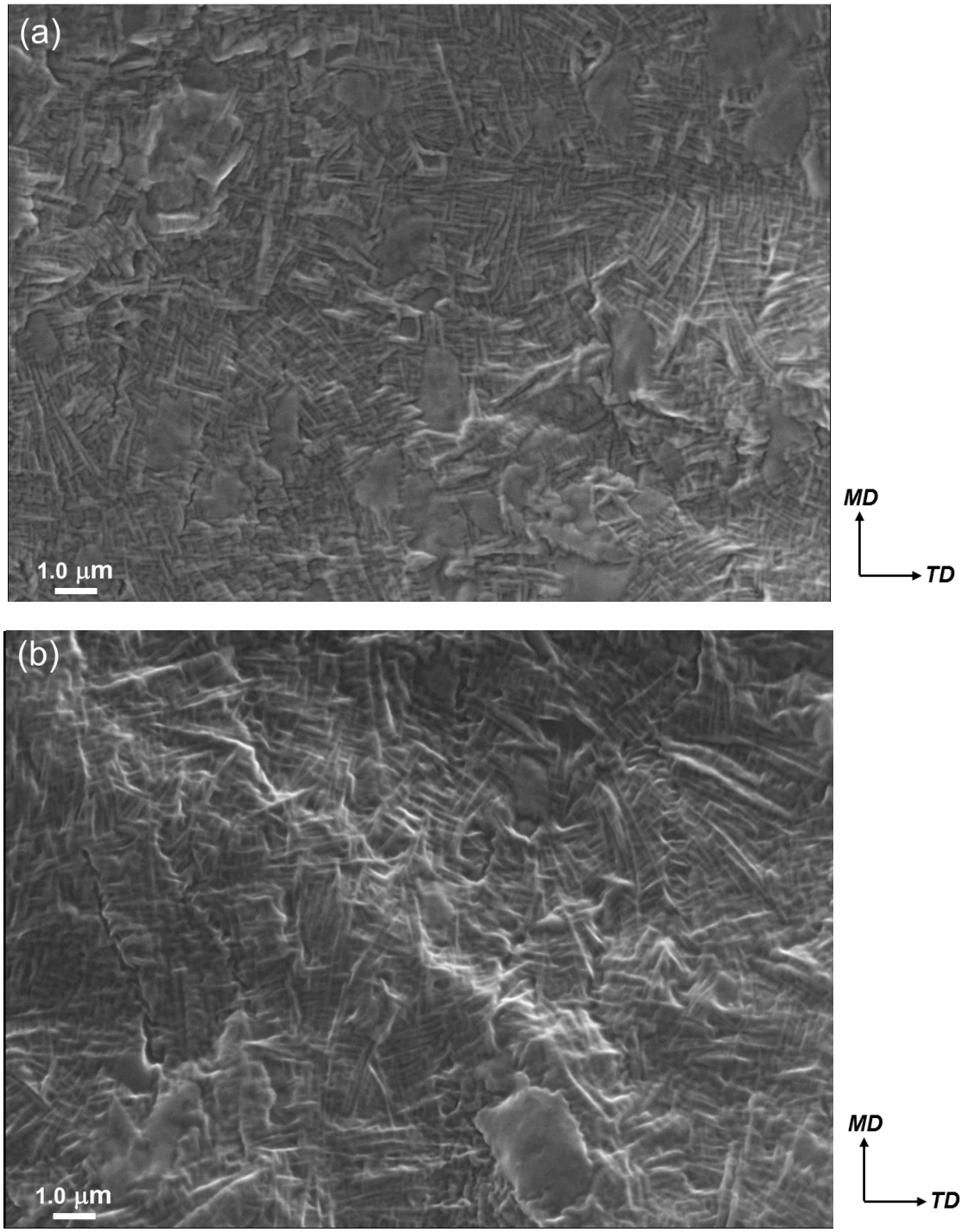

Figure 5.6 Cross-hatching and organoclay orientation in blown films from various nanocomposites (a) PPNC6, (b) PPNC7, (c) PPNC8. The dispersed nanolayers were marked with yellow circles.

Figure 5.6 (cont'd)

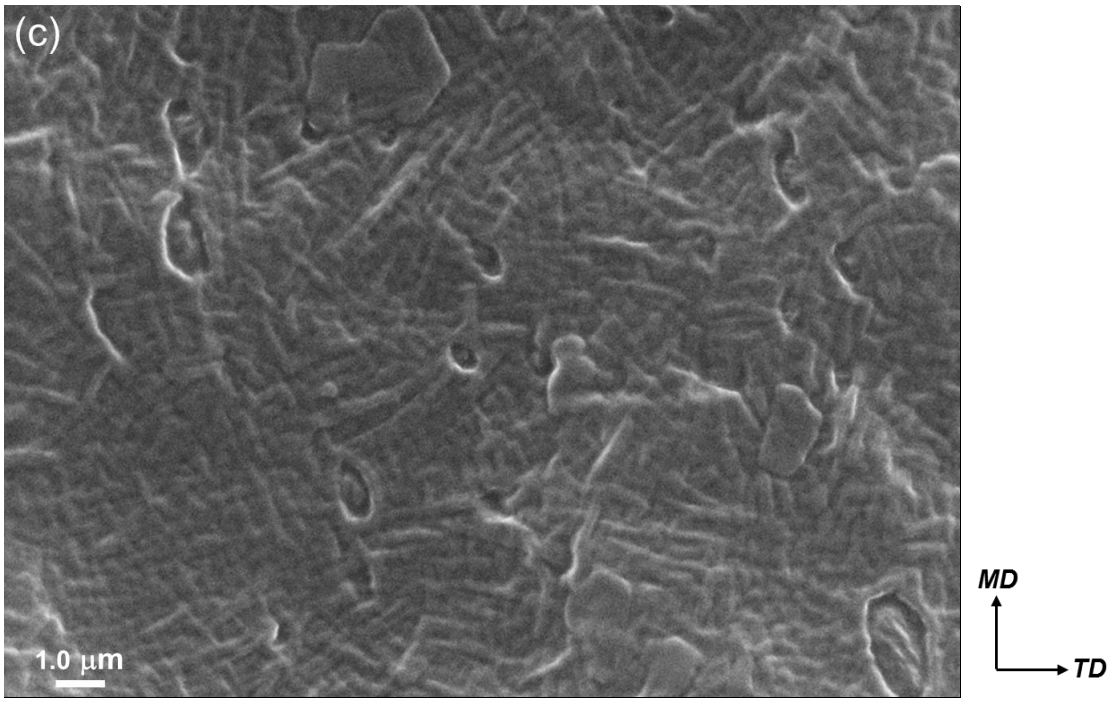

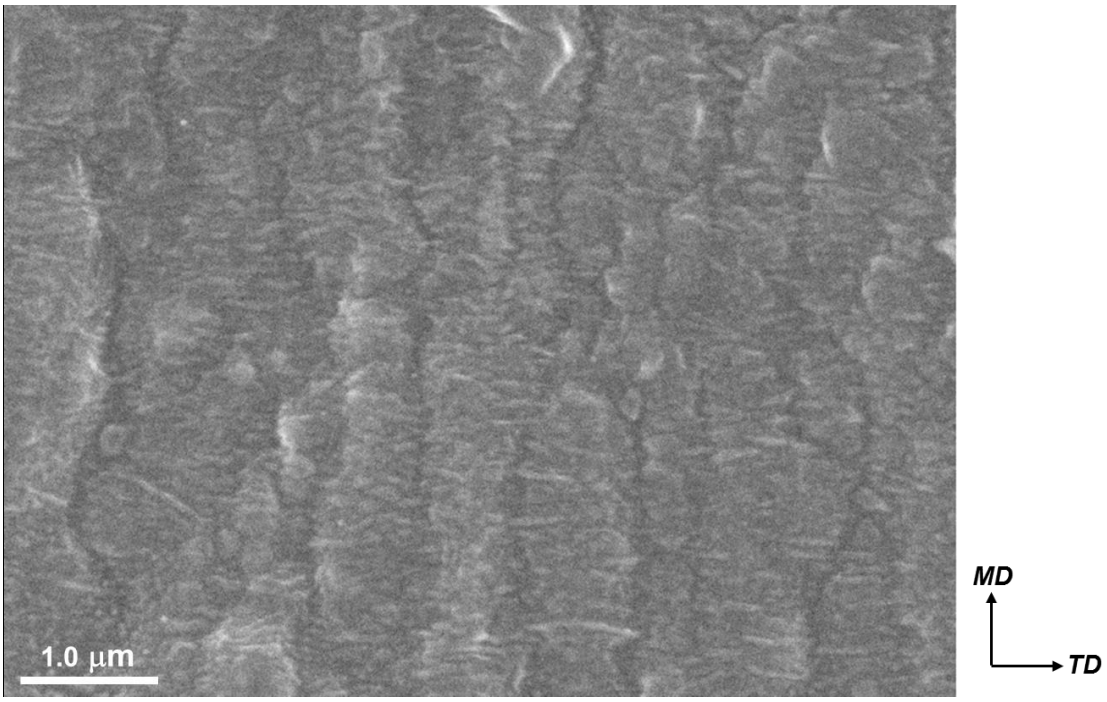

Figure 5.7 Lamellar orientation in nanocomposites blown film with stacked lamellar. The nanocomposite was prepared with the use of I.44P organoclay modified with aminoalkyltrimethoxysilane based on the wet process.

The dispersed organoclay particles were also observed in Figure 5.6. Exfoliated silicate layers aligned parallel to the plane of the films. The orientation of clay particles was further illustrated with TEM images. The TEM micrograph of PPNC7 film sliced by the TD-ND plane has been presented in Figure 5.8. The silicate layers represented by dark lines were oriented along the TD and were exfoliated and well dispersed in polymer matrix. Also, it should be pointed out that the actual amounts of dispersed clay particles as characterized by TEM is far more than what can be seen under FESEM.

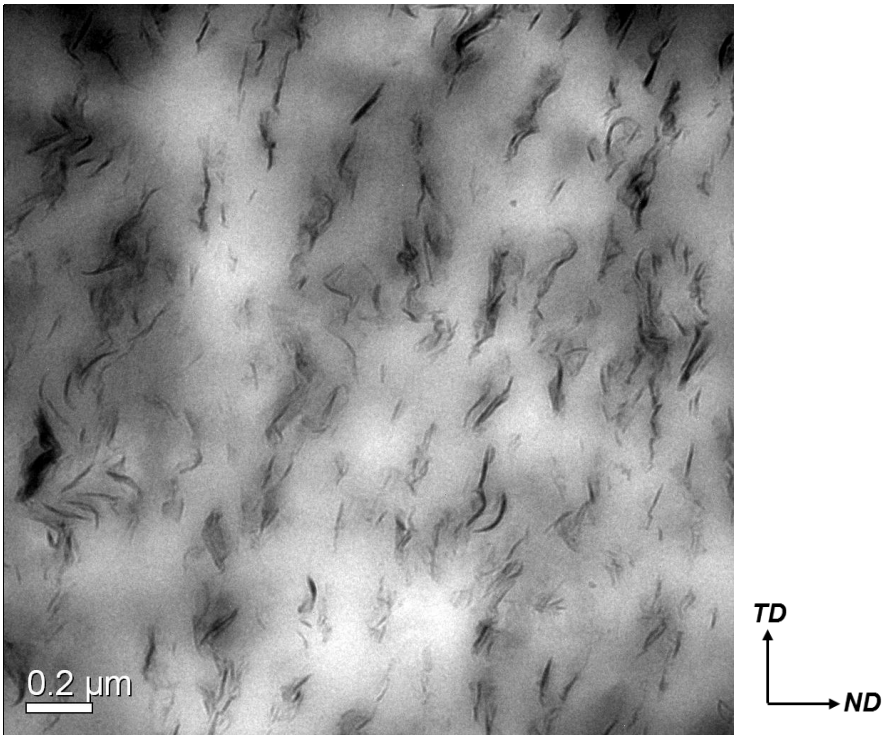

Figure 5.8 TEM micrographs of PPNC7 blown film in cross section.

The pole figures for crystal axes labeled 100 (*a**), 010 (*b*), and 001 (*c*) based on a linear intensity scale for blown films have been presented in Figure 5.9 to characterize the crystalline chain orientation. The *b* axis of all specimens was oriented strongly along the ND, while *a** and *c* axis were in the flow plane (MD-TD). The 001 pole figure of PPC300 films shows that the distribution of crystal *c* axis was between two quadrants of the pole figure with a maximum at around + 45° from TD, indicating a uniaxial orientation of polymer chains in the crystalline phase. For nanocomposite films with both 5 and 8 wt% organoclay, Figure 5.9 shows that while the maximum intensity of *c* axis at around + 45° from TD was preserved, an additional *c* axis distribution along two other quadrants of the MD-TD plane became noticeable, which, according to the analysis of crystalline structure, attributes to the presence of daughter lamellae in nanocomposite films. Also as indicated by the intensity profile, the amount of daughter lamellae of is lowest for PPNC8 among all nanocomposites films. This is probably caused by the relative

weak polymer-particle interaction and limited dispersion of PPNC8 compared to PPNC6 and PPNC7.

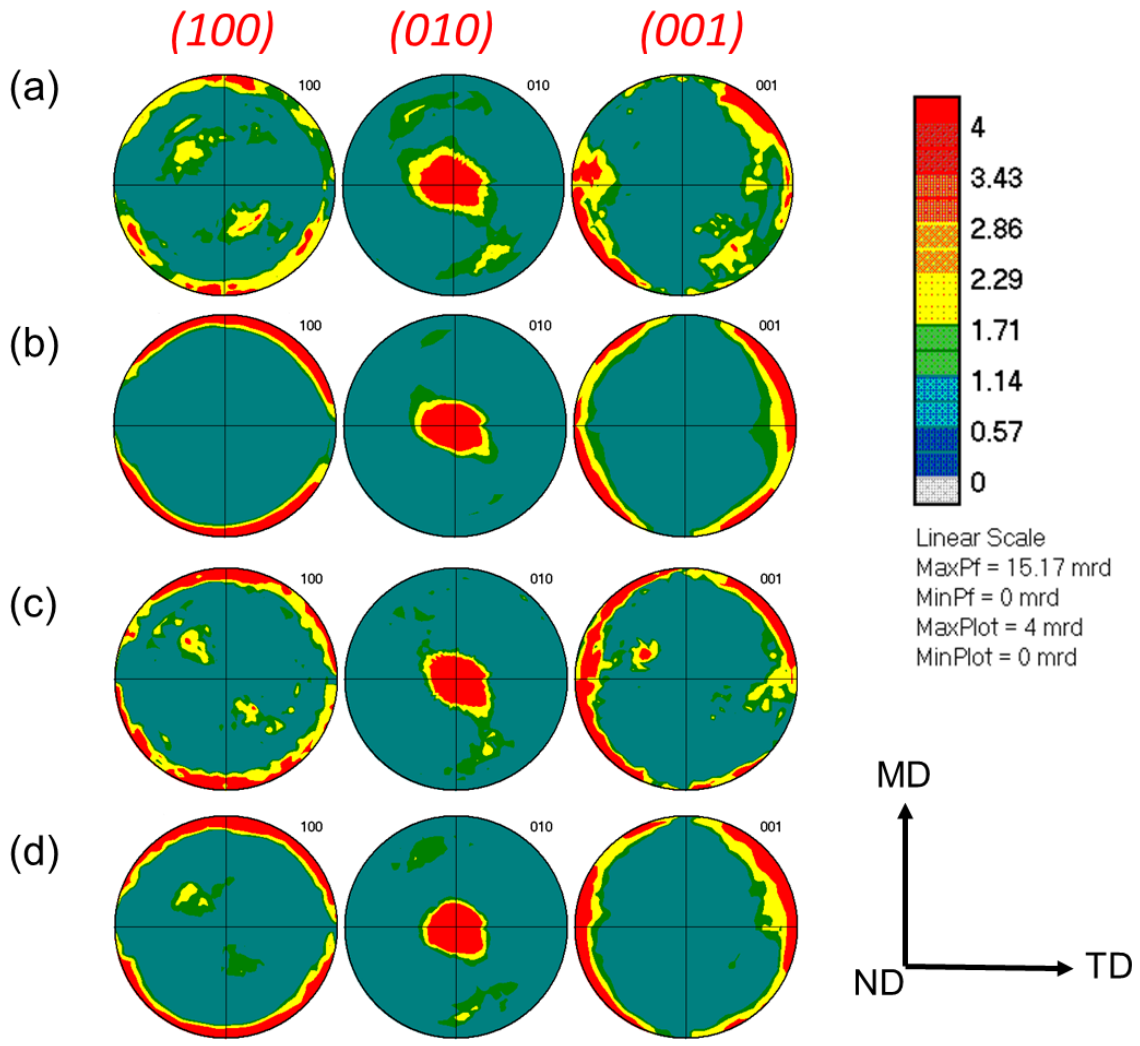

Figure 5.9 Pole figures of crystal axes of (a) PP C300, (b) PPNC6, (c) PPNC7 and (d) PPNC8 nanocomposite blown films

For semi-crystalline blown films, the birefringence data of blown films have been presented in Table 5.4. For semi-crystalline polymers, the birefringence data corresponds to the overall molecular orientation including both the crystalline and amorphous ordering. As amorphous segments present between crystal lamellae with aligned segments, it is expected that

the stretching may orient the amorphous chains similarly as the crystal lamellae. In the case of organoclay nanocomposite, the orientation of particle also contributes to the measured birefringence value. It has been reported that for blown films of uniaxial orientation, $\Delta n_{12} \approx \Delta n_{13}$, and $\Delta n_{12} \approx 0$, while in the case of approximately biaxial film, $\Delta n_{13} \approx \Delta n_{13} > \Delta n_{12}$.[46] Therefore, table 4 shows that PPC300 film exhibited highly anisotropic chain orientation as a result of imbalanced stretching along MD and TD during the blowing process. With the incorporation of organoclay of various amounts, a more isotropic orientation of nanocomposite blown films was obtained.

Table 5.4 Refractive index and birefringence of blown films of PPC300 and nanocomposites.

Compound	Refractive index			n_{11}-n_{22}	n_{11}-n_{33}	n_{22}-n_{33}
	MD (n_{11})	TD (n_{22})	ND (n_{33})			
PPC300	1.5218	1.5136	1.5139	0.0083	0.0079	0
PPNC6	1.5190	1.5155	1.5122	0.0035	0.0068	0.0033
PPNC7	1.5188	1.5167	1.5114	0.0021	0.0074	0.0053
PPNC8	1.5184	1.5168	1.5121	0.0016	0.0063	0.0047

Tensile properties of blown films have been presented in Table 5.5. It must be noted in comparing mechanical properties of blown films that the PP used as matrix for nanocomposites in this study was a block copolymer of propylene with ethylene which is tougher than homopolymer PP and has high elongation to failure (500% along MD and 170% along TD). The elongation to break for the nanocomposite films was similar along the machine direction and was found to be much higher along the transverse direction (TD). The 1% secant modulus of blown films increases as the organoclay clay content increases due to the intrinsic high modulus of organoclay particles. It has been reported that the orientation of organoclay along the flow direction also contributes to the enhancement in modulus of nanocomposites[176]. Under the

same clay loading, PPNC8 with lower compatibilizer content displayed a higher modulus than PPNC7 in both MD and TD, as the compatibilizer used in this study has a much lower molecular weight so as the modulus than the neat PP. The yield strength of the nanocomposite films was greater by up to 24% along the MD and by up to 90% along the TD. The tensile strength of films made with MB1 was increased by 50 to 67% along the transverse direction along with 10% decrease along the MD. It has been reported by Hotta and Paul[177] in the study of low density polyethylene and organoclays nanocomposite that at clay loading greater than 2.5 wt%, addition of compatibilizer resulted in greater tensile properties due to the promotion of interfacial adhesion between polymer matrix and organoclay. In our study, the enhanced mechanical strength is attributed to the strong coupling obtained at faces and edges of nanolayers. Also, a higher improvement in yield strength and tensile strength was obtained for PPNC7 compared to PPNC8 due to the presence of more compatibilizers in the former case.

The tear strength of blown films tabulated in Table 5 shows that tear strength of PPC300 film along the TD was much higher than along the MD. This is attributed to the highly anisotropic structure of the film, with the oriented chain along MD leading to lower tear resistance in this direction. With the addition of organoclay, the tear strength of PPNC6 and PPNC7 films became more balanced in the plane of the film. The reduced tear strength in TD is caused by the lower chain alignment along the MD due to the development of cross-hatching structure. In PPNC8 films, because the presence of cross-hatching structure is to a less extent as indicated by the pole figures, the high tear resistance along the TD was maintained.

Table 5.5 Mechanical properties of blown films of PPC300 and nanocomposites in machine and transverse directions.

	1% Secant Modulus (GPa)		Yield strength (MPa)		Tensile strength (MPa)		Elongation to break (%)		Tear strength (g)	
Compound	MD	TD	MD	TD	MD	TD	MD	TD	MD	TD
PPC300	0.826	0.529	18.8	9.3	35.1	15.6	500.3	169.7	30.9	354
PPNC6	0.877	0.655	20.4	17.6	29.7	26.0	474.7	538.7	28.4	64.4
PPNC7	1.003	0.845	23.3	17.1	31.3	23.6	476.3	456.3	14.6	59.2
PPNC8	1.189	1.001	22.9	9.7	30.7	18.7	538.7	341.7	9.2	496.6

5.4 Conclusion

The incorporation of 1 wt% silane in organoclay through a dry process was more effective in obtaining good coupling at the gallery faces through penetration of silane into the galleries. The masterbatch made with a 2:1 ratio by weight of maleated polypropylene compatibilizer to this silylated organoclay produced very good dispersions of the nanolayers after let-down with the bulk polypropylene at both loadings – 5 wt% and 8 wt%. The dry process of organoclay silylation also led to prominent strain hardening in uniaxial extensional flow of the let-down composites with 5 to 8 wt% organoclay. Film blowing with these nanocomposites gives films with a smaller spread in thickness (12%) than with the neat polypropylene (26%).

The anisotropy of various blown films was evaluated from mechanical tests and from refractive index measurements and both estimates were consistent. The anisotropy of the films estimated from mechanical properties of the films along the machine direction and the transverse direction was less in the nanocomposite films with the 2:1 masterbatch (MB1) than in the neat PP films. The anisotropy of overall orientation in these films, estimated with refractive index

measurements was also highest for the neat PP and decreased progressively with clay loading in the nanocomposite films.

The crystalline lamellar orientation, imaged by means of FESEM was seen to be primarily along the transverse direction (TD) for the neat PP film; the lamellar orientation was seen to be more evenly distributed in the plane of the film for the nanocomposite films. The orientation of the nanolayers in the nanocomposite films with dry phase silylated organoclay was normal to the transverse direction (i.e. the plane normal were along TD).

CHAPTER 6

RHEOLOGY OF POLYPROPYLENE - ORGANOCLAY NANOCOMPOSITES: CHEMICAL INTERACTIONS AND HINDERED CHAIN RELAXATION

6.1 Introduction

Rheology of nanocomposites at small strains exhibits a linear viscoelastic response generally deviating from the classical theory of linear viscoelasticity. A liquid-to-solid transition, evidenced by the increase of dynamic moduli and dynamic viscosity at low frequencies are commonly observed with the incorporation of nanoparticles[135, 176, 178-181]. A modulus plateau can eventually appear due to the formation of percolated particle network. This can be achieved directly by particle-particle interactions with increased filler volume fraction in well-dispersed nanocomposites, as illustrated in Figure 6.1[182]. In nanocomposites with attractive polymer-particle interactions, the filler particles tend to absorb the surrounding polymer chains. This can also lead to the formation of percolated particle network indirectly by chain bridging among neighboring particles at a reduced filler loading[137, 152, 153]. It has been demonstrated that the molecular weight of polymer matrix plays a crucial role in boosting dynamic moduli of nanocomposites since it is easier for longer chains to bridge among particles[183].

With a low filler loading where no percolated particle network is presented, rheological properties of nanocomposites are very sensitive to the molecular dynamics of polymer chains. The slowdown of mobility for chains attached to the particle surface as a result of attractive polymer-particle interactions has been demonstrated directly by nuclear magnetic resonance and indirectly by the elevated glass transition temperature in nanocomposites[184-190]. Several studies have also shown an increase of relaxation time of attached chains in nanocomposites

based on computer simulation[191, 192]. Because the attached chains on the particle surface can form trapped entanglements with free chains of the matrix, this leads to a change in the relaxation spectrum of the overall nanocomposites, consequently resulting in an enhancement of dynamic moduli at low frequencies with respect to the pure melt. Depending on the strength of interfacial interactions, considerable increase of viscoelastic properties can be achieved for strong interactions while less increase is expected with weak polymer-particle affinity.

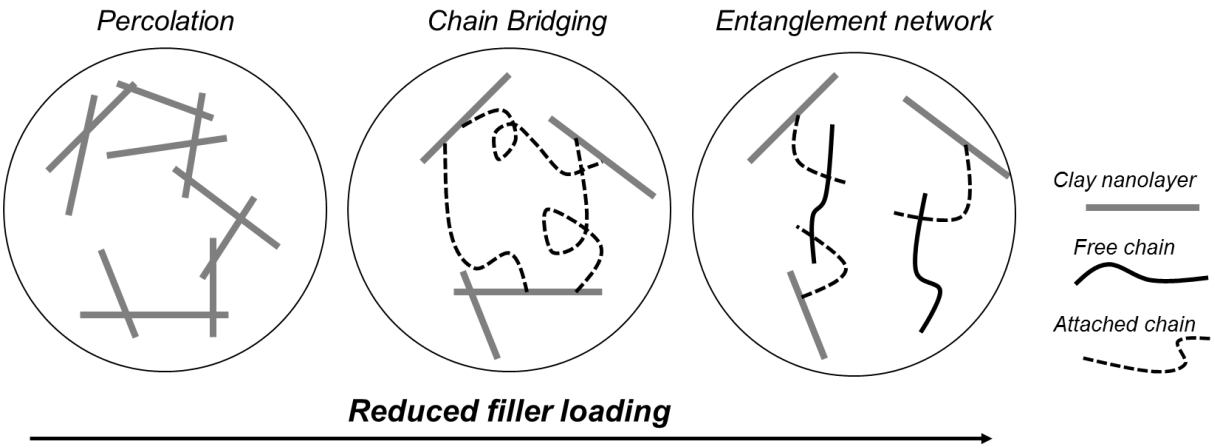

Figure 6.1 Schematic representation of filler and entanglement network as a function of filler loading.

In polypropylene-layered silicate nanocomposite, where the maleic anhydride grafted PP is generally used as a compatibilizer, mobility of matrix chains can be retarded by mainly reversible attachments of PP-g-MA on edges and faces of nanoclays via hydrogen bonds[193]. The polymer−clay interface may be strengthened further by means of silane coupling agents that interact with the either sites at one end and with the functionalized polymeric compatibilizer at the other end[194-198], which results in irreversible attachments of polymer chains via covalent bonds.

In this chapter, the dynamic shear rheology of polypropylene-layered silicate

nanocomposites as affected by variation of polymer-clay interactions was investigated. Pure PP-g-MA, rather than a blend of PP and PP-g-MA, was used as the polymer matrix to keep clear of the type of matrix chains presented in the system. Three types of nanoclays, which were organically modified I.44P and its silane treated derivatives via dry process and wet process, were used. The different silylation process resulted in silane coupling at either both faces and edges or at edges alone of clay nanolayers. A viscoelastic model based on the one proposed by Sarvestani[154] was applied to model the rheology of nanocomposites with two entanglement networks – particle attached chains and free chains. Specifically, this model described the dynamics of free chains and particle-attached chains that formed two different types of entanglements to account for the effects of attractive polymer-particle interactions on chain relaxation and the frequency-dependent dynamic shear moduli of nanocomposites.

The incorporation of nanoclay has also been reported to modify the extensional flow behavior of the polymer melts. For example, Park et al. investigated the uniaxial extensional behavior of PP/clay nanocomposites[91], and reported that in systems where clay particles were exfoliated, strain hardening was imparted to the transient uniaxial extensional viscosity, where the matrix polymer did not exhibit this property. However, the opposite effect has been reported of reduced strain hardening after adding the same high aspect ratio nanoparticles to a matrix polymer that displayed strain hardening by itself[140-142]; the cause of the varied effects remains unclear. In this work, by means of silane coupling at the edges and/or faces of nanoclay, the key factors that affect strain hardening behavior of PP-g-MA/clay nanocomposites were discussed.

6.2 Experimental Details

6.2.1 Materials

The polymer matrix used in this study was maleic anhydride grafted PP (Exxelor 1015 from ExxonMobil) with molecular weight of 122,000, and maleic content of 0.42%. It is a random copolymer of propylene and ethylene with a melting temperature of 145°C. The organoclay used was Nanomer I.44P from Nanocor, which has a quaternary onium ion surfactant with two C18 tails. The organoclay was treated with silane coupling agent (aminoalkyldimethoxy silane, from Evonik Industries) based on both dry process and wet process as described in Chapter 2. The resulting silylated organoclays were designated as VS-I.44P and SS-I.44P, respectively. The three kinds of organoclays were used to prepare nanocomposites with 95 wt% of PP-g-MA and 5 wt% of nanoclay.

6.2.2 Processing Procedures

The PP-g-MA and organoclay were compounded in a Brabender batch mixer for 10 min at 165°C with continuous nitrogen purge. Before compounding, both materials were dried overnight in a vacuum oven. The PP-g-MA alone was also processed under the same condition to account for the effect of processing on any structural change of polymer matrix.

Compression molding by a hydraulic press was used to make composite specimens for TEM analysis and rheological characterizations. Dynamic shear tests were carried out on a TA Instruments AR2000 rheometer with parallel plates of diameter 40 mm over a frequency range from 0.01 to 100 rad/s at 155°C under nitrogen flow. A fixed strain of 1% was used for all nanocomposites, which was confirmed by a strain sweep to be within the linear viscoelastic regime of each material. For the oscillatory frequency sweep of PP-g-MA matrix, a 5% strain,

was used so that the torque signal was enlarged to obtain more reliable result. The melt extensional viscosity of nanocomposite melts was measured using an extensional viscosity fixture (EVF) on a TA-ARES instrument. The extensional viscosity measurements were carried out at 155°C and at four strain rates (0.1, 0.5, 1.0, and 2.0 s^{-1}) over Hencky strains up to 3. The details of all the preparation and characterization procedures were provided in Chapter 2.

6.3 Results and Discussion

6.3.1 Dispersion and Structure of Polymer Nanocomposites.

The dispersion of I.44P, VS-I.44P and VS-I.44P organoclays was characterized by TEM analysis and typical examples of these images have been presented in Figure 6.2. It appears that for all compounds clay particles were almost completely exfoliated to single silicate layers that were uniformly dispersed in the polymer matrix. This fine dispersion of nanoclay of 5 wt% even without the presence of silane coupling is attributed to the sufficient interfacial interactions when maleic anhydride grafted PP is used as the polymer matrix.

To testify whether a percolated network has arisen via polymer chains bridging among nanoclays, the average spacing between dispersed silicate layers was evaluated by measuring the closest distance between several pairs of clay particles in a continuous path for each nanocomposite and the result has been tabulated in Table 6.1. Meanwhile, the average diameter of random coils of PP-g-MA molecules in the melt state was calculated based on the following equation

$$D = 2R_g = \sqrt{\frac{2}{3}}R \tag{6.1}$$

where R is the end-to-end distance of polymer chains. With known value of $\frac{<R^2>}{M_w}$ for isotactic polypropylene[199], the average diameter of PP-g-MA coil was estimated to be 23.7 nm, which was smaller than the particle distance tabulated in Table 6.1. Since multiple maleic anhydride functional groups as the sites of attachments are distributed along the chain of PP-g-MA, a strongly compressed conformation is expected for the attached chains compared to that of the free chains[200, 201]. Together, these observations appear to provide support for the idea that formation of particle network via direct chain bridging is not likely to occur.

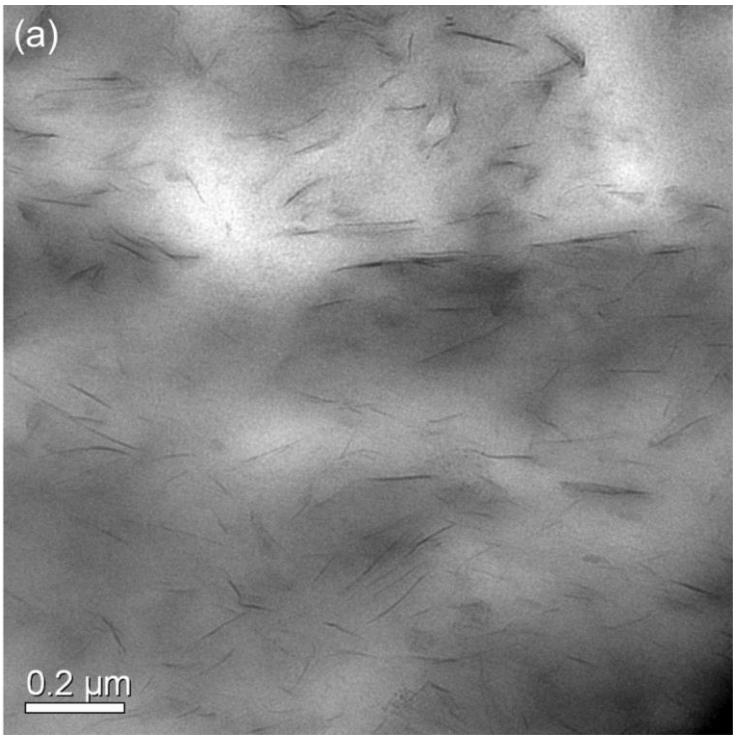

Figure 6.2 TEM micrographs of nanocomposites with (a) non-silylated I.44P, (b) VS-I.44P and (c) SS-I.44P.

Figure 6.2 (cont'd)

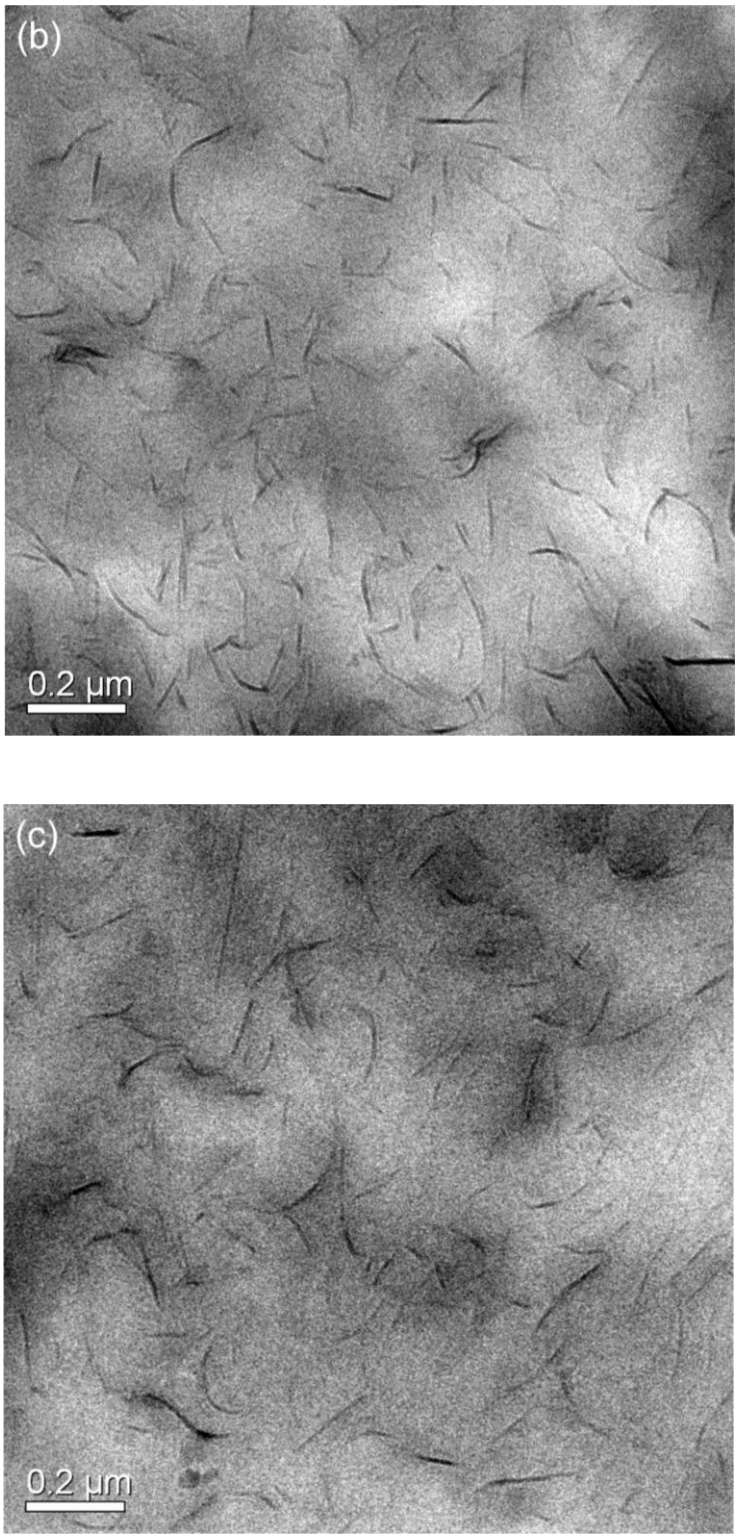

Table 6.1 Estimated mean particle distance and particle number density for various nanocomposites.

Compound	Mean particle distance (nm)	Particle number density (μm^{-2})
PO1015-I.44P	35.2	70
PO1015-VSI.44P	38.2	75
PO1015-SSI.44P	31.1	45

6.3.2 Dynamic Shear Rheology of Nanocomposite Melts

The frequency-dependent dynamic shear storage modulus and dynamic viscosity at 155°C have been presented in Figure 6.3 for the matrix and in Figure 6.4 for nanocomposites. The data of PP-g-MA matrix below 0.37 rad/s was removed, as the torque values during test were below the acceptable lower torque-sensing limit of the transducer and the data showed poor reproducibility. At high frequencies, the storage modulus and dynamic viscosity of all nanocomposites were increased by roughly 200% from the matrix, as a result of the shear amplification effect. At low frequencies, the addition of organoclays increased the storage modulus and dynamic viscosity more dramatically. In nanocomposite melts, attractive polymer-particle interactions lead to reversible or irreversible attachments of PP-g-MA chains on faces and edges of clay nanolayers. When entanglements are formed between attached chains and free chains, relaxation of this type of entanglements is retarded compared to that of entanglements between free chains and free chains, leading to the enhancements in dynamic shear rheology at low frequencies. This effect depends strongly on the strength and the amount of polymer attachments on nanolayers. Nanocomposite with stronger and more chain attachments is expected to display higher storage modulus values.

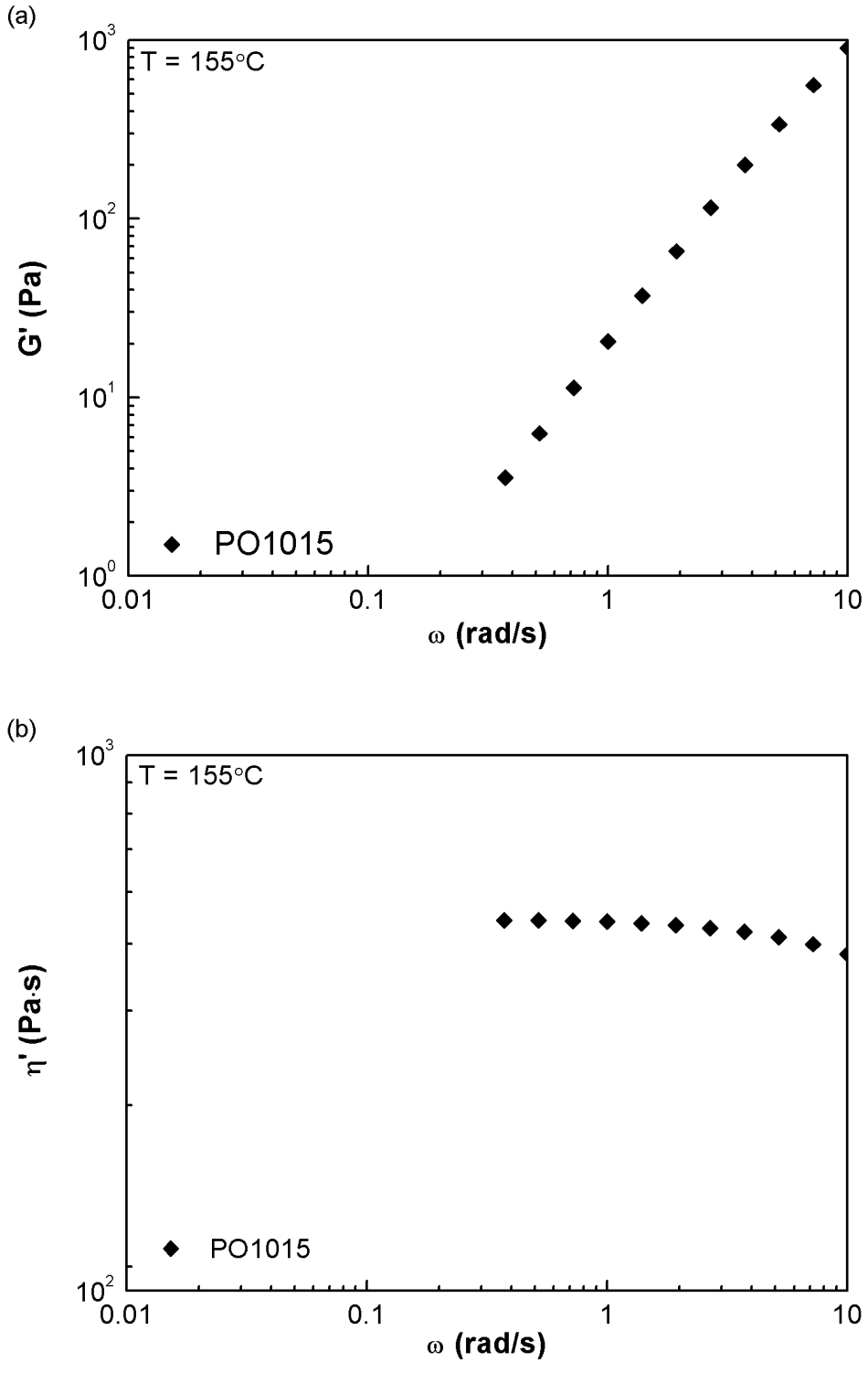

Figure 6.3 (a) Storage modulus and (b) dynamic viscosity of PP-g-MA matrix.

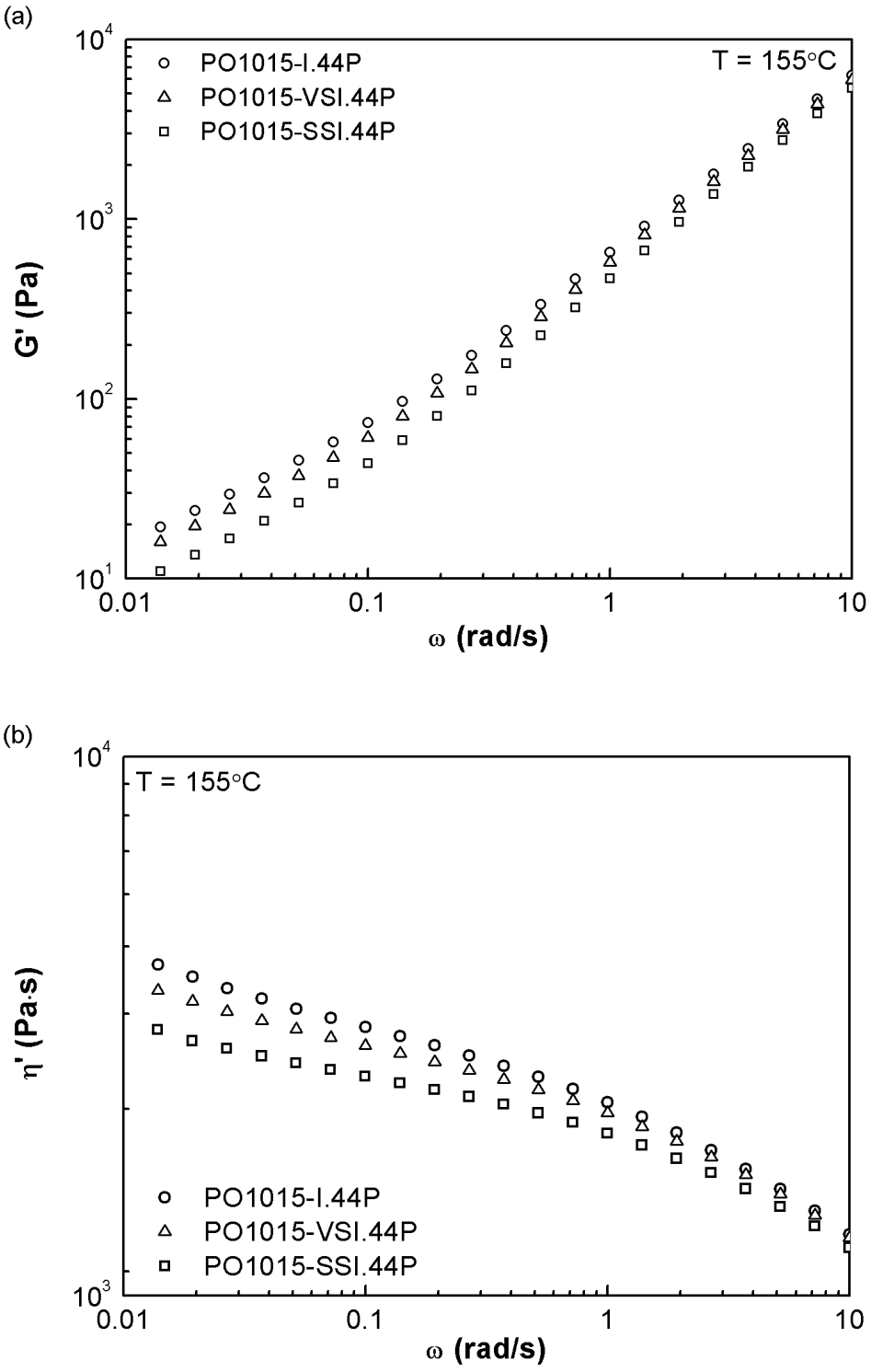

Figure 6.4 (a) Storage modulus and (b) dynamic viscosity of nanocomposites with unmodified I.44P and silane treated I.44P via wet and dry process.

Figure 6.4 also shows that the storage modulus curve is lower for nanocomposites prepared with silane treated organoclays, with the one with SS-I.44P organoclay displaying the lowest values. This was caused by the decrease of chain attachments in the presence of silane coupling agents. As illustrated in Figure 6.5, the anhydride or acid group of PP-g-MA chains reacted with the amine end of the silane, which in turn tied up two sites on the clay surface as each silane molecule contains two silanol groups. In the case of PO1015-SSI.44P, the smaller number density of clay nanolayers as tabulated in Table 6.1 compared with the other nanocomposites was responsible for the low storage modulus values, because less surface area was available for chain attachment to occur.

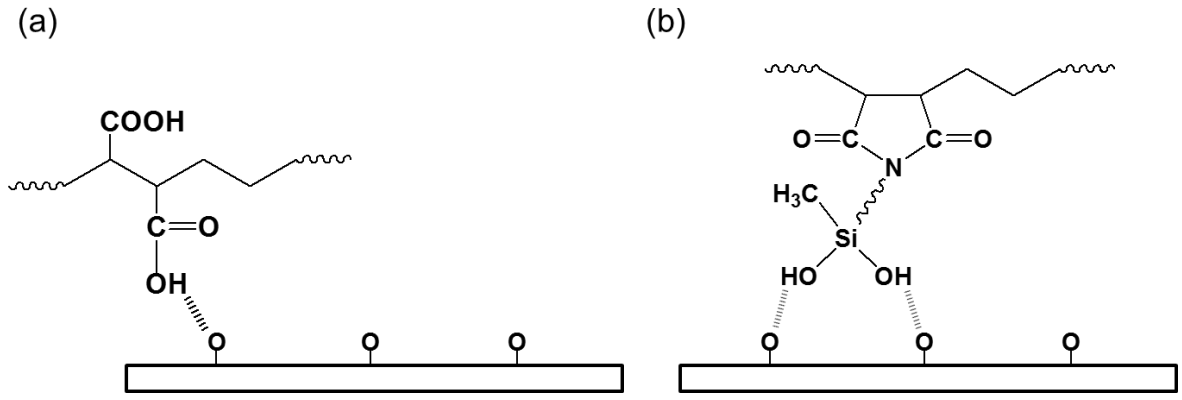

Figure 6.5 (a) Hydrogen bond between the PP-g-MA chain and the oxygen group on the gallery face of non-silylated I.44P, (b) covalent bond between the PP-g-MA chain and the silane, which occupies two sites on the gallery face of silylated I.44P.

6.3.3 Linear Viscoelastic Model of Nanocomposites

In this section, a viscoelastic model was developed to quantitatively capture the linear rheological behavior of PP-g-MA/clay nanocomposites, and also to illustrate its dependence on surface modification of nanoclays examined in this study. As discussed above, the entangled chain relaxation in the presence of attractive nanoclays is considered to include two parts: free

chains with no attachment to silicate layer and particle attached chains. While the repetitive motion of free chains is unaffected, that of attached chains is restricted to a certain extent, which gives rise to the enhancement in the dynamic moduli and viscosity at low frequencies. The disentanglement time of chains attached to clay nanolayers ($\lambda_{d,a}$) can be related to that of the matrix chains ($\lambda_{d,m}$) by the following expressions

$$\lambda_{d,a} = c * \lambda_{d,m} \tag{6.2}$$

where c is an experimentally fitted parameter describing the degree of restriction of chain relaxation at the interface, which depends on the strength of polymer-clay interactions[154, 202]. Also, for a system composed of chains with both fast and slow dynamics, the polymer chains relax in the manner of double reptation[203, 204], where a chain end on either chain passing through the entanglement point by reptation leads to loss of entanglement to both chains. Therefore, the shear stress relaxation function of polymer chains in the nanocomposite can be written in the form that includes the reptation of the free chains and attached chains as well as the tube renewal due to constraint release of the surrounding chains[154]

$$G_c(t) = B \cdot G_0[\left(1 - \phi_a\right)\mu_m(t) + \phi_a\mu_a(t)]^{1+\delta} \tag{6.3}$$

where B is the strain amplification factor evaluated as G^*_c/G^*_m at ω = 100 rad/s, representing the increase of strain in polymer matrix compared to the external strain applied for nanocomposites due to the non-deformed nature of rigid particles[205]. G_0 is the plateau modulus, ϕ_a is the fraction of adsorbed chains on silicate layers, and $\mu_m(t)$ and $\mu_a(t)$ are the survival fraction of the free chains and adsorbed chains, respectively. δ represents the dilution exponent in the theory of dynamic dilution, which accounts for the accelerated relaxation of long chains in the presence of short chains as a "solvent" for the unrelaxed long chains. δ was taken to

be 1 following the double reputation model. It should be noted that expansion of equation 6.3 leads to cross terms with relaxation time depending on the that of both components according to the double reptation model. For example,

$$\frac{1}{\lambda_{d,cross}} = \frac{1}{\lambda_{d,m}} + \frac{1}{\lambda_{d,a}} \tag{6.4}$$

An analysis of the reptation process leads to the expressions for survival fraction, which are defined by

$$\mu_m(t) = \frac{8}{\pi^2}\sum_{i_{odd}} \frac{1}{i^2}\exp(-\frac{i^2 t}{\lambda_{d,m}}) \tag{6.5}$$

$$\mu_a(t) = \frac{8}{\pi^2}\sum_{i_{odd}} \frac{1}{i^2}\exp(-\frac{i^2 t}{\lambda_{d,a}}) \tag{6.6}$$

Finally, the storage modulus of polymer chains as a function of frequency can be calculated by applying a Fourier transform to equation 6.3 with

$$G'(\omega) = \omega \int_0^\infty G(t)\sin(\omega t)\, dt \tag{6.7}$$

Because of the insufficient data at low frequencies, the matrix curves were not used for fitting of the G_0 and relaxation time for free chains ($\lambda_{d,m}$). Instead, the storage modulus of PPNC-I.44P nanocomposite was fitted with G_0, $\lambda_{d,m}$, ϕ_a and c as fitting parameters in the frequency range from 0.01 to 1 rad/s. The emphasis on low frequency portion originated from the dominated contribution of attached chains for the increase of storage modulus while the high frequency portion of the curves is dominated by the free chain behavior. With the same G_0 and $\lambda_{d,m}$ as that of PPNC-I.44P, $G'(\omega)$ of PO1015-SSI.44P and PO1015-VSI.44P were fitted to derive ϕ_a and c values for each case.

Fitting results of $G'(\omega)$ for all nanocomposite have been presented in Figure 6.6. The fitting parameters have been tabulated in Table 6.2, which reveals the effect of variation in polymer-clay interactions by silane treatment on chain attachments, and consequently the linear dynamic storage modulus of nanocomposite melts. For nanocomposites with reactive coupling, higher c values were obtained. This is expected because of the replacement of some weak hydrogen bonds between the organoclay and PP-g-MA chains with strong covalent bonds. On the other hand, silane treatment of organoclay led to smaller ϕ_a values or decreased amounts of attached chains, especially for SSI.44P, leading to the lower storage modulus of the corresponding nanocomposites at low frequencies.

Table 6.2 Parameters for theoretical fit to experimental data of PP-g-MA matrix and various nanocomposites.

Compound	$\lambda_{d,m}$	G_0	B	ϕ_a	c
PO1015-I.44P	1.97	1758	2.42	0.126	56
PO1015-VSI.44P	1.97	1758	2.41	0.11	62
PO1015-SSI.44P	1.97	1758	2.36	0.090	66

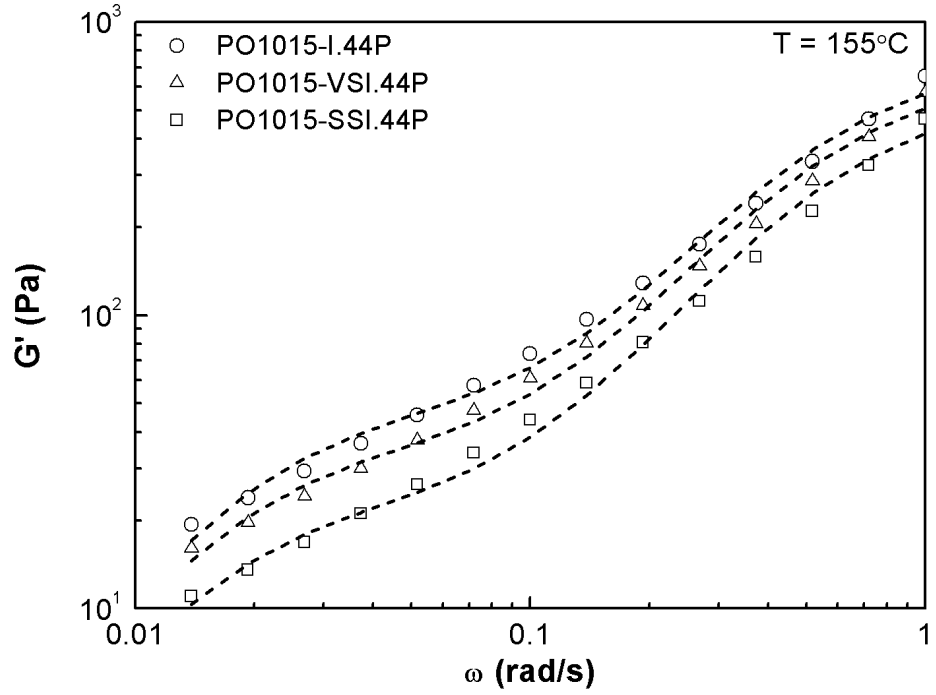

Figure 6.6 Comparison of the model prediction (dash lines) with experimental results of all nanocomposite for storage modulus.

6.3.4 Transient Uniaxial Extensional Viscosity

The effect of polymer−clay interactions on melt extensional viscosity for various nanocomposite melts at several strain rates has been presented in Figure 6.7. For all specimens, the transient extensional flow curves displayed strain hardening behaviors, while the PP-g-MA used in this study did not. The maximum strain hardening parameter (χ_{max}) at highest strains before the stretched strand breaks or deforms non-uniformly was evaluated. Plots of the maximum strain hardening ratio against strain rate have been presented in Figure 6.8. It is seen that the presence of silane coupling increased χ_{max} at all strain rates. Moreover, when silane coupling occurs at both faces and edges of nanoclays, the highest extent of strain hardening was obtained, as in the case of PO1015-VSI.44P.

The observed strain hardening behavior of polymer nanocomposites in extensional flow may be understood in terms of the formation of trapped entanglement between chains attached to surface of clay nanolayers and free chains in the bulk matrix. This is analogous to the slow relaxation of entanglements formed between backbone of branched polymers and surrounding branches, which has been reported to be crucial in inducing the strain hardening behavior[206, 207]. Accordingly, a strong polymer-clay interaction as evidenced by the higher c and ϕ_a values, especially for nanocomposites prepared with VS-I.44P plays a dominant role for a high value of χ_{max}.

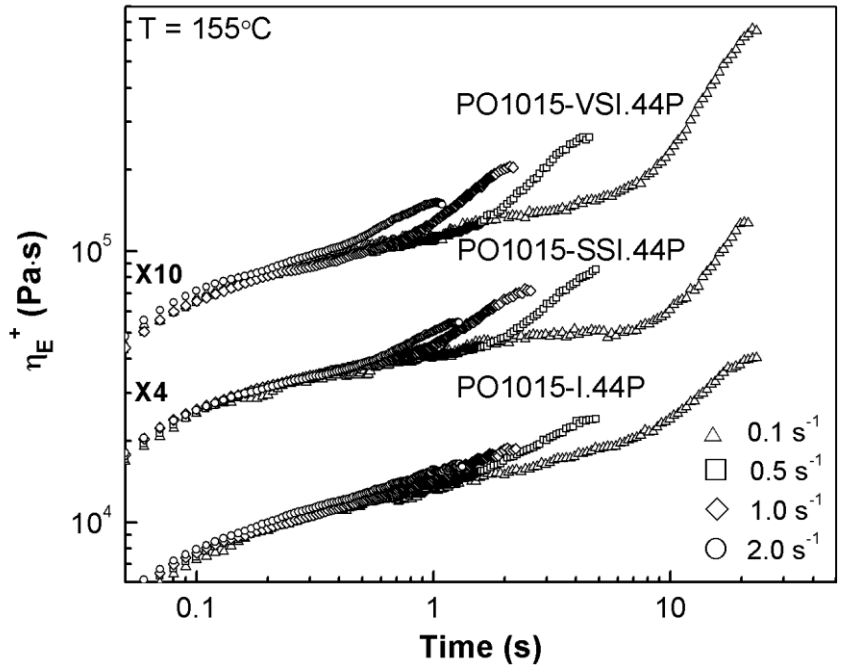

Figure 6.7 Uniaxial extensional viscosity transients (η_E^+) at several strain rates for nanocomposite melts.

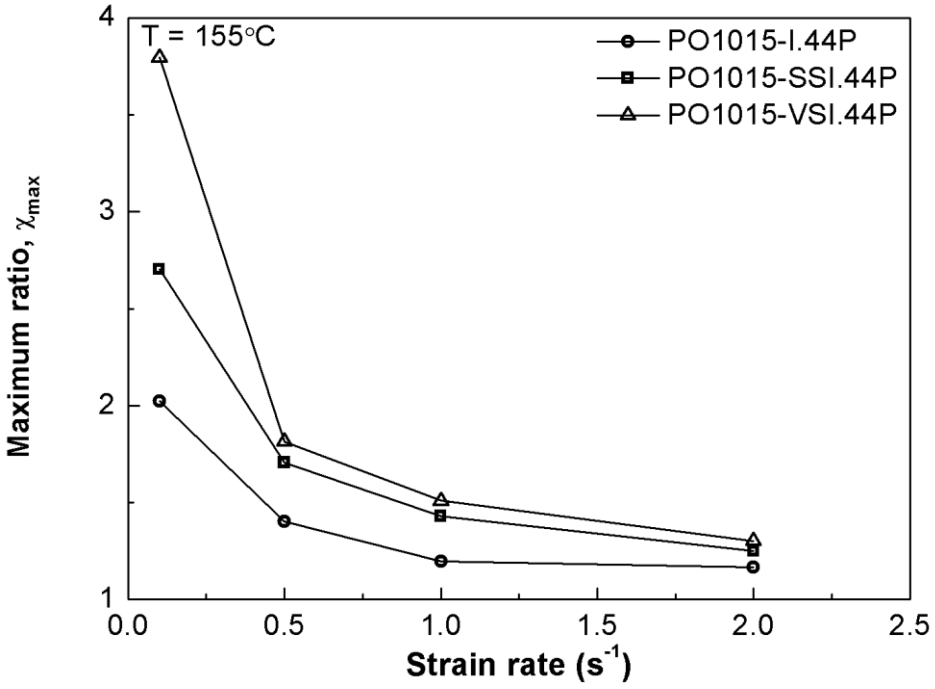

Figure 6.8 Maximum strain hardening ratio for the nanocomposite melts at 155°C.

6.4 Conclusion

A viscoelastic model was applied to illustrate effects of attractive polymer-clay interactions on the dynamic shear rheology of nanocomposite melts. The nanocomposites were prepared by compounding 5 wt% of unmodified and silane treated organoclay, respectively, with PP-g-MA as the polymer matrix. Without the presence of percolated clay network, the enhancement of dynamic moduli and dynamic viscosity at low frequencies compared to that of the matrix was attributed to the restricted relaxation of particle attached chains. This was correlated in the model by the interaction strength between the PP-g-MA and nanoclay (c) and the fraction of particle attached chains (ϕ_a) at the interface. The surface treatment of nanoclay with silane led to increased c values due to the replacement of some of the weak polymer-clay interactions via hydrogen bonds with stronger covalent bonds in the systems. Meanwhile, silane

coupling reduced the fraction of attached chains (ϕ_a), because each dimethoxy silane molecule took up two sites that could interact with the PP-g-MA chains. Therefore, experimental result of the low frequency dynamic storage modulus was lower for nanocomposites prepared with silylated organoclay. The uniaxial extensional viscosity of nanocomposites with silane coupling displayed greater strain hardening, especially in the case of coupling at faces and edges. Analysis of fitting parameters based on the viscoelastic model revealed the crucial role of polymer-clay interaction strength with high amount of chain attachments in enhancing the strain hardening behavior of nanocomposites.

CHAPTER 7

CONCLUSIONS AND RECOMMENDATIONS

7.1 Conclusions

This research focused on the development of thin blown films from linear polypropylene that exhibited both good processing stabilities as well as end-use properties. This was achieved by formulating polypropylene nanocomposites with alkyl ammonium surfactants modified nanoclays, maleic anhydride grafted PP compatibilizers and suitable reactive silane coupling agents.

Organoclay consists of several tens of two-dimensional silicate layers stacked together with long chain alkyl ammonium surfactants intercalating between galleries. Two different types of interface sites are available on organoclay: edges with hydroxyl groups and gallery faces with oxygen atoms. The compatibilizers in polypropylene nanocomposites can interact with organoclay at either site mainly through hydrogen bonding. In order to reinforce the polymer-clay interface of nanocomposites, aminoalkyldisssmethoxysilane was used to treat the nanoclay in this study. This allowed the formation of covalent bonds between the amino groups of silane treated organoclays and the maleic anhydride groups of functionalized compatibilizers. The silane treatment was first carried out using a solvent mediated method on two different organoclays: I.44P nanoclay with 40% dialkyl quaternary onium ion surfactant and I.30P nanoclay with 30% alkyl primary onium ion surfactant. Characterization of the silylated nanoclays using BET, TGA, and XRD revealed that in the case of I.44P, the silanols reacted only at the nanolayer edges while in the case of I.30P, the silanes entered the interlayer galleries. Because of the large face area of nanoclays, the number of interactive sites on the face is far

greater than that on the edge. Therefore, locating the coupling agents at both types of sites is important for effectively enhancing polymer-clay interactions.

In nanocomposites prepared with 3 wt% of organoclay and 12 wt% of PP-g-MA compatibilizer, the effect of reactive coupling was noticeably improved dispersion with thinner stacks of nanolayers, as evidenced by the mean stack thickness based on TEM images analysis. The uniaxial extensional viscosity of these melts displayed significantly greater strain hardening behavior. Especially in the case of reactive coupling at both faces and edges, the evaluated maximum strain hardening ratio was higher than 2 over the entire range of strain rates. These results demonstrated the potential for rheology modification to reinforce the melt strength of linear polypropylene by means of organoclay nanocomposites with coupling agents and long chain polymeric compatibilizers.

The stability of morphology and rheology for these nanocomposites was also investigated by reprocessing in a capillary rheometer under a specific shear rate. Frequency-dependent dynamic shear results showed lower dynamic viscosity values at the high frequency end in all reprocessed compounds, indicating some degradation of the polymer matrix. For nanocomposite with silylated I.44P, reprocessing led to better exfoliation of nanoclays as a result of additional shear stresses applied. Also, a drop of 15% to 30% in the maximum extensional viscosity was observed, which was caused by some loss of entanglements due to the matrix degradation. In sharp contrast, severe degradation of both morphology and strain hardening behavior, as evidenced by the formation of particle agglomerate and 70% to 90% drop in extensional viscosity magnitudes, respectively, was obtained for reprocessed nanocomposite with silylated I.30P. This was attributed to the low thermal stability of physically absorbed silanes at the gallery faces as evidenced in the TGA profile. Upon reprocessing, detachments of these silanes

along with the reacted polymer compatibilizers led to the loss of polymer-clay interactions for the nanocomposite.

To formulate nanocomposite compounds that exhibited both high melt strength and processing stability, a vapor phase silylation process was introduced to treat the I.44P organoclay. XRD and TGA results showed that compared to wet process, the dry process made it possible for the silylation to occurs at both edges and faces of I.44P organoclay without losing its thermal stability. This silylated I.44P was then used to prepare masterbatch additives by blending with compatibilizers with ratios of 1:2 and 2:3. 20 wt% of a high molecular weight polypropylene was also added in the masterbatch to ensure high torque values for better mixing. The masterbatch was let down with the same polypropylene of various concentrations to prepare nanocomposites for film blowing. It was shown that despite the low amount of compatibilizer used, nanocomposites with 5 wt% and 8 wt% organoclay displayed excellent particle dispersion and significant strain hardening behavior. During film blowing process, the nanocomposites exhibited strongly improved bubble stability compard to the neat polypropylene. Meanwhile, better thickness uniformity along the circumference was obtained for nanocomposite blown films based on calculated standard deviation values of the film thickness. While the mechanical properties of nanocomposite films along the machine direction remained roughly unchanged, an improvement of yield stress, tensile strength and elongation at break was seen in the transverse direction. Meanwhile, the mechanical properties of nanocomposite blown films were more isotropic in the plane of the film than that of the film from the neat PP. These trends were understood in terms of the orientation distributions of crystalline lamellae in the films. FESEM images revealed that cross-hatching of lamellae, which correlated to isotropy of film properties, was absent from the blown film of unfilled PP but pervasive in the blown films of

nanocomposites. This might be attributed to the strong mobility reduction of chains attached to the nanolayers, which led to a comparable growth rate for the parent and daughter crystals of polypropylene, and consequently the formation of cross-hatching structure in nanocomposite films. Beyond the scope of blown film application, the masterbatch additives have also been demonstrated for its capability of boosting rheological properties and processability of reprocessed or recycled linear polypropylene and nanocomposites.

A viscoelastic model was applied to investigate the dynamic shear rheology of polypropylene nanocomposites prepared by compounding 5 wt% of non-silylated and silylated I.44P organoclays with the functional compatibilizer as the matrix. The absence of percolated clay network in nanocomposites was first confirmed by TEM analysis where the average particle-to-particle distance was observed to be larger than the radius of gyration of particle attached chains. This allowed the model to represent the frequency-dependent storage modulus of nanocomposites solely by the relaxation of free chains and attached chains on faces and edges of the nanoclay. Two variables were introduced in the model to describe the degree of chain mobility restriction: c and ϕ_a, which correlated with the interaction strength and the fraction of particle attached chains, respectively. Evaluation of fitting parameters revealed that nanocomposites with reactive silane coupling at either interactive site displayed larger c values and lower ϕ_a values. The latter was responsible for the lower storage modulus and dynamic viscosity at low frequencies compared to the nanocomposite with non-silylated I.44P. The uniaxial extensional viscosity of these nanocomposites was also evaluated. The result showed that the presence of silane coupling led to greater strain hardening behavior, especially in the case of coupling at both faces and edges. Analysis of fitting parameters revealed the crucial role

of polymer-clay interaction strength with high amount of chain attachments in enhancing the strain hardening behavior of nanocomposites.

7.2 Recommendations

As mentioned above, nanocomposites developed with organically modified nanoclays, high molecular weight functional compatibilizers and reactive coupling agents resulted in rheology modification of linear polypropylene with enhanced melt strength. Such reinforcement can be further improved by a dry process for silylation and a two-step mixing protocol (masterbatch and let-down) for nanocomposite preparation. These results are promising and lead into a number of technically and commercially significant directions. But it has not been fully explored and few of the obvious questions that emerge from the above study are that, what is the optimized silane concentration to use for vapor phase silylation that can maximize the attractive polymer-clay interactions? To what extent does such optimization affect the melt rheology of nanocomposites? How does the incorporation of bulk polypropylene of various concentrations and molecular weights in masterbatch affect state of nanoclay dispersion and physical properties of the final products?

In the present work, maleic anhydride grafted polypropylene, Exxelor PO1015, was used as compatibilizers for nanocomposite preparation. However, the function of compatibilizers in promoting strain hardening behavior of polypropylene-clay nanocomposites has not been completely understood. It would be intriguing to synthesize PP-g-MA with finely controlled maleic anhydride content, molecular weight and molecular structure, and investigate effects of these factor on strain hardening properties of the resulting nanocomposites.

In blown film application, it has been established that the melt strength, as a function of nanocomposite formulations, dominates the bubble stability and processing window. Yet it still remains to find out the process/structure/property relationships of nanocomposite blown films. With this argument, another recommendation in the context of our study is to investigate how the processing parameters, such as BUR and TUR, nip speed, frost line height, etc., and nanocomposite formations affect the crystalline structure and chain orientation and therefore physical properties of the blown films.

BIBLIOGRAPHY

BIBLIOGRAPHY

1. Cantor and K. Cantor, *Blown Film Extrusion*. 2011, Carl Hanser Verlag GmbH & Co. KG,: S.l.

2. Han, C.D. and J.Y. Park, *Studies on Blown Film Extrusion .1. Experimental Determination of Elongational Viscosity.* Journal of Applied Polymer Science, 1975. **19**(12): p. 3257-3276.

3. Kim, Y.M. and J.K. Park, *Effect of short chain branching on the blown film properties of linear low density polyethylene.* Journal of Applied Polymer Science, 1996. **61**(13): p. 2315-2324.

4. Lu, J.J., H.J. Sue, and T.P. Rieker, *Morphology and mechanical property relationship in linear low-density polyethylene blown films.* Journal of Materials Science, 2000. **35**(20): p. 5169-5178.

5. Bafna, A., G. Beaucage, F. Mirabella, G. Skillas, and S. Sukumaran, *Optical properties and orientation in polyethylene blown films.* Journal of Polymer Science Part B-Polymer Physics, 2001. **39**(23): p. 2923-2936.

6. Hobbs, S.Y. and C.F. Pratt, *The Development of Surface Texture in Blown Polypropylene Film.* Polymer Engineering and Science, 1982. **22**(10): p. 594-600.

7. Bheda, J.H. and J.E. Spruiell, *The Effect of Process and Polymer Variables on the Light Transmission Properties of Polypropylene Tubular Blown Films.* Polymer Engineering and Science, 1986. **26**(11): p. 736-745.

8. Sadeghi, F., A. Ajji, and P.J. Carreau, *Study of polypropylene morphology obtained from blown and cast film processes: Initial morphology requirements for making porous membrane by stretching.* Journal of Plastic Film & Sheeting, 2005. **21**(3): p. 199-216.

9. Choi, D. and J.L. White, *Crystallization and orientation development in fiber and film processing of polypropylenes of varying stereoregular form and tacticity.* Polymer Engineering and Science, 2004. **44**(2): p. 210-222.

10. Choi, D. and J.L. White, *Crystal structures and orientation development in tubular film extrusion of syndiotactic polypropylene and isotactic polypropylene.* Polymer Engineering and Science, 2001. **41**(10): p. 1743-1751.

11. Auinger, T. and M. Stadlbauer, *Inter-Relationship Between Processing Conditions and Mechanical Properties of Blown Film from Different Polypropylenes and High Melt Strength Polypropylene Blends.* Journal of Applied Polymer Science, 2010. **117**(1): p. 155-162.

12. Di Maio, L., P. Scarfato, L. Incarnato, and D. Acierno, *Biaxial orientation of polyamide films: Processability and properties.* Macromolecular Symposia, 2002. **180**: p. 1-8.

13. Yeh, J.T., C.J. Chang, F.C. Tsai, K.N. Chen, and K.S. Huang, *Oxygen barrier and blending properties of blown films of blends of modified polyamide and polyamide-6 clay mineral nanocomposites.* Applied Clay Science, 2009. **45**(1-2): p. 1-7.

14. Patel, R.M., P. Saavedra, C. Hinton, and J. deGroot, *Comparison of EVA and polyolefin plastomer as blend components in various film applications.* Journal of Plastic Film & Sheeting, 1998. **14**(4): p. 344-355.

15. Nostro, A., R. Scaffaro, G. Ginestra, M. D'Arrigo, L. Botta, A. Marino, and G. Bisignano, *Control of biofilm formation by poly-ethylene-co-vinyl acetate films incorporating nisin.* Applied Microbiology and Biotechnology, 2010. **87**(2): p. 729-737.

16. Stenhouse, P.J., J.A. Ratto, and N.S. Schneider, *Structure and properties of starch/poly(ethylene-co-vinyl alcohol) blown films.* Journal of Applied Polymer Science, 1997. **64**(13): p. 2613-2622.

17. Yeh, J.T. and H.Y. Chen, *Blending and oxygen permeation properties of the blown films of blends of modified polyamide and ethylene vinyl alcohol copolymer with varying vinyl alcohol contents.* Journal of Materials Science, 2007. **42**(14): p. 5742-5751.

18. Li, L., Q. Wang, and R. Wang, *Enhancing mechanical properties of poly(vinyl alcohol) blown films by drawing and surface crosslinking.* Journal of Applied Polymer Science, 2005. **98**(2): p. 774-779.

19. Ma, T.C. and C.D. Han, *Processing Structure Property Relationships in Poly(Ethylene-Terephthalate) Blown Film.* Journal of Applied Polymer Science, 1988. **35**(7): p. 1725-1757.

20. Sedlarik, V., N. Saha, J. Sedlarikova, and P. Saha, *Biodegradation of Blown Films Based on Poly(lactic acid) under Natural Conditions.* Macromolecular Symposia, 2008. **272**: p. 100-103.

21. Mallet, B., K. Lamnawar, and A. Maazouz, *Improvement of Blown Film Extrusion of Poly(Lactic Acid): Structure-Processing-Properties Relationships.* Polymer Engineering and Science, 2014. **54**(4): p. 840-857.

22. Nouri, S., P.G. Lafleur, and C. Dubois, *Enhanced Film Blowing of Polylactide by Incorporating Branched Chains and Stereocomplex Crystals.* International Polymer Processing, 2015. **30**(4): p. 500-510.

23. Choi, K.J., J.L. White, and J.E. Spruiell, *Orientation Development in Tubular Film Extrusion of Polystyrene.* Journal of Applied Polymer Science, 1980. **25**(12): p. 2777-2788.

24. Fang, Y., F. Sadeghi, G. Fleuret, and P.J. Carreau, *Properties of blends of linear and branched polypropylenes in film blowing.* Canadian Journal of Chemical Engineering, 2008. **86**(1): p. 6-14.

25. Kim, S., Y.L. Fang, P.G. Lafleur, and P.J. Carreau, *Dynamics and criteria for bubble instabilities in a single layer film blowing extrusion.* Polymer Engineering and Science, 2004. **44**(2): p. 283-302.

26. Munstedt, H., S. Kurzbeck, and J. Stange, *Importance of elongational properties of polymer melts for film blowing and thermoforming.* Polymer Engineering and Science, 2006. **46**(9): p. 1190-1195.

27. Munstedt, H., T. Steffl, and A. Malmberg, *Correlation between rheological behaviour in uniaxial elongation and film blowing properties of various polyethylenes.* Rheologica Acta, 2005. **45**(1): p. 14-22.

28. Kolarik, R., M. Zatloukal, and M. Martyn, *The effect of polyolefin extensional rheology on non-isothermal film blowing process stability.* International Journal of Heat and Mass Transfer, 2013. **56**(1-2): p. 694-708.

29. Micic, P., S.N. Bhattacharya, and G. Field, *Transient elongational viscosity of LLDPE/LDPE blends and its relevance to bubble stability in the film blowing process.* Polymer Engineering and Science, 1998. **38**(10): p. 1685-1693.

30. Micic, P. and S.N. Bhattacharya, *Rheology of LLDPE, LDPE and LLDPE/LDPE blends and its relevance to the film blowing process.* Polymer International, 2000. **49**(12): p. 1580-1589.

31. Stange, J., C. Uhl, and H. Munstedt, *Rheological behavior of blends from a linear and a long-chain branched polypropylene.* Journal of Rheology, 2005. **49**(5): p. 1059-1079.

32. Tabatabaei, S.H., P.J. Carreau, and A. Ajji, *Rheological Long-Chain Properties of Blends of Linear and Branched Polypropylenes.* Polymer Engineering and Science, 2010. **50**(1): p. 191-199.

33. Gururajan, G. and A.A. Ogale, *Real-time crystalline orientation measurements during low-density polyethylene blown film extrusion using wide-angle X-ray diffraction.* Polymer Engineering and Science, 2012. **52**(7): p. 1532-1536.

34. Ajji, A., X. Zhang, and S. Elkoun, *Biaxial orientation in HDPE films: comparison of infrared spectroscopy, X-ray pole figures and birefringence techniques.* Polymer, 2005. **46**(11): p. 3838-3846.

35. Tabatabaei, S.H., P.J. Carreau, and A. Ajji, *Effect of processing on the crystalline orientation, morphology, and mechanical properties of polypropylene cast films and microporous membrane formation.* Polymer, 2009. **50**(17): p. 4228-4240.

36. Troisi, E.M., M. van Drongelen, H.J.M. Caelers, G. Portale, and G.W.M. Peters, *Structure evolution during film blowing: An experimental study using in-situ small angle X-ray scattering.* European Polymer Journal, 2016. **74**: p. 190-208.

37. Zhang, X.M., S. Elkoun, A. Ajji, and M.A. Huneault, *Oriented structure and anisotropy properties of polymer blown films: HDPE, LLDPE and LDPE.* Polymer, 2004. **45**(1): p. 217-229.

38. Prasad, A., R. Shroff, S. Rane, and G. Beaucage, *Morphological study of HDPE blown films by SAXS, SEM and TEM: a relationship between the melt elasticity parameter and lamellae orientation.* Polymer, 2001. **42**(7): p. 3103-3113.

39. Somani, R.H., L. Yang, and B.S. Hsiao, *Effects of high molecular weight species on shear-induced orientation and crystallization of isotactic polypropylene.* Polymer, 2006. **47**(15): p. 5657-5668.

40. van Drongelen, M., D. Cavallo, L. Balzano, G. Portale, I. Vittorias, W. Bras, G.C. Alfonso, and G.W.M. Peters, *Structure Development of Low-Density Polyethylenes During Film Blowing: A Real-Time Wide-Angle X-ray Diffraction Study.* Macromolecular Materials and Engineering, 2014. **299**(12): p. 1494-1512.

41. Cherukupalli, S.S., S.E. Gottlieb, and A.A. Ogale, *Real-time Raman spectroscopic measurement of crystallization kinetics and its effect on the morphology and properties of polyolefin blown films.* Journal of Applied Polymer Science, 2005. **94**(4): p. 1740-1747.

42. Yu, T.H. and G.L. Wilkes, *Orientation determination and morphological study of high density polyethylene (HDPE) extruded tubular films: Effect of processing variables and molecular weight distribution.* Polymer, 1996. **37**(21): p. 4675-4687.

43. Patel, R.M., T.I. Butler, K.L. Walton, and G.W. Knight, *Investigation of Processing-Structure-Properties Relationships in Polyethylene Blown Films.* Polymer Engineering and Science, 1994. **34**(19): p. 1506-1514.

44. Godshall, D., G. Wilkes, R.K. Krishnaswamy, and A.M. Sukhadia, *Processing-structure-property investigation of blown HDPE films containing both machine and transverse direction oriented lamellar stacks.* Polymer, 2003. **44**(18): p. 5397-5406.

45. Pazur, R.J. and R.E. Prudhomme, *X-ray pole figure and small angle scattering measurements on tubular blown low-density poly(ethylene) films.* Macromolecules, 1996. **29**(1): p. 119-128.

46. Choi, K.J., J.E. Spruiell, and J.L. White, *Orientation and Morphology of High-Density Polyethylene Film Produced by the Tubular Blowing Method and Its Relationship to Process Conditions.* Journal of Polymer Science Part B-Polymer Physics, 1982. **20**(1): p. 27-47.

47. Shimomura, Y., J.E. Spruiell, and J.L. White, *Orientation Development in the Tubular Film Extrusion of Polypropylene.* Journal of Applied Polymer Science, 1982. **27**(7): p. 2663-2674.

48. Kwack, T.H. and C.D. Han, *Development of Crystalline-Structure during Tubular Film Blowing of Low-Density Polyethylene.* Journal of Applied Polymer Science, 1988. **35**(2): p. 363-389.

49. Saffar, A., A. Ajji, P.J. Carreau, and M.R. Kamal, *The impact of new crystalline lamellae formation during annealing on the properties of polypropylene based films and membranes.* Polymer, 2014. **55**(14): p. 3156-3167.

50. Sadeghi, F., A. Ajji, and P.J. Carreau, *Analysis of row nucleated larnellar morphology of polypropylene obtained from the cast film process: Effect of melt rheology and process conditions.* Polymer Engineering and Science, 2007. **47**(7): p. 1170-1178.

51. Lu, J., H.J. Sue, and T.P. Rieker, *Dual crystalline texture in HDPE blown films and its implication on mechanical properties.* Polymer, 2001. **42**(10): p. 4635-4646.

52. Krishnaswamy, R.K. and M.J. Lamborn, *Tensile properties of linear low density polyethylene (LLDPE) blown films.* Polymer Engineering and Science, 2000. **40**(11): p. 2385-2396.

53. Zhou, H.Y. and G.L. Wilkes, *Orientation-dependent mechanical properties and deformation morphologies for uniaxially melt-extruded high-density polyethylene films having an initial stacked lamellar texture.* Journal of Materials Science, 1998. **33**(2): p. 287-303.

54. Lee, L.B.W., R.A. Register, and D.M. Dean, *Tear anisotropy in films blown from polyethylenes of different macromolecular architectures.* Journal of Polymer Science Part B-Polymer Physics, 2005. **43**(4): p. 413-420.

55. Chen, H.Y., M.T. Bishop, B.G. Landes, and S.P. Chum, *Orientation and property correlations for LLDPE blown films.* Journal of Applied Polymer Science, 2006. **101**(2): p. 898-907.

56. Krishnaswamy, R.K. and A.M. Sukhadia, *Orientation characteristics of LLDPE blown films and their implications on Elmendorf tear performance.* Polymer, 2000. **41**(26): p. 9205-9217.

57. Kojima, Y., A. Usuki, M. Kawasumi, A. Okada, T. Kurauchi, and O. Kamigaito, *One-Pot Synthesis of Nylon-6 Clay Hybrid.* Journal of Polymer Science Part a-Polymer Chemistry, 1993. **31**(7): p. 1755-1758.

58. Kojima, Y., A. Usuki, M. Kawasumi, A. Okada, T. Kurauchi, and O. Kamigaito, *Synthesis of Nylon-6-Clay Hybrid by Montmorillonite Intercalated with Epsilon-Caprolactam.* Journal of Polymer Science Part a-Polymer Chemistry, 1993. **31**(4): p. 983-986.

59. Okada, A., M. Kawasumi, T. Kurauchi, and O. Kamigaito, *Synthesis and Characterization of a Nylon 6-Clay Hybrid.* Abstracts of Papers of the American Chemical Society, 1987. **194**: p. 10-Macr.

60. Usuki, A., Y. Kojima, M. Kawasumi, A. Okada, Y. Fukushima, T. Kurauchi, and O. Kamigaito, *Synthesis of Nylon 6-Clay Hybrid.* Journal of Materials Research, 1993. **8**(5): p. 1179-1184.

61. Samyn, F., S. Bourbigot, C. Jama, S. Bellayer, S. Nazare, R. Hull, A. Castrovinci, A. Fina, and G. Camino, *Crossed characterisation of polymer-layered silicate (PLS) nanocomposite morphology: TEM, X-ray diffraction, rheology and solid-state nuclear magnetic resonance measurements.* European Polymer Journal, 2008. **44**(6): p. 1642-1653.

62. Dennis, H.R., D.L. Hunter, D. Chang, S. Kim, J.L. White, J.W. Cho, and D.R. Paul, *Effect of melt processing conditions on the extent of exfoliation in organoclay-based nanocomposites.* Polymer, 2001. **42**(23): p. 9513-9522.

63. Fornes, T.D., P.J. Yoon, H. Keskkula, and D.R. Paul, *Nylon 6 nanocomposites: the effect of matrix molecular weight.* Polymer, 2001. **42**(25): p. 9929-9940.

64. de Paiva, L.B., A.R. Morales, and F.R.V. Diaz, *Organoclays: Properties, preparation and applications.* Applied Clay Science, 2008. **42**(1-2): p. 8-24.

65. Heinz, H., R.A. Vaia, R. Krishnamoorti, and B.L. Farmer, *Self-assembly of alkylammonium chains on montmorillonite: Effect of chain length, head group structure, and cation exchange capacity.* Chemistry of Materials, 2007. **19**(1): p. 59-68.

66. Reichert, P., H. Nitz, S. Klinke, R. Brandsch, R. Thomann, and R. Mulhaupt, *Poly(propylene)/organoclay nanocomposite formation: Influence of compatibilizer functionality and organoclay modification.* Macromol. Mater. Eng., 2000. **275**(2): p. 8-17.

67. Wang, K.H., M.H. Choi, C.M. Koo, Y.S. Choi, and I.J. Chung, *Synthesis and characterization of maleated polyethylene/clay nanocomposites.* Polymer, 2001. **42**(24): p. 9819-9826.

68. Fornes, T.D., D.L. Hunter, and D.R. Paul, *Nylon-6 nanocomposites from alkylammonium-modified clay: The role of alkyl tails on exfoliation.* Macromolecules, 2004. **37**(5): p. 1793-1798.

69. Fornes, T.D., P.J. Yoon, and D.R. Paul, *Effect of organoclay structure on nylon 6 nanocomposite morphology and properties.* Abstracts of Papers of the American Chemical Society, 2002. **224**: p. U493-U493.

70. Chrissopoulou, K. and S.H. Anastasiadis, *Polyolefin/layered silicate nanocomposites with functional compatibilizers.* European Polymer Journal, 2011. **47**(4): p. 600-613.

71. Marchant, D. and K. Jayaraman, *Strategies for optimizing polypropylene−clay nanocomposite structure.* Industrial & Engineering Chemistry Research, 2002. **41**(25): p. 6402-6408.

72. Kim, D.H., P.D. Fasulo, W.R. Rodgers, and D.R. Paul, *Structure and properties of polypropylene-based nanocomposites: Effect of PP-g-MA to organoclay ratio.* Polymer, 2007. **48**(18): p. 5308-5323.

73. Perrin-Sarazin, F., M.T. Ton-That, M.N. Bureau, and J. Denault, *Micro- and nano-structure in polypropylene/clay nanocomposites.* Polymer, 2005. **46**(25): p. 11624-11634.

74. Dubnikova, I.L., S.M. Berezina, Y.M. Korolev, G.M. Kim, and S.M. Lomakin, *Morphology, deformation behavior and thermomechanical properties of polypropylene/maleic anhydride grafted polypropylene/layered silicate nanocomposites.* Journal of Applied Polymer Science, 2007. **105**(6): p. 3836-3850.

75. Arunvisut, S., S. Phummanee, and A. Somwangthanaroj, *Effect of clay on mechanical and gas barrier properties of blown film LDPE/Clay nanocomposites.* Journal of Applied Polymer Science, 2007. **106**(4): p. 2210-2217.

76. Wang, K.H., C.M. Koo, and I.J. Chung, *Physical properties of polyethylene/silicate nanocomposite blown films.* Journal of Applied Polymer Science, 2003. **89**(8): p. 2131-2136.

77. Lotti, C., C.S. Isaac, M.C. Branciforti, R.M.V. Alves, S. Liberman, and R.E.S. Bretas, *Rheological, mechanical and transport properties of blown films of high density polyethylene nanocomposites.* European Polymer Journal, 2008. **44**(5): p. 1346-1357.

78. Zhong, Y. and D. De Kee, *Morphology and properties of layered silicate-polyethylene nanocomposite blown films.* Polymer Engineering and Science, 2005. **45**(4): p. 469-477.

79. Kashyap, M.J. and A.K. Ghosh, *Processing, rheology and characterization of polypropylene nanocomposites and their blown films.* Journal of Plastic Film & Sheeting, 2013. **29**(3): p. 228-248.

80. Xu, W.C., D.L. Li, Y.B. Fu, R.J. Liao, J.Z. Shi, Y.J. Wang, and X.H. He, *Influence of nanovermiculites with a high aspect ratio and stretch orientation on the microstructure of polypropylene films.* Journal of Applied Polymer Science, 2016. **133**(1).

81. Sharma, S.K., A.K. Nema, and S.K. Nayak, *Polypropylene Nanocomposite Film: A Critical Evaluation on the Effect of Nanoclay on the Mechanical, Thermal, and Morphological Behavior.* Journal of Applied Polymer Science, 2010. **115**(6): p. 3463-3473.

82. Mirzadeh, A. and M. Kokabi, *The effect of composition and draw-down ratio on morphology and oxygen permeability of polypropylene nanocomposite blown films.* European Polymer Journal, 2007. **43**(9): p. 3757-3765.

83. Shah, R.K., R.K. Krishnaswamy, S. Takahashi, and D.R. Paul, *Blown films of nanocomposites prepared from low density polyethylene and a sodium ionomer of poly(ethylene-co-methacrylic acid).* Polymer, 2006. **47**(17): p. 6187-6201.

84. Dadfar, S.M.A., I. Alemzadeh, S.M.R. Dadfar, and M. Vosoughi, *Studies on the oxygen barrier and mechanical properties of low density polyethylene/organoclay nanocomposite films in the presence of ethylene vinyl acetate copolymer as a new type of compatibilizer.* Materials & Design, 2011. **32**(4): p. 1806-1813.

85. Ren, W.J., A.K. Chaudhary, and K. Jayaraman, *Processing Polypropylene Nanocomposites with Silylated Organoclays: Coupling at Edges versus Gallery Faces.* Industrial & Engineering Chemistry Research, 2015. **54**(16): p. 4264-4273.

86. Lee, S.H., E. Cho, and J.R. Youn, *Rheological behavior of polypropylene/layered silicate nanocomposites prepared by melt compounding in shear and elongational flows.* Journal of Applied Polymer Science, 2007. **103**(6): p. 3506-3515.

87. Lee, S.H., S.Y. Kim, and J.R. Youn, *Rheological Behavior and Theoretical Modeling of Uniaxial Elongational Flow Properties of Polypropylene/Layered Silicate Nanocomposites.* Polymer Composites, 2009. **30**(10): p. 1426-1436.

88. Okamoto, M., P.H. Nam, P. Maiti, T. Kotaka, N. Hasegawa, and A. Usuki, *A house of cards structure in polypropylene/clay nanocomposites under elongational flow.* Nano Letters, 2001. **1**(6): p. 295-298.

89. Okamoto, M., P.H. Nam, P. Maiti, T. Kotaka, T. Nakayama, M. Takada, M. Ohshima, A. Usuki, N. Hasegawa, and H. Okamoto, *Biaxial flow-induced alignment of silicate layers in polypropylene/clay nanocomposite foam.* Nano Letters, 2001. **1**(9): p. 503-505.

90. Chaudhary, A.K. and K. Jayaraman, *Extrusion of linear polypropylene-clay nanocomposite foams.* Polymer Engineering and Science, 2011. **51**(9): p. 1749-1756.

91. Park, J.U., J.L. Kim, D.H. Kim, K.H. Ahn, S.J. Lee, and K.S. Cho, *Rheological behavior of polymer/layered silicate nanocomposites under uniaxial extensional flow.* Macromolecular Research, 2006. **14**(3): p. 318-323.

92. Lim, H.T., K.H. Ahn, S.J. Lee, and J.S. Hong, *Design of new HDPE/silica nanocomposite and its enhanced melt strength.* Rheologica Acta, 2012. **51**(2): p. 143-150.

93. Akelah, A. and A. Moet, *Polymer-clay nanocomposites: Free-radical grafting of polystyrene on to organophilic montmorillonite interlayers.* Journal of Materials Science, 1996. **31**(13): p. 3589-3596.

94. Krishnamoorti, R. and E.P. Giannelis, *Rheology of end-tethered polymer layered silicate nanocomposites.* Macromolecules, 1997. **30**(14): p. 4097-4102.

95. Messersmith, P.B. and E.P. Giannelis, *Polymer-Layered Silicate Nanocomposites - in-Situ Intercalative Polymerization of Epsilon-Caprolactone in Layered Silicates.* Chemistry of Materials, 1993. **5**(8): p. 1064-1066.

96. Paul, M.A., M. Alexandre, P. Degee, C. Calberg, R. Jerome, and P. Dubois, *Exfoliated polylactide/clay nanocomposites by in-situ coordination-insertion polymerization.* Macromolecular Rapid Communications, 2003. **24**(9): p. 561-566.

97. Yeh, J.M., S.J. Liou, M.C. Lai, Y.W. Chang, C.Y. Huang, C.P. Chen, J.H. Jaw, T.Y. Tsai, and Y.H. Yu, *Comparative studies of the properties of poly(methyl methacrylate)-clay nanocomposite materials prepared by in situ emulsion polymerization and solution dispersion.* Journal of Applied Polymer Science, 2004. **94**(5): p. 1936-1946.

98. Vaia, R.A., B.B. Sauer, O.K. Tse, and E.P. Giannelis, *Relaxations of confined chains in polymer nanocomposites: Glass transition properties of poly(ethylene oxide) intercalated in montmorillonite.* Journal of Polymer Science Part B-Polymer Physics, 1997. **35**(1): p. 59-67.

99. Jeon, H.G., H.T. Jung, S.W. Lee, and S.D. Hudson, *Morphology of polymer/silicate nanocomposites - High density polyethylene and a nitrile copolymer.* Polymer Bulletin, 1998. **41**(1): p. 107-113.

100. Ogata, N., G. Jimenez, H. Kawai, and T. Ogihara, *Structure and thermal/mechanical properties of poly(l-lactide)-clay blend.* Journal of Polymer Science Part B-Polymer Physics, 1997. **35**(2): p. 389-396.

101. Kawasumi, M., N. Hasegawa, M. Kato, A. Usuki, and A. Okada, *Preparation and mechanical properties of polypropylene-clay hybrids.* Macromolecules, 1997. **30**(20): p. 6333-6338.

102. Hasegawa, N., M. Kawasumi, M. Kato, A. Usuki, and A. Okada, *Preparation and mechanical properties of polypropylene-clay hybrids using a maleic anhydride-modified polypropylene oligomer.* Journal of Applied Polymer Science, 1998. **67**(1): p. 87-92.

103. Lee, H.S., P.D. Fasulo, W.R. Rodgers, and D.R. Paul, *TPO based nanocomposites. Part 1. Morphology and mechanical properties.* Polymer, 2005. **46**(25): p. 11673-11689.

104. Shi, Y., S. Peterson, and D.Y. Sogah, *Surfactant-free method for the synthesis of poly(vinyl acetate) masterbatch nanocomposites as a route to ethylene vinyl acetate/silicate nanocomposites.* Chemistry of Materials, 2007. **19**(7): p. 1552-1564.

105. Treece, M.A., W. Zhang, R.D. Moffitt, and J.P. Oberhauser, *Twin-screw extrusion of polypropylene-clay nanocomposites: Influence of masterbatch processing, screw rotation mode, and sequence.* Polymer Engineering and Science, 2007. **47**(6): p. 898-911.

106. Etelaaho, P., K. Nevalainen, R. Suihkonen, J. Vuorinen, K. Hanhi, and P. Jarvela, *Effects of Direct Melt Compounding and Masterbatch Dilution on the Structure and Properties*

of Nanoclay-filled Polyolefins. Polymer Engineering and Science, 2009. **49**(7): p. 1438-1446.

107. Wang, Y., F.B. Chen, and K.C. Wu, *Twin-screw extrusion compounding of polypropylene/organoclay nanocomposites modified by maleated polypropylenes.* Journal of Applied Polymer Science, 2004. **93**(1): p. 100-112.

108. Fornes, T.D. and D.R. Paul, *Modeling properties of nylon 6/clay nanocomposites using composite theories.* Polymer, 2003. **44**(17): p. 4993-5013.

109. Brunauer, S., P.H. Emmett, and E. Teller, *Adsorption of gases in multimolecular layers.* Journal of the American Chemical Society, 1938. **60**: p. 309-319.

110. Vermogen, A., K. Masenelli-Varlot, R. Seguela, J. Duchet-Rumeau, S. Boucard, and P. Prele, *Evaluation of the structure and dispersion in polymer-layered silicate nanocomposites.* Macromolecules, 2005. **38**(23): p. 9661-9669.

111. Wagener, R. and T.J.G. Reisinger, *A rheological method to compare the degree of exfoliation of nanocomposites.* Polymer, 2003. **44**(24): p. 7513-7518.

112. Vermant, J., S. Ceccia, M.K. Dolgovskij, P.L. Maffettone, and C.W. Macosko, *Quantifying dispersion of layered nanocomposites via melt rheology.* Journal of Rheology, 2007. **51**(3): p. 429-450.

113. Solomon, M.J., A.S. Almusallam, K.F. Seefeldt, A. Somwangthanaroj, and P. Varadan, *Rheology of polypropylene/clay hybrid materials.* Macromolecules, 2001. **34**(6): p. 1864-1872.

114. Krishnamoorti, R. and K. Yurekli, *Rheology of polymer layered silicate nanocomposites.* Current Opinion in Colloid & Interface Science, 2001. **6**(5-6): p. 464-470.

115. Chatterjee, T., R. Patel, J. Garnett, R. Paradkar, S.R. Ge, L.Z. Liu, K.T. Forziati, and N. Shah, *Machine direction orientation of high density polyethylene (HDPE): Barrier and optical properties.* Polymer, 2014. **55**(16): p. 4102-4115.

116. Srinivas, S., P. Brant, Y. Huang, and D.R. Paul, *Structure and properties of oriented polyethylene films.* Polymer Engineering and Science, 2003. **43**(4): p. 831-849.

117. Shi, H., T. Lan, and T.J. Pinnavaia, *Interfacial Effects on the Reinforcement Properties of Polymer−Organoclay Nanocomposites.* Chemistry of Materials, 1996. **8**(8): p. 1584-1587.

118. Manias, E., A. Touny, L. Wu, K. Strawhecker, B. Lu, and T.C. Chung, *Polypropylene/montmorillonite nanocomposites. Review of the synthetic routes and materials properties.* Chemistry of Materials, 2001. **13**(10): p. 3516-3523.

119. Jayaraman, K. and S. Kumar, *Polypropylene layered silicate nanocomposites*, in *Polymer Nanocomposites*. 2006, Woodhead Publishing. p. 130-150.

120. Herrera, N.N., J.-M. Letoffe, J.-P. Reymond, and E. Bourgeat-Lami, *Silylation of laponite clay particles with monofunctional and trifunctional vinyl alkoxysilanes.* Journal of Materials Chemistry, 2005. **15**(8): p. 863-871.

121. Carrado, K.A., L. Xu, R. Csencsits, and J.V. Muntean, *Use of Organo- and Alkoxysilanes in the Synthesis of Grafted and Pristine Clays.* Chemistry of Materials, 2001. **13**(10): p. 3766-3773.

122. He, H.P., Q. Tao, J.X. Zhu, P. Yuan, W. Shen, and S.Q. Yang, *Silylation of clay mineral surfaces.* Appl. Clay Sci., 2013. **71**: p. 15-20.

123. Lu, H.D., Y. Hu, M. Li, Z.Y. Chen, and W.C. Fan, *Structure characteristics and thermal properties of silane-grafted-polyethylene/clay nanocomposite prepared by reactive extrusion.* Composites Science and Technology, 2006. **66**(15): p. 3035-3039.

124. Buggy, M., G. Bradley, and A. Sullivan, *Polymer-filler interactions in kaolin/nylon 6,6 composites containing a silane coupling agent.* Composites Part a-Applied Science and Manufacturing, 2005. **36**(4): p. 437-442.

125. Choi, Y.Y., S.H. Lee, and S.H. Ryu, *Effect of silane functionalization of montmorillonite on epoxy/montmorillonite nanocomposite.* Polymer Bulletin, 2009. **63**(1): p. 47-55.

126. Lee, J.W., M.H. Kim, W.M. Choi, and O.O. Park, *Effects of organoclay modification on microstructure and properties of polypropylene–organoclay nanocomposites.* Journal of Applied Polymer Science, 2006. **99**(4): p. 1752-1759.

127. Yazdani, H., J. Morshedian, and H.A. Khonakdar, *Effects of silane coupling agent and maleic anhydride grafted polypropylene on the morphology and viscoelastic properties of polypropylene-mica composites.* Polymer Composites, 2006. **27**(5): p. 491-496.

128. Shanmugharaj, A.M., K.Y. Rhee, and S.H. Ryu, *Influence of dispersing medium on grafting of aminopropyltriethoxysilane in swelling clay materials.* Journal of Colloid and Interface Science, 2006. **298**(2): p. 854-859.

129. Song, K. and G. Sandi, *Characterization of montmorillonite surfaces after modification by organosilane.* Clays and Clay Minerals, 2001. **49**(2): p. 119-125.

130. Le Pluart, L., J. Duchet, H. Sautereau, and J.F. Gerard, *Surface modifications of montmorillonite for tailored interfaces in nanocomposites.* Journal of Adhesion, 2002. **78**(7): p. 645-662.

131. Krishnamoorti, R., I. Banik, and L. Xu, *Rheology and processing of polymer nanocomposites.* Reviews in Chemical Engineering, 2010. **26**(1-2): p. 3-12.

132. Ren, J.X. and R. Krishnamoorti, *Nonlinear viscoelastic properties of layered-silicate-based intercalated nanocomposites.* Macromolecules, 2003. **36**(12): p. 4443-4451.

133. Letwimolnun, W., B. Vergnes, G. Ausias, and P.J. Carreau, *Stress overshoots of organoclay nanocomposites in transient shear flow.* Journal of Non-Newtonian Fluid Mechanics, 2007. **141**(2-3): p. 167-179.

134. Ghanbari, A., M.-C. Heuzey, P. Carreau, and M.-T. Ton-That, *Morphological and rheological properties of PET/clay nanocomposites.* Rheologica Acta, 2013. **52**(1): p. 59-74.

135. Cassagnau, P., *Melt rheology of organoclay and fumed silica nanocomposites.* Polymer, 2008. **49**(9): p. 2183-2196.

136. Cassagnau, P., *Linear viscoelasticity and dynamics of suspensions and molten polymers filled with nanoparticles of different aspect ratios.* Polymer, 2013. **54**(18): p. 4762-4775.

137. Zhang, Q., Archer, L., *Polyethylene oxide/silica nanocomposites; structure and rheology.* Langmuir, 2002. **18**: p. 10435-10442.

138. Durmus, A., A. Kasgoz, and C.W. Macosko, *Linear low density polyethylene (LLDPE)/clay nanocomposites. Part I: Structural characterization and quantifying clay dispersion by melt rheology.* Polymer, 2007. **48**(15): p. 4492-4502.

139. Baldi, F., A. Franceschini, F. Bignotti, G. Tieghi, and T. Ricco, *Rheological behaviour of nano-composites based on polyamide 6 under shear and elongational flow at high strain rates.* Rheologica Acta, 2009. **48**(1): p. 73-88.

140. Gupta, R.K., V. Pasanovic-Zujo, and S.N. Bhattacharya, *Shear and extensional rheology of EVA/layered silicate-nanocomposites.* Journal of Non-Newtonian Fluid Mechanics, 2005. **128**(2-3): p. 116-125.

141. Pasanovic-Zujo, V., R.K. Gupta, and S.N. Bhattacharya, *Effect of vinyl acetate content and silicate loading on EVA nanocomposites under shear and extensional flow.* Rheologica Acta, 2004. **43**(2): p. 99-108.

142. Singh, S., A.K. Ghosh, S.N. Maiti, S. Raha, R.K. Gupta, and S. Bhattacharya, *Morphology and rheological behavior of polylactic acid/clay nanocomposites.* Polymer Engineering and Science, 2012. **52**(1): p. 225-232.

143. Ku, K.H. and S.C. Kim, *Polypropylene nanocomposite using maleated PP and diamine.* Journal of Applied Polymer Science, 2009. **113**(3): p. 1539-1549.

144. Hameed, T., D.K. Potter, and E. Takacs, *Reactions of low molecular weight highly functionalized maleic anhydride grafted polyethylene with polyetherdiamines.* Journal of Applied Polymer Science, 2010. **116**(4): p. 2285-2297.

145. Orr, C.A., J.J. Cernohous, P. Guegan, A. Hirao, H.K. Jeon, and C.W. Macosko, *Homogeneous reactive coupling of terminally functional polymers.* Polymer, 2001. **42**(19): p. 8171-8178.

146. Lu, Q.W., C.W. Macosko, and J. Horrion, *Melt amination of polypropylenes.* Journal of Polymer Science Part a-Polymer Chemistry, 2005. **43**(18): p. 4217-4232.

147. Song, Z.Q. and W.E. Baker, *Chemical reactions and reactivity of primary, secondary, and tertiary diamines with acid functionalized polymers.* Journal of Polymer Science Part a-Polymer Chemistry, 1992. **30**(8): p. 1589-1600.

148. Pathak, T.J., *Ph.D. Dissertation, Michigan State University*. 2014.

149. Najjar, W., S. Azabou, S. Sayadi, and A. Ghorbel, *Catalytic wet peroxide photo-oxidation of phenolic olive oil mill wastewater contaminants: Part 1. Reactivity of tyrosol over (Al-Fe)PILC.* Applied Catalysis B-Environmental, 2007. **74**(1-2): p. 11-18.

150. Wibulswas, R., *Batch and fixed bed sorption of methylene blue on precursor and QACs modified montmorillonite.* Separation and Purification Technology, 2004. **39**(1-2): p. 3-12.

151. Yang, T., X.D. Wen, J.F. Li, and L.M. Yang, *Theoretical and experimental investigations on the structures of purified clay and acid-activated clay.* Applied Surface Science, 2006. **252**(18): p. 6154-6161.

152. Aranguren, M.I., E. Mora, J.J.V. DeGroot, and C.W. Macosko, *Effect of reinforcing fillers on the rheology of polymer melts.* Journal of Rheology, 1992. **36**(6): p. 1165-1182.

153. Xu, L., H. Nakajima, E. Manias, and R. Krishnamoorti, *Tailored nanocomposites of polypropylene with layered silicates.* Macromolecules, 2009. **42**(11): p. 3795-3803.

154. Sarvestani, A.S., *Modeling the solid-like behavior of entangled polymer nanocomposites at low frequency regimes.* European Polymer Journal, 2008. **44**(2): p. 263-269.

155. Russo, G.M., V. Nicolais, L. Di Maio, S. Montesano, and L. Incarnato, *Rheological and mechanical properties of nylon 6 nanocomposites submitted to reprocessing with single and twin screw extruders.* Polymer Degradation and Stability, 2007. **92**(10): p. 1925-1933.

156. Shah, R.K. and D.R. Paul, *Organoclay degradation in melt processed polyethylene nanocomposites.* Polymer, 2006. **47**(11): p. 4075-4084.

157. Phuong, N.T., V. Gilbert, and B. Chuong, *Preparation of recycled polypropylene/organophilic modified layered silicates nanocomposites part I: The recycling process of polypropylene and the mechanical properties of recycled polypropylene/organoclay nanocomposites.* Journal of Reinforced Plastics and Composites, 2008. **27**(18): p. 1983-2000.

158. La Mantia, F.P., M.C. Mistretta, and M. Morreale, *Recycling and thermomechanical degradation of LDPE/modified clay nanocomposites.* Macromolecular Materials and Engineering, 2014. **299**(1): p. 96-103.

159. Silvano, J.d.R., S.A. Rodrigues, J. Marini, R.E.S. Bretas, S.V. Canevarolo, B.d.M. Carvalho, and L.A. Pinheiro, *Effect of reprocessing and clay concentration on the degradation of polypropylene/montmorillonite nanocomposites during twin screw extrusion.* Polymer Degradation and Stability, 2013. **98**(3): p. 801-808.

160. Touati, N., M. Kaci, S. Bruzaud, and Y. Grohens, *The effects of reprocessing cycles on the structure and properties of isotactic polypropylene/cloisite 15A nanocomposites.* Polymer Degradation and Stability, 2011. **96**(6): p. 1064-1073.

161. Thompson, M.R. and K.K. Yeung, *Recyclability of a layered silicate–thermoplastic olefin elastomer nanocomposite.* Polymer Degradation and Stability, 2006. **91**(10): p. 2396-2407.

162. Incarnato, L., P. Scarfato, G. Gorrasi, V. Vittoria, and D. Acierno, *Structural modifications induced by recycling of polypropylene.* Polymer Engineering and Science, 1999. **39**(9): p. 1661-1666.

163. Incarnato, L., P. Scarfato, and D. Acierno, *Rheological and mechanical properties of recycled polypropylene.* Polymer Engineering and Science, 1999. **39**(4): p. 749-755.

164. Fornes, T.D., P.J. Yoon, and D.R. Paul, *Polymer matrix degradation and color formation in melt processed nylon 6/clay nanocomposites.* Polymer, 2003. **44**(24): p. 7545-7556.

165. de la Orden, M.U., D. Pascual, C. Munoz, V. Lorenzo, and J.M. Urreaga, *Clay-induced degradation during the melt reprocessing of waste polycarbonate.* Journal of Applied Polymer Science, 2014. **131**(5).

166. Shen, W., H.P. He, J.X. Zhu, P. Yuan, and R.L. Frost, *Grafting of montmorillonite with different functional silanes via two different reaction systems.* Journal of Colloid and Interface Science, 2007. **313**(1): p. 268-273.

167. He, H., J. Duchet, J. Galy, and J.-F. Gérard, *Influence of cationic surfactant removal on the thermal stability of organoclays.* Journal of Colloid and Interface Science, 2006. **295**(1): p. 202-208.

168. Filippone, G., G. Romeo, and D. Acierno, *Viscoelasticity and Structure of Polystyrene/Fumed Silica Nanocomposites: Filler Network and Hydrodynamic Contributions.* Langmuir, 2010. **26**(4): p. 2714-2720.

169. Tabatabaei, S.H. and A. Ajji, *Structure-orientation-properties relationships for polypropylene nanoclay composite films.* Journal of Plastic Film & Sheeting, 2011. **27**(1-2): p. 87-115.

170. Manikantan, M.R. and N. Varadharaju, *Preparation and Properties of Polypropylene-Based Nanocomposite Films for Food Packaging.* Packaging Technology and Science, 2011. **24**(4): p. 191-209.

171. Shah, R.K. and D.R. Paul, *Nylon 6 nanocomposites prepared by a melt mixing masterbatch process.* Polymer, 2004. **45**(9): p. 2991-3000.

172. He, H.P., Q. Tao, J.X. Zhu, P. Yuan, W. Shen, and S.Q. Yang, *Silylation of clay mineral surfaces.* Applied Clay Science, 2013. **71**: p. 15-20.

173. Lee, J.W., M.H. Kim, W.M. Choi, and O.O. Park, *Effects of organoclay modification on microstructure and properties of polypropylene-organoclay nanocomposites.* Journal of Applied Polymer Science, 2006. **99**(4): p. 1752-1759.

174. Roozemond, P.C., Z. Ma, K.P. Cui, L.B. Li, and G.W.M. Peters, *Multimorphological Crystallization of Shish-Kebab Structures in Isotactic Polypropylene: Quantitative Modeling of Parent-Daughter Crystallization Kinetics.* Macromolecules, 2014. **47**(15): p. 5152-5162.

175. Roozemond, P.C., M. van Drongelen, Z. Ma, M.A. Hulsen, and G.W.M. Peters, *Modeling flow-induced crystallization in isotactic polypropylene at high shear rates.* Journal of Rheology, 2015. **59**(3): p. 613-642.

176. Galgali, G., S. Agarwal, and A. Lele, *Effect of clay orientation on the tensile modulus of polypropylene-nanoclay composites.* Polymer, 2004. **45**(17): p. 6059-6069.

177. Hotta, S. and D.R. Paul, *Nanocomposites formed from linear low density polyethylene and organoclays.* Polymer, 2004. **45**(22): p. 7639-7654.

178. Ren, J.X., A.S. Silva, and R. Krishnamoorti, *Linear viscoelasticity of disordered polystyrene-polyisoprene block copolymer based layered-silicate nanocomposites.* Macromolecules, 2000. **33**(10): p. 3739-3746.

179. Hyun, Y.H., S.T. Lim, H.J. Choi, and M.S. Jhon, *Rheology of poly(ethylene oxide)/organoclay nanocomposites.* Macromolecules, 2001. **34**(23): p. 8084-8093.

180. Rohlmann, C.O., M.D. Failla, and L.M. Quinzani, *Linear viscoelasticity and structure of polypropylene-montmorillonite nanocomposites.* Polymer, 2006. **47**(22): p. 7795-7804.

181. Devendra, R., S.G. Hatzikiriakos, and R. Vogel, *Rheology of metallocene polyethylene-based nanocomposites: Influence of graft modification.* Journal of Rheology, 2006. **50**(4): p. 415-434.

182. Akcora, P., S.K. Kumar, J. Moll, S. Lewis, L.S. Schadler, Y. Li, B.C. Benicewicz, A. Sandy, S. Narayanan, J. Illavsky, P. Thiyagarajan, R.H. Colby, and J.F. Douglas, *"Gel-like" Mechanical Reinforcement in Polymer Nanocomposite Melts.* Macromolecules, 2010. **43**(2): p. 1003-1010.

183. Zhu, Z.Y., T. Thompson, S.Q. Wang, E.D. von Meerwall, and A. Halasa, *Investigating linear and nonlinear viscoelastic behavior using model silica-particle-filled polybutadiene.* Macromolecules, 2005. **38**(21): p. 8816-8824.

184. Lorthioir, C., F. Laupretre, J. Soulestin, and J.M. Lefebvre, *Segmental Dynamics of Poly(ethylene oxide) Chains in a Model Polymer/Clay Intercalated Phase: Solid-State NMR Investigation.* Macromolecules, 2009. **42**(1): p. 218-230.

185. Faghihi, F., N. Mohammadi, and P. Hazendonk, *The effect of rigid polymeric particles addition on the local dynamic heterogeneity and the ultrasound attenuation of butyl acrylate-methyl methacrylate copolymers.* Polymer, 2013. **54**(12): p. 3038-3046.

186. Papon, A., H. Montes, M. Hanafi, F. Lequeux, L. Guy, and K. Saalwachter, *Glass-Transition Temperature Gradient in Nanocomposites: Evidence from Nuclear Magnetic Resonance and Differential Scanning Calorimetry.* Physical Review Letters, 2012. **108**(6).

187. Papon, A., K. Saalwachter, K. Schaler, L. Guy, F. Lequeux, and H. Montes, *Low-Field NMR Investigations of Nanocomposites: Polymer Dynamics and Network Effects.* Macromolecules, 2011. **44**(4): p. 913-922.

188. Dreiss, C.A., T. Cosgrove, N.J. Benton, D. Kilburn, M.A. Alam, R.G. Schmidt, and G.V. Gordon, *Effect of crosslinking on the mobility of PDMS filled with polysilicate nanoparticles: Positron lifetime, rheology and NMR relaxation studies.* Polymer, 2007. **48**(15): p. 4419-4428.

189. Chen, F., A. Clough, B.M. Reinhard, M.W. Grinstaff, N. Jiang, T. Koga, and O.K.C. Tsui, *Glass Transition Temperature of Polymer-Nanoparticle Composites: Effect of Polymer-Particle Interfacial Energy.* Macromolecules, 2013. **46**(11): p. 4663-4669.

190. Tsagaropoulos, G. and A. Eisenberg, *Direct Observation of 2 Glass Transitions in Silica-Filled Polymers - Implications for the Morphology of Random Ionomers.* Macromolecules, 1995. **28**(1): p. 396-398.

191. Hattemer, G.D. and G. Arya, *Viscoelastic Properties of Polymer-Grafted Nanoparticle Composites from Molecular Dynamics Simulations.* Macromolecules, 2015. **48**(4): p. 1240-1255.

192. V, P. and G. V, *Origins of linear viscoelastic behavior of polymer-nanoparticle composites.* Macromolecules, 2006. **39**(2): p. 844-856.

193. Coiai, S., D. Prevosto, M. Bertoldo, L. Conzatti, V. Causin, C. Pinzino, and E. Passaglia, *Chemistry of Interfacial Interactions in a LDPE-Based Nanocomposite and Their Effect on the Nanoscale Hybrid Assembling.* Macromolecules, 2013. **46**(4): p. 1563-1572.

194. Leu, C.M., Z.W. Wu, and K.H. Wei, *Synthesis and properties of covalently bonded layered silicates/polyimide (BTDA-ODA) nanocomposites.* Chemistry of Materials, 2002. **14**(7): p. 3016-3021.

195. Zhao, C.G., M. Feng, F.L. Gong, H.L. Qin, and M.S. Yang, *Preparation and characterization of polyethylene-clay nanocomposites by using chlorosilane-modified clay.* Journal of Applied Polymer Science, 2004. **93**(2): p. 676-680.

196. Chen, G.X., J.B. Choi, and J.S. Yoon, *The role of functional group on the exfoliation of clay in poly(L-lactide).* Macromolecular Rapid Communications, 2005. **26**(3): p. 183-187.

197. Wheeler, P.A., J.Z. Wang, J. Baker, and L.J. Mathias, *Synthesis and characterization of covalently functionalized laponite clay.* Chemistry of Materials, 2005. **17**(11): p. 3012-3018.

198. Bailly, M., M. Kontopoulou, and K. El Mabrouk, *Effect of polymer/filler interactions on the structure and rheological properties of ethylene-octene copolymer/nanosilica composites.* Polymer, 2010. **51**(23): p. 5506-5515.

199. Dealy, J.M. and R.G. Larson, *Structure and Rheology of Molten Polymers From Polymerization to Processability Via Rheology*. 2006, Hanser Publications: Cincinnati.

200. Robbes, A.S., F. Cousin, F. Meneau, F. Dalmas, R. Schweins, D. Gigmes, and J. Jestin, *Polymer-Grafted Magnetic Nanoparticles in Nanocomposites: Curvature Effects, Conformation of Grafted Chain, and Bimodal Nanotriggering of Filler Organization by Combination of Chain Grafting and Magnetic Field (vol 45, pg 9220, 2012).* Macromolecules, 2013. **46**(3): p. 1260-1260.

201. Roe, R.J., *Conformation of an Isolated Polymer Molecule at an Interface .2. Dependence on Molecular Weight.* Journal of Chemical Physics, 1965. **43**(5): p. 1591-&.

202. Kabanemi, K.K. and J.F. Hetu, *A reptation-based model to the dynamics and rheology of linear entangled polymers reinforced with nanoscale rigid particles.* Journal of Non-Newtonian Fluid Mechanics, 2010. **165**(15-16): p. 866-878.

203. Tsenoglou, C., *Viscoelasticity of Binary Homopolymer Blends.* Abstracts of Papers of the American Chemical Society, 1987. **194**: p. 219-POLY.

204. Descloizeaux, J., *Double Reptation Vs Simple Reptation in Polymer Melts.* Europhysics Letters, 1988. **5**(5): p. 437-442.

205. Vilgis, T.A., G. Heinrich, and M. Kluppel, *Reinforcement of polymer nano-composites : theory, experiments and applications*. 2009, Cambridge, UK ; New York: Cambridge University Press.

206. McLeish, T.C.B. and R.G. Larson, *Molecular constitutive equations for a class of branched polymers: The pom-pom polymer.* Journal of Rheology, 1998. **42**(1): p. 81-110.

207. Lentzakis, H., D. Vlassopoulos, D.J. Read, H. Lee, T. Chang, P. Driva, and N. Hadjichristidis, *Uniaxial extensional rheology of well-characterized comb polymers.* Journal of Rheology, 2013. **57**(2): p. 605-625.